

UNIVERSITA' DEGLI STUDI DI NAPOLI "FEDERICO II"

FACOLTA' DI INGEGNERIA

**DIPARTIMENTO DI INGEGNERIA CHIMICA DEI MATERIALI E
DELLA PRODUZIONE INDUSTRIALE**



**DOTTORATO DI RICERCA IN INGEGNERIA DEI MATERIALI E DELLE
STRUTTURE**

Ciclo XXVI

**Manipulating the Morphology and Properties of
Immiscible Polymer Blends Using Nanoparticles – A
Viable Route to Enlarge the Fields of Application of
Biopolymers**

Scientific Committee

PhD Student

Supervisors: Dr. Giovanni Filippone

Anna Nuzzo

Prof. Domenico Acierno

Coordinator of the PhD Program:

Prof. Giuseppe Mensitieri

TRIENNIO 2011/2014

Acknowledgements

I would like to express my sincere gratitude to my supervisors Prof. Domenico Acierno and Dr. Giovanni Filippone, for their support and guidance throughout my PhD life. I am thankful for all the opportunities they initiated such as presenting at national and international conferences, research collaborations, the experience in Queen Mary University and journal publishing.

This work was supported by the FIRB 2010-Futuro in ricerca project (No. RBFR10DCS7) funded by the Italian Ministry of University and Research (MIUR). I would like to thank all the members of the project: Dr. Serena Coiai, Dr. Sabrina C. Carroccio, Dr. Nadka Tz. Dintcheva, Dr. Cristian Gambarotti.

Dr. Sabrina C. Carroccio (Consiglio Nazionale delle Ricerche, CNR-ICTP UOS Catania, Catania, Italy) is kindly acknowledge for the SEC-MALLS analyses and the valuable discussions.

I wish to thank Prof. Ton Peijs for giving me the possibility to join his group in Queen Mary University of London, Materials Department, for his fruitful suggestions and hospitality. Thanks are especially given to Dr. Emiliano Bilotti for his constant support and invaluable guidance, for his trust and constant encouragement throughout all the period I spent in Queen Mary. I wish to thank all the group members and support staff in Queen Mary for the suggestions and the assistance with the experimental work and above all for their hospitality: I felt like an effective member of Ton's group and not only as a visiting PhD student. Thanks are especially given to Eric Asare, Dr. Urszula Stachewicz, Dr. Wei Tu, Fang Mai and Dr. Krystelle Mafina.

I wish to thank Dr. Lorenzo Botto for the critical comments and discussions.

Ringrazio tutti i miei amici e colleghi del Dipartimento di Ingegneria Chimica, dei Materiali e della Produzione Industriale, dove ho svolto la gran parte dell'attività di ricerca. Grazie di cuore a tutti voi ragazzi, per il vostro aiuto e supporto, per l'incoraggiamento, i consigli, le chiacchierate, la pazienza, i sorrisi e gli innumerevoli momenti di gioia e divertimento trascorsi insieme.

Un ringraziamento speciale va a Barbara e Giorgio. Grazie ragazzi per la vostra amicizia costante e sincera e grazie perché ci siete sempre stati e mi date perenne conferma che continuerete a esserci.

Ringrazio poi i miei amici di una vita: Teresa, Valeria, Pina e Gianluca.

Ringrazio inoltre Sara per l'amicizia e i bellissimi momenti trascorsi insieme a Londra e in Cornovaglia e per essermi stata vicina nei periodi più difficili.

Infine, vorrei esprimere la più sincera gratitudine alla mia famiglia per il costante supporto durante questi anni.

Abstract

The overall aim of the research activity has been identifying bio-based and eco-sustainable polymeric formulations potentially suitable for applications of technological interest. Together with the typically high costs, the major technical challenge to widespread acceptance of bio-polymers is the difficulty in achieving physical and mechanical properties comparable with those of conventional petroleum-based polymers. Among bio-polymers, poly lactic acid (PLA) is one of the most promising candidate for the substitution, totally or partially, of many petroleum-based polymers. In fact, PLA exhibits the best compromise among eco-sustainability, physical and mechanical features and industrial development prospect. However, the low mechanical resistance at high temperature (Heat Deflection Temperature = 50÷60°C) has prevented its complete access to relevant industrial sectors.

In the present work, the poor mechanical properties of the amorphous PLA above its glass transition are corrected by blending it with Polyamide 11 (PA11), a semicrystalline bio-based polymer, and promoting the continuity of the latter phase through the addition of nanoparticles. Specifically, three different kinds of nanoparticles, inclined to enrich PA11 phase, have been used: an organo-modified montmorillonite (OMMT), an organo-modified sepiolite (MS) and carbon nanotubes (CNTs).

The preferential positioning of the three fillers inside the PA11 minor phase of PLA/PA11 blends has resulted effective in inducing its phase continuity. In particular, provided a critical nanoparticles loading is exceeded, the drops-matrix morphology of a blend at 70% wt of PLA converts in a co-continuous one. In such a way, remarkable improvements of the high temperature mechanical performances are achieved owing to the filled PA11 framework, which interpenetrates the PLA major phase and contributes to bear stress up to ~160°C, i.e. ~100°C above the PLA glass transition. Nanoparticles-induced co-continuity in immiscible polymer blends has been previously observed in many systems, but the underlying mechanism is still unclear. An additional goal of this work is to better clarify the mechanism behind the co-continuity development observed in our bio-based nanocomposite polymer blend. In particular, we focus on the roles played by *(i)* bulk rheology of filled phase, *(ii)* self-networking propensity of nanoparticles, and *(iii)* properties of the blend interface. The latter are differently affected by changing chemistry and geometrical features of the nanoparticles. Among others, two issues are examined more in depth: how effective it is to promote co-continuity by kinetically arresting the relaxation dynamics of the bulk polymer phases by

means of nanoparticles? And, if so, is the self-networking ability of the particles the only relevant parameter? The cross-check of the experimental data obtained from morphological, dynamical-mechanical and rheological analyses reveals that simply slowing down the melt state relaxation dynamics of the minor phase through the aggregation of nanoparticles in a space-spanning elastic network may be not sufficient to promote co-continuity. The effect of the geometrical features of the particles is discussed, as well as their ability to affect interfacial tension. In particular, the lowering of the latter seems to play a crucial role, stabilizing irregularly-shaped domains whose merging eventually results into co-continuity. Concluding, the results obtained in the present thesis provide the experimental evidence that a judicious selection of the blend constituents, combined with a clever manipulation of the blend microstructure through the addition of nanoparticles, may effectively result in “engineered” materials with enhanced properties. Applying such an approach to bio-based polymers represents a viable route to expand and diversify the field of possible applications of such promising materials.

Table of Contents

List of Tables	8
List of Figures	9

1.INTRODUCTION **12**

1.1 Bio-based plastics	12
1.1.1 What is a bio-plastic?	12
1.1.2 Bio-plastics: market scenario	13
1.1.3 Eco-sustainability: bio-plastics vs petroleum-based plastics	16
1.1.4 Bio-plastics: weaknesses and challenges	19
1.2 State of the art and aim of the research activity	20
1.2.1 Materials selection: motivations	22
1.2.2 Structure of the thesis	25
1.3 References	27

PART 1: HEAT RESISTANT FULLY BIO-BASED NANOCOMPOSITE BLENDS BASED ON POLY(LACTIC ACID) **31**

2.1 Introduction	32
2.2 Materials and Methods	37
2.2.1 Materials and blends preparation	37
2.2.2 Characterization methods	38
2.3 Results and discussion	39
2.3.1 Morphological Analysis	39
2.3.2 Crystallization behavior	46
2.3.3 Thermo-mechanical behavior	49
2.3.4 Optimizing the formulation-High vs room temperature mechanical properties	52
2.4 Conclusions	54
2.5 References	56

PART 2: NANOPARTICLE-INDUCED CO-CONTINUITY IN IMMISCIBLE POLYMER BLENDS – A COMPARATIVE STUDY USING CLOISITE, SEPIOLITE, CARBON NANOTUBES **60**

3.1 Introduction	61
3.2 Materials and Methods	63
2.2.1 Materials and blends preparation	63
2.2.2 Characterization methods	64

<u>3.3 Results and discussion</u>	<u>66</u>
3.3.1 Selective localization of nanofillers	66
3.3.2 Nanoparticles-induced co-continuity	68
<i>Effect of the shape of the nanoparticles: OMMT- and MS-based blend</i>	68
<i>Role of bulk rheology</i>	73
<i>CNTs-based blends</i>	75
3.3.3 Role of the interfacial features	81
<u>3.4 Conclusions</u>	<u>84</u>
<u>3.5 References</u>	<u>86</u>

4. CONCLUSIONS **90**

APPENDIX **93**

<u>A.1 Melt state stability: linear viscoelasticity and thermal degradation phenomena</u>	<u>93</u>
A.1.1 Experimental procedure	94
A.1.2 Thermal degradation of pure PLA	95
A.1.3 Thermal degradation of pure PA11	97
A.1.4 Thermal degradation of PA11/OMMT nanocomposites	99
<u>A.2 References</u>	<u>103</u>

List of Tables

1.1	<u>Comparison of Typical PLA Properties with Several Petroleum-Based Commodity Thermoplastic Resins</u>	23
2.1	<u>Primary transition temperatures of selected PLA copolymers</u>	33
2.2	<u>Compositions of samples</u>	37
2.3	<u>Measured contact angles and computed surface energies for PLA and PA11 at 25°C (a) and 215°C (b). The data for Cloisite 30B are experimental values from [24]</u>	41
2.4	<u>The calculated values of interfacial energies and wetting coefficient</u>	41
2.5	<u>Crystallization temperature (T_c) and enthalpy (ΔH_c), Cold Crystallization temperature (T_{cc}) and enthalpy (ΔH_{cc}), Melting temperature (T_m) and enthalpy (ΔH_m) for the samples as in Figure 2.7. The degree of crystallinity (χ_{PA11}) is the mass percentage crystallinity of PA11 calculated by $\chi_{PA11}=100 \times \Delta H_{m(PA11)} / 200m$, where $\Delta H_{m(PA11)}$ is the measured melting enthalpy of PA11 phase from the second heating scan, 200 J/g was taken as the enthalpy of melting for PA11 perfect crystal [58], m is the weight fraction of PA11 in the blends</u>	47
2.6	<u>Values of Young's modulus, tensile strength, elongations at break and toughness</u>	53
3.1	<u>Compositions of samples</u>	64
3.2	<u>Experimental values of contact angle and surface energies</u>	82
3.3	<u>Interfacial tensions between PLA and various PA11-based nanocomposites</u>	82
A.1	<u>SEC-MALLS of PA11 before and after the rheological characterization</u>	99
A.2	<u>SEC-MALLS of some representative samples</u>	101

List of Figures

1.1	<u>Current and emerging (partially) bio-based plastics and their biodegradability</u>	13
1.2	<u>Projection of the worldwide production capacity of bio-based plastics until 2020</u>	15
1.3	<u>Global carbon cycle during a product life</u>	19
2.1	<u>Synthesis of PLA from L- and D-lactic acid [1, 2]</u>	32
2.2	<u>Stereoforms of lactides [2]</u>	32
2.3	<u>(a) TEM micrograph of the sample PLA90-C3. A magnification of a OMMT-rich PA11 droplet is shown in (b)TEM micrographs of the sample PLA90-C3</u>	42
2.4	<u>WAXD patterns of the pristine OMMT and the sample PLA90-C3</u>	43
2.5	<u>SEM micrographs of the samples PLA90 (a), PLA70 (b), PLA50 (c), PLA90-C3 (d), PLA70-C3 (e), and PLA50-C6 (f)</u>	43
2.6	<u>Schematic illustration of the morphology evolution of the unfilled and filled blends as a function of composition as emerged from SEM and TEM analyses</u>	45
2.7	<u>DSC traces of the neat polymers and the unfilled and filled blends upon cooling (left) and heating (right) at 10°C min⁻¹</u>	46
2.8	<u>(a) Elastic modulus of the neat polymers and the unfilled blends and (b) the OMMT-filled samples. The error bars are the standard deviations estimated on three independent tests</u>	49
2.9	<u>(a) Sample deflection recorded during creep tests for the sample PLA (squares), PA11 (diamonds), PLA70 (circles) and PLA70-C3 (triangles). The pictures show the samples PLA70 (b) and PLA70-C3 (c) at the end of the test, that is after the temperature had reached ~160°C</u>	52
2.10	<u>(a) Sample deflection recorded during the creep tests for the blends PLA80-C3 (circles), PLA70-C1(squares), PLA70-C3 (triangles) and PLA70-C6 (diamonds). The pictures show the samples PLA70-C1 (b) and PLA70-C6 (c) soon after the end of the test</u>	54
2.11	<u>Representative stress-strain curves. (a) PLA (circles), PA11 (triangles) and PLA70 (squares). (b) PLA70-C1 (diamonds), PLA70-C3 (triangles) and PLA70-C6 (circles); the reference curve of the sample PLA70 is reported as well (squares)</u>	56
3.1	<u>(a) TEM micrograph of the sample PLA90-S1.5. A magnification of a MS-rich PA11 droplet is shown in (b)</u>	67
3.2	<u>SEM micrographs of the sample PLA90-S1.5 at different magnifications. The arrows indicate part of MS</u>	68
3.3	<u>SEM micrographs of the samples PLA70-C1 (a), PLA70-C2 (b), PLA70-C3 (c), PLA70-S1 (d), PLA70-S5 (e) and PLA70-S6 (f). Apparently continuous domains of filled PA11 are highlighted in (e) and (f). (Scale bar = 10 µm)</u>	69
3.4	<u>Storage modulus as a function of Temperature of the (a) neat polymers, the unfilled blend PLA70, the OMMT-filled samples PLA-C3 and PLA70-Cx and (b) the MS-filled samples PLA-S6 and PLA70-Sy; the reference curve of the unfilled blend</u>	

	PLA70 is reported as well. (c) Storage modulus at 90°C as a function of filler content for OMMT- (green symbols and line) and MS-based samples (violet symbols and line)	71
3.5	Pictures of (a) PLA70-S1 and (b) PLA70-S6 soon after a creep test performed applying a constant load of 0.455 MPa while heating at 2°C/min from room temperature up to 180°C	73
3.6	ω -dependent elastic modulus (full symbols, left axis) and loss factor $\tan\delta$ (open symbols, right axis) of PA11/based (a) OMMT- and (b) MS-nanocomposites at different filler content: (a) PA11-C1 (circles), PA11-C3 (triangles), PA11-C6 (squares), PA11-C8 (diamonds); (b) PA11-S1 (triangles), PA11-S3 (circles), PA11-S6 (squares), PA11-S15 (diamonds). The modulus and the loss factor of the neat PA11 are reported as the continuous (G') and dashed line ($\tan\delta$)	74
3.7	TEM micrographs of CNT-rich PA11 droplets. The arrows indicate nanotubes protruding from the domain (b) or connecting contiguous drops (c)	76
3.8	(a) SEM micrograph of the sample PLA90-N0.75. A magnification of a CNTs-rich PA11 droplet is shown in (b). The arrows indicate part of CNTs	77
3.9	ω -dependent elastic modulus (full symbols, left axis) and loss factor $\tan\delta$ (open symbols, right axis) of the samples PA11-N0.5 (circles), PA11-S15 (diamonds), PA11-C6 (squares) and PA11-N1 (triangles). The modulus and the loss factor of the neat PA11 are reported as the continuous (G') and dashed line ($\tan\delta$)	78
3.10	(a) Storage modulus as a function of Temperature of the CNTs-filled blends PLA/PA11 70/30. The reference curve of the unfilled sample PLA70 is reported as well. (b) Storage modulus at 90°C of the CNTs-filled blends at 70% of PLA as a function of CNTs content	79
3.11	SEM micrographs of the CNTs-filled samples (a) PLA70-N0.3 (b) PLA70-N1 (c) PLA70-N2	80
3.12	Resistivity versus CNTs content for the PLA/PA11 70/30 blends (left axis). E'_{90° as a function of CNTs content is reported, as well (right axis)	81
3.13	Schematic illustration of the morphology of the filled blends at 70 % wt of PLA when the filled PA11 phase is at the gel-point: (a) PLA70-C3; (b) PLA70-N0.75; (c) PLA70-S6	83
A.1	Time evolution of the PLA complex viscosity η^* and linearization of the rheological data	95
A.2	(a) Frequency dependence of elastic G' (triangles) and viscous G'' (circles) moduli obtained during the four consecutive frequency scans (from I to IV, empty symbols) performed on PLA sample. Full symbols are the moduli extrapolated at time-zero according to the procedure described in (b). The moduli are plotted as a function of the time at which they were acquired. Colored symbols are the extrapolated moduli at time-zero for some representative frequencies	96
A.3	Time evolution of the PA11 complex viscosity η^*	97

A.4	Frequency dependence of elastic G' (triangles) and viscous G'' (circles) moduli obtained during the four consecutive frequency scans performed on PA11 (from I to IV, empty symbols). Full symbols are the moduli extrapolated at “time-zero”	98
A.5	Van Gulp plots computed from the four consecutive frequency scans performed on PA11 (from I to IV, empty symbols). The Van Gulp plot extrapolated at “time-zero” is reported as well (full symbols)	99
A.6	The Hofmann elimination reaction for quaternary ammonium compounds: (a) general reaction scheme and (b) a proposed scheme for organically modified MMT	100
A.7	Elastic modulus (normalized over its value at time zero) as a function of time for the neat and OMMT-filled PA11	102

INTRODUCTION

1.1. BIO-BASED PLASTICS

1.1.1. *What is a bioplastic?*

Nowadays the environmental concerns and a shortage of petroleum resources have driven efforts aiming at bulk production of *bio-polymers*. The difference between *biopolymers* and *petroleum-based polymers* is that the monomers of a biopolymer are derived from a living source. There are three principal ways to produce bio-based plastics [1]: (i) to make use of natural polymers which may be modified but remain intact to a large extent (e.g. starch plastics); (ii) to make use of monomers from natural resources and to polymerize these monomers in a second step (e.g. polylactic acid, PLA); (iii) to produce bio-based polymers directly in microorganisms or in genetically modified crops (e.g. polyhydroxyalcanoates, PHAs).

Bioplastics are plastics made out of biopolymers. Some, like bio-polyethylene, are identical to their oil derived form, except that the source of the monomers is different. Others are unique and have no petroleum-based polymer equivalent. Some bioplastics are biodegradable while others are not. Indeed, the rigorous definition of the term “bio-plastics or biopolymers for plastic application” is still the subject of debate in the industrial and academic world. In fact, it can indicate both (i) not necessarily biodegradable/compostable polymers which entirely derive from renewable resources, and (ii) biodegradable/compostable polymers which are not necessarily obtained from renewable resources. Today, several certifications [2] exist in order to define the conditions where the tests have to be done in order to evaluate the property of biodegradability/compostability.

Figure 1.1 shows the classification of the main polymers according to their origin and biodegradability.

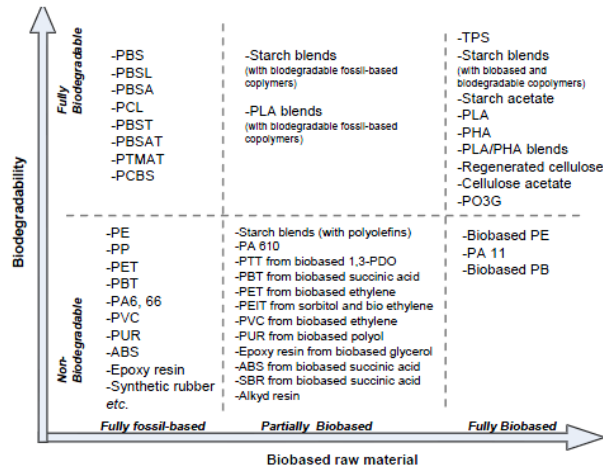


Fig. 1.1: Current and emerging (partially) bio-based plastics and their biodegradability (taken from [3]).

The feedstocks for bioplastics come from a variety of biological sources. Starch based bioplastics are usually made from wheat, corn, rice, potatoes, barley, and sorghum. Cellulose based bioplastics are commonly made from wood. Natural oils from soy, palm, and other plants have also been used to make bioplastics. Other bioplastics rely on bacteria to supply raw materials. An example of an animal derived monomer is hyaluronic acid (HA). It can also be extracted from bacteria. Genetically engineered organisms have been made to increase the yield of certain bioplastic components and in some cases to actually produce specific biopolymers.

1.1.2. Bioplastics: market scenario

The field of bioplastics is still in its infancy but is developing rapidly. The development in the past five years in emerging bio-based plastics is amazing from a technological point of view. Many old processes have been revisited, such as the chemical dehydration of ethanol which leads to ethylene, an important intermediate chemical which can be subsequently converted into polyethylene (PE), polyvinyl chloride (PVC) and other plastics. For numerous types of plastics, first-of-its-kind industrial plants were recently set up and the optimization of these plants is ongoing. Hence, we are at the very beginning of the learning curve. Some of the plant capacities are still rather small when compared to petrochemical plants (e.g. the capacity of Tianan's PHA plant is only 2 kt), but others are very sizable (e.g. Dow-Crystalsev's biobased PE plant will have a capacity of 350 kt). With growing demand for bio-based plastics, it is probably just a matter of time until turn-key plants with large capacities will be commercially available for more bio-based plastics, thereby allowing substantially accelerated growth.

The annual report made by the University of Utrecht in 2009 [3] estimates the global capacity of emerging bio-based plastics at 0.36 Mt (million metric tonnes) by the end of 2007. This is approximately 0.3% of the worldwide production of all plastics (dominated by petrochemical plastics). The current production capacity of bio-based plastics is even smaller compared to “conventional bio-products”: They represent only 2% of the global production of established bio-polymers (20 Mt; comprising cellulose polymers, alkyd resins and non-food starch without starch for fuel ethanol) and only 0.1% of the world paper and board production. However, the market of emerging bio-based plastics has been experiencing rapid growth. From 2003 to the end of 2007, the global average annual growth rate was 38%. In Europe, the annual growth rate was as high as 48% in the same period.

Always looking at ref. [3], the total maximum technical substitution potential of bio-based polymers replacing their petrochemical counterparts is estimated at 270 Mt, or 90% of the total polymers (including fibres) that were consumed in 2007 worldwide. It will not be possible to exploit this technical substitution potential in the short to medium term. The main reasons are economic barriers (especially production costs and capital availability), technical challenges in scale-up, the short-term availability of bio-based feedstocks and the need for the plastics conversion sector to adapt to the new plastics. Nevertheless, from a *technical* point of view, there are very large opportunities for the replacement of petrochemical by bio-based plastics. As shown in Figure 1.2, the worldwide capacity of bio-based plastics, according to company announcements, will increase from 0.36 Mt in 2007 to 2.33 Mt in 2013 and to 3.45 Mt in 2020. This is equivalent to average annual growth rates of 37% between 2007 and 2013 and 6% between 2013 and 2020. In 2007, the most important products in terms of volumes were starch plastics (0.15 Mt) and PLA (0.15 Mt). Based on the company announcements it is projected that the most important representatives projected by 2020 will be starch plastics (1.3 Mt), PLA (0.8 Mt), bio-based PE (0.6 Mt) and PHA (0.4 Mt). Figure 1.2 also shows three PROPIB 2009 (Projection of the worldwide production capacity of bio-based plastics until 2020, final report June, 2009) scenarios, denoted as “BAU” (business-as-usual), “HIGH” and “LOW”. These scenarios are based on expected influencing factors, namely, technical barriers, bulk applications, cost and raw material supply security. The BAU scenario assumes a steady growth of the four key plastics (i.e. starch plastics, PLA, bio-based PE and bio-based epoxy resin) and a modest growth for cellulose films, PHA and bio-based Polyurethane (PUR). The BAU projection results in global production capacity of approximately 3 Mt for 2020. The HIGH scenario shows a fast growing bio-based plastics sector, the four key plastics

are expected to grow strongly, while a steady growth rate is foreseen for cellulose films, PHA and bio-based PUR. Polyamide 11 (PA11) and Polytrimethylene terephthalate (PTT) will not enjoy substantial growth because of their limited use in bulk applications. The HIGH scenario projects that the global production will reach 4.4 Mt by 2020, approximately 30% higher than the projections based on company announcement (3.45 Mt) and the companies' expectations (3.44 Mt). The LOW scenario describes a relatively pessimistic future. The four key plastics will grow relatively slowly and the growth from the remaining plastics will be insignificant. Little progress will be made for bio-based succinic acid, bio-based Polyamide 6 (PA6) and Polyamide 66 (PA66), and bio-based Polypropylene (PP). The LOW scenario estimates that only 1.47 Mt capacity will be installed by 2020. This is approximately 60% lower than the projections. If the overall bio-based plastics industry grows under a BAU condition, the 2020 market will reach 2.49 Mt. The "LOW" growth rate implies that half of the total capacity announced for 2013 will not be implemented even by 2020. In the "HIGH" scenario, on the other hand, the total installed capacity in 2020 will increase nearly twice as much as the capacity announced for 2013. Figure 1.2 shows that for 2020, the projections based on company announcements (3.45 Mt) falls between the former projection, which was published by Crank et al. in 2005 [4], without policies and measures (PM) (2.50 Mt) and PM (4.17 Mt). Based on the previous market analysis, it can be concluded that the long-term expectations coincide rather well with the former projections published in 2005. This gives support to about the reliability of the mid- and long-term projections, which clearly indicate a promising growth rate for the market of bioplastics.

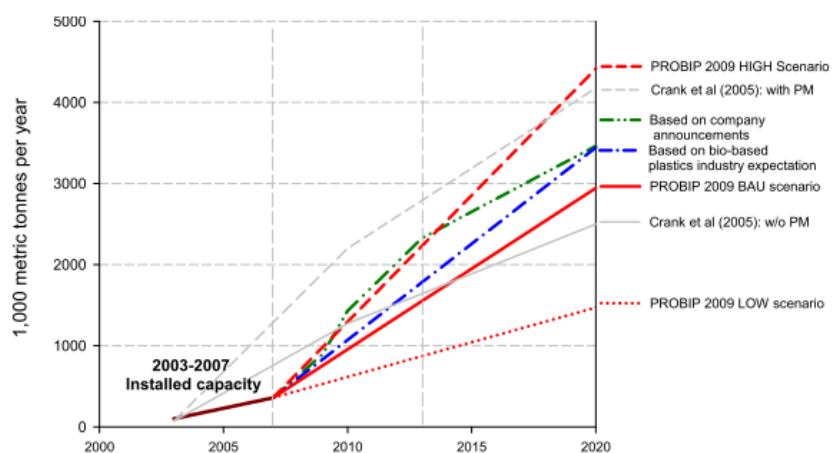


Fig. 1.2: Projection of the worldwide production capacity of bio-based plastics until 2020.

1.1.3 Eco-sustainability: Bioplastics vs Petroleum-based plastics

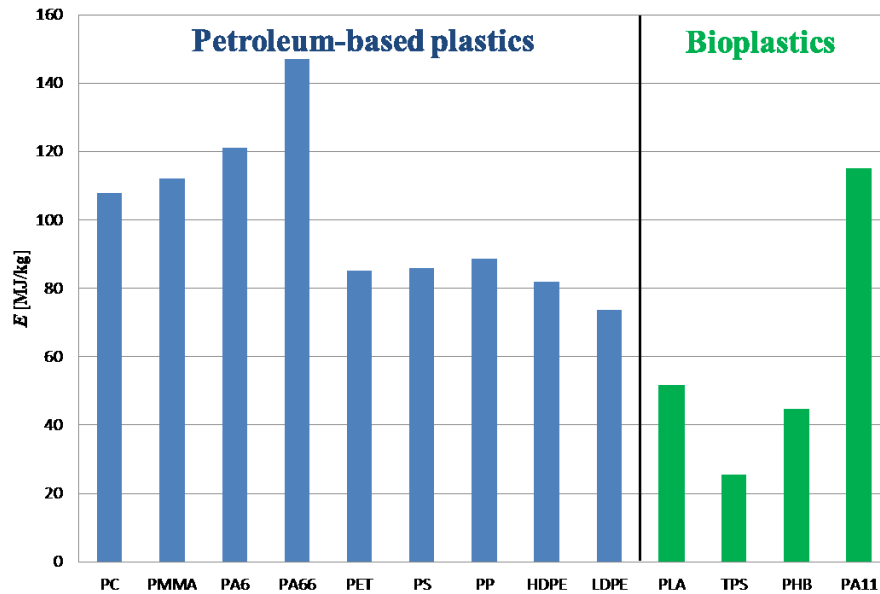
Sustainable development is the driving force for acting more responsibly to protect our world for future generations. It encompasses a combination of environmental, social and economic aspects. In these three aspects, plastics play a vital role. The plastics industry continues to innovate in order to advance its contribution to a more sustainable society. Among all the reasons for the success of plastics, the key one is that plastics are a better alternative for many applications in comparison to metal, not only on the basis of sustainable considerations, but also in term of properties. The main advantages of plastics are low specific weight, flexibility, resistance to corrosive attacks, better processability (less energy requirement), and versatility. A recent study has estimated the effects on climate change if plastics were to be replaced by alternative materials wherever possible across the whole of Western Europe [5]. The results indicate that there would be an additional energy requirement of around 10%, or about 25 million tons of crude oil, corresponding to 105 million tons of CO₂ greenhouse gas emissions per year.

Eco-profiles assessments demonstrate that the bioplastics, at equivalent properties, are usually more eco-sustainable than their homologue based on fossil raw materials. Eco-profile assessment is a method to account for the environmental impacts associated with a certain product. The term “Eco-profile” indicates that all stages of the material lifecycle, from resource extraction up to the product, are taken into account (i.e. “from cradle to pellet”). Eco-profile differentiates from “life cycle assessment” (LCA) as it does not deal with the use of the product and its disposal, whereas LCA does (i.e. “from cradle to grave”).

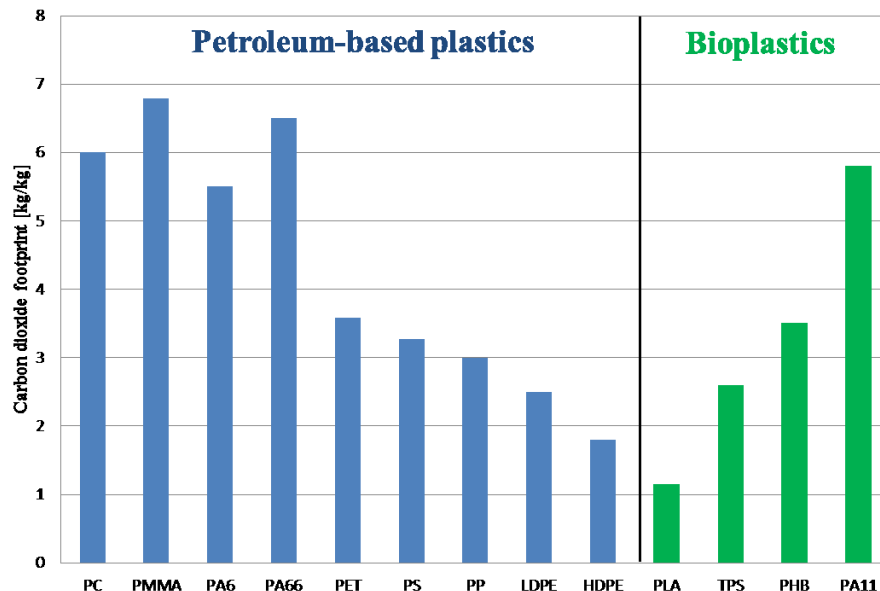
Here the environmental impacts of various bio-plastics and petro-plastics eco-profiles was evaluated through the software CES Edupack 2012. The results have been compared with data reported in literature. We focused on two categories of impacts, which have an increasing importance around the world today: fossil energy requirement (E) and global warming potential or CO₂ footprint ([CO₂]). The fossil energy requirement represents the total amount of fossil feedstocks consumption related to the polymer production, from the raw materials to the pellets. The feedstocks (fossil or biological) are transported to the production plant, consuming energy. The fraction, synthesis, polymerization, extrusion and chopping of polymer requires energy, as does the heating, lighting and general support and maintenance of the plant. E is expressed in MJ per kg of polymer. The global warming potential or the CO₂ footprint represents the CO₂ equivalent mass, in kg, of greenhouse gases produced and released into the atmosphere as a consequence of the production of 1 kg of the material. There

are a variety of “greenhouse gases” that contribute to global warming, including carbon dioxide, methane and nitrous oxide. The “potency” of these gases can vary significantly from a global warming perspective, and therefore it is conventional to report these emissions in terms of an equivalent mass of carbon dioxide.

Graph 1.1 and 1.2 give the fossil energy requirement and the CO₂ footprint of some petro-plastics and bio-plastics, respectively.



Graph 1.1: Fossil energy requirement E for some petroleum-based plastics and bio-plastics.



Graph 1.2: Carbon dioxide footprint in kg/kg for some petroleum-based plastics and bio-plastics.

By definition, the feedstocks of a bioplastic are not derived from petroleum, while the feedstocks of petro-plastics are almost entirely fossil fuel-based. Actually, bioplastics

production consumes fossil fuels because the farming and processing operations commonly use fossil fuel as energy sources. Thus, the production method an individual company uses dictates the amount of fossil fuels that can be saved by a switch to bioplastics. NatureWorks, a manufacturer of polylactic acid (PLA), claims a 68% reduction of fossil fuel use over traditional plastics [6]. Metabolix claims a 95% reduction in fossil fuel use over petroleum plastics for its Mirel brand of Polyhydroxybutyrates (PHB) [7]. The energy for the farm equipment, fertilizer production, and the bioplastics factories does not necessarily have to come from fossil fuels. Alternative energy like solar, nuclear, hydroelectric, biomass, geothermal, and wind could supply all the necessary energy if the required investment was made. However, the fact that the starting feedstock is biomass is one of the main reasons why most bioplastics are more energy saving than petro-polymers with comparable properties. For example, PHB require less energy, when the energy of production and feedstocks are combined, than petroleum based plastics with similar characteristics, like Low Density Polyethylene (LDPE), High Density Polyethylene (HDPE) or PP. The energy requirements for PHB are 44.7 MJ per Kg plastic produced while PP requires 88.6 MJ per Kg, HDPE uses 73.7 MJ per Kg, and LDPE uses 81.8 MJ per Kg produced. PLA requires 54.1 MJ per kg of energy input during its production, which is significantly less than the energy consumption for most petro-plastics with comparable properties like Polystyrene (PS) and Poly(ethylene terephthalate) (PET). The PA11 fossil fuel energy requirements are lower than PA66 and are in the range of competing performance petro-plastics such as Polycarbonate (PC), PA6 or Poly(methyl methacrylate) (PMMA). Thermoplastic starch (TPS) has the lowest energy requirements of the bioplastic examples given. The energy requirement for TPS is 25.4 MJ per Kg plastic produced, less than a third of the energy required to produce most petro-plastics. TPS has the potential for the most energy savings but also has the most limited potential use for its low mechanical properties.

The analysis of Graph 1.2 demonstrates that bio-plastics production enjoys also a lower contribution to global climate change. In fact, the bioplastics at equivalent properties are generally more CO₂ neutral than their homologue based on fossil raw materials. To explain this last point, we have to consider the global carbon cycle during the whole life of a product, which is illustrated in Figure 1.3.

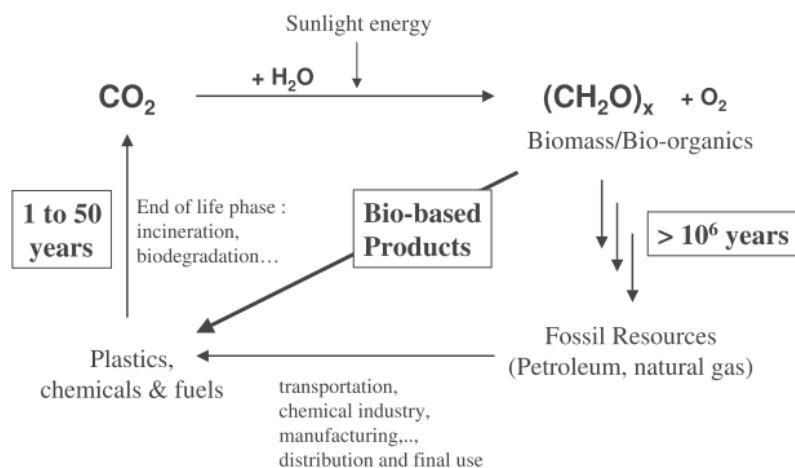


Fig. 1.3: Global carbon cycle during a product life.

When consuming fossil resources to produce polymers, chemicals and fuels, carbon back is released into the atmosphere as CO₂ in a short time frame of 1-50 years, unbalancing the carbon cycle. The rate at which biomass is converted to fossil resources is in imbalance with the rate at which they are consumed and liberated (>10⁶ years vs. 1-50 years). Thus, during petroleum-based plastics production more CO₂ is released than we sequester as fossil resources, resulting in a kinetic problem. However, using annually renewable crops or biomass as feedstocks for manufacturing carbon based polymers, chemicals and fuels, the rate at which CO₂ is fixed ideally can equal the rate at which it is consumed and liberated, since renewable crops or biomass production requires a big atmospheric CO₂ consumption.

1.1.4 Bioplastics: weaknesses and challenges

Several attributes make a switch to bioplastics attractive. Among others, there are the limited and therefore uncertain supply with fossil fuels (especially oil and gas), the related economic aspects, environmental considerations (especially savings of non-renewable energy and greenhouse abatement), innovation offering new opportunities (technical, employment etc.). All these traits would encourage the transition to bioplastics, but this is not the whole story. Bioplastics also have several serious shortfalls. They cost more than petroleum-based plastics, although the price difference between petroleum-based plastics and bioplastics can largely be attributed to the immaturity of the bioplastics industry. Lower prices for bioplastics are expected in the near future. One of the most serious problems of bioplastics production is the impact on the food supply. Since bioplastics are commonly derived from food crops, shortages and price increases could result from scaled up production. To sum it up, the disadvantages of bioplastics take away much of their appeal. Therefore, challenges that need

to be successfully addressed in the next years are their relatively high cost for production and processing and the need to minimize the agricultural land use and forests, thereby also avoiding competition with food production and adverse effects on biodiversity and other environmental aspects.

However, one thing above all others inhibits a switch to bioplastics. Despite all the advantages and disadvantages, the limiting factor that makes a major shift to bioplastics production impractical is the fact that bioplastics exhibit physical properties and mechanical performances typically lower than the competing conventional plastics. Most bio-polymers suffer from of brittleness, low softening point, poor heat resistance, limited gas barrier properties, moisture sensibility. All the benefits that we have illustrated above are irrelevant if the product cannot be used due to its low performances. This is the key point that most of the industrial and academic world underlines, and is facing and this has been the main challenge of the present work.

1.2. STATE OF THE ART AND AIM OF THE RESEARCH ACTIVITY

The overall aim of the present research activity has been identifying bio-based and eco-sustainable formulations potentially suitable for applications of technological interest. As previously discussed, along with their typically high costs, the major technical challenge to widespread acceptance of bio-polymers is the difficulty in achieving physical and mechanical properties comparable with those of conventional petroleum-based polymers. Many studies have been done to improve the properties of bio-polymers. Some interesting and noteworthy results have been summarized in recent reports [1, 8-10]. As in the case of petroleum-based polymers, also for bio-polymers the main strategies adopted to overcome some of their principal drawbacks are *(i)* blending with other polymers with complementary properties, either bio-based or not, and *(ii)* adding (nano)fillers.

Blending polymers has been widely used because of the possibility to combine in a unique material the properties of the blend components at a relatively low cost when compared to the development of a new polymer. Many binary and ternary biodegradable and/or biorenewable blends have been prepared and characterized. Some of them are also produced on industrial scale, such as starch-based blends with polyolefins, or bio-polyesters, PLA/Poly(butylene adipate-co-butylene terephthalate (PBAT), PLA/PHA, Poly(3-hydroxybutyrate-co-3-

hydroxyvalerate) PHBV/PBAT blends [3]. Unfortunately, most polymers are thermodynamically immiscible because of a negligible entropy gain as a result of blending. Therefore, the final properties of the material strictly depend on the nature of phase morphology and the interface adhesion. Various compatibilizers and additives like block or graft copolymers, premade or formed in situ, combined with particular processing techniques, have been developed to improve the phase morphology and the properties of the interface of fully or partially bio-based blends, leading to significant improvements in the overall mechanical properties [11-18].

It is well-known that small amounts of nanoparticles can enhance the properties and/or impart new functional features to hosting polymer matrices. Many examples exist of nanofilled homopolymers having excellent mechanical, optical, thermal and transport properties [19-21]. Although not as abundant as that concerning not bio-based polymers, recent literature indicates the possibility of noticeable property enhancements at very low filler content also for nanocomposites based on bio-polymers. Large improvements in the mechanical properties both in solid and melt state, thermal stability, gas barrier properties, flame resistance, and biodegradability have been observed and documented, especially for bio-nanocomposites with nanometre-size clays [9, 10]. During the last years, the dispersion of solid nanoparticles throughout a polymer blend with an existing phase-separated morphology, has provided a generally viable route towards the development of functional nanocomposites. When nanoparticles are combined with an immiscible polymer blend, they often distribute heterogeneously. The selective filling of specific regions of the blend may lead to novel opportunities, such as preferential reinforcement of one phase, targeted reinforcement of the interphase, filler induced changes in phase morphology, phase alignment, filler induced compatibilization of immiscible polymer phases, and changes of thermo-mechanical transitions [22]. The most recent trend is using nanoparticles as a mean to drive the space arrangements of polymer phases towards desired morphologies to impart new or improved performances to the material. In fact, the heterogeneous distribution of nanoparticles has been reported to minimize and stabilize the polymer domains and in some cases, it has been found effective in promoting phase co-continuity over a large composition range [23]. The co-continuous morphology consists of continuous and interconnected phases percolated throughout the blend volume, in which each phase contributes in parallel to the properties of the blend in all directions. Such morphology is of practical interest due to the synergistic combination of mechanical, electrical, optical, and transport properties of each phase [24].

The ability of nanoparticles to promote fine co-continuous microstructures in immiscible blends has attracted great interest as it allows for a fine tuning of the final performances of the blend.

In the light of the previous considerations, the first aim of the present research activity has been exploiting the great potential of adding nanoparticles to immiscible polymer blends to properly design bio-based and eco-sustainable materials suitable for a wider range of technological application. The goal has been pursued through a judicious selection of the bio-polymers and a clever manipulation of the microstructure using nanoparticles. In particular, efforts have been made to promote co-continuous morphologies.

Nanoparticle-induced co-continuity in immiscible polymer blends has been observed in many systems, the underlying mechanism being still unclear. Therefore, an additional goal of the present work has been to clarify the mechanisms behind the co-continuity development in our bio-based nanocomposites polymer blends. In particular, we focused on the roles played by (i) bulk rheology, (ii) interfacial rheology and (iii) interfacial tension, which are all affected by changing chemistry, shape and aspect ratio of nanoparticles. Among others, two issues have been examined more in depth: how effective is it to promote co-continuity by kinetically arresting the relaxation dynamics of the bulk polymer phases by means of nanoparticles? And, if so, is the self-networking ability of the particles the only relevant parameter? The achievement of such additional goal has important technological implications. In fact, it provides the possibility to govern the phenomena of nanoparticles-induced morphological changes in immiscible polymer blends, which represent a viable route to enlarge the fields of possible applications of bio-polymers.

1.2.1. *Materials selection: motivations*

To achieve our goals, the first step of the present research activity has been a proper selection of the bio-based blend constituents.

Among bio-polymers, poly lactic acid (PLA) is one of the most promising candidate for the substitution, totally or partially, of many petroleum-based polymers. In fact, PLA exhibits the best compromise among eco-sustainability, physical and mechanical features and industrial development prospect. Eco-profile assessments (see Graph 1.1 and 1.2, page 17) show that PLA requires 25-55% less energy to be produced than petroleum-based polymers. In addition, the PLA production has the lowest carbon dioxide footprint not only with respect to conventional polymers, but also in comparison to bio-based ones. As shown in Table 1.1,

PLA exhibits mechanical and thermal properties comparable with several petroleum-based commodity thermoplastic polymers [25].

Table 1.1: Comparison of Typical PLA Properties with Several Petroleum-Based Commodity Thermoplastic Resins.

	PLA	PET	PS	HIPS	PP
T_g (°C) ^a	55	75	105	–	–10
Tensile strength @ break (MPa) ^a	53	54	45	23	31
Tensile modulus (GPa) ^a	3.4	2.8	2.9	2.1	0.9
Elongation @ break (%) ^a	6	130	7	45	120
Notched Izod IS (J/m) ^a	13	59 ¹	27	123	27 ⁶ (i-PP)
Gardner impact (J) ^a	0.06	0.32	0.51	11.30	0.79
Cost (\$/lb) ^b	1–1.5	0.70–0.72	0.99–1.01	1.01–1.03	1.15–1.17

Furthermore, the recent breakthroughs in lactide and polymerization technology have significantly reduced the production cost, opening up possibility for PLA production in bulk volumes. However, the low mechanical resistance at high temperature (Heat Deflection Temperature HDT = 50–60°C) has prevented its complete access to relevant industrial sectors [26]. The slow crystallization rate of PLA, in fact, results in amorphous articles that lose their structural integrity soon as the glass transition is approached, that is around 60°C. During the last years three main strategies have been adopted to overcome such a drawback: (i) promoting PLA crystallization through annealing and/or adding nucleating agent [27-30]; (ii) adding reinforcing nanoparticles [31-33]; (iii) blending PLA with heat resistant polymers [34]. The latter approach is the one used in this work, but the PLA-based blends have been properly designed aiming at different targets. Among the possible heat resistant polymers to blend with PLA we have selected the bio-based Polyamide-11. PA11 is produced from renewable castor seeds and has a long hydrophobic C₁₀ aliphatic chain. It is a high performance, lightweight bioplastic (plastic produced with 100% of the carbons coming from plant based renewable resources) with a unique combination of various advantageous properties, such as high temperature and cold impact resistance, lower moisture pick-up and superior ageing resistance with respect to conventional high performance polyamides [35, 36]. In addition, among the heat resistant polymers, PA11 has a relatively low processing temperature, and this feature allows to minimize the thermo-mechanical degradation of PLA during melt blending [37]. Furthermore, eco-profile assessments (see Graph 1.1 and 1.2, page 17) show that, if compared to petroleum-based high performance plastics like PA6, PMMA and PC, PA11 is more energy saving and its production has lower carbon dioxide footprint, since it starts with a big atmospheric CO₂ consumption (castor seed cultivation). However, it

must be said that PA11 has the major environmental impact when compared to other bioplastics.

To sum it up, thanks to its physical, thermal and mechanical features, PA11 can be considered as a good candidate to correct the poor heat resistance of PLA. Nevertheless, in the light of the eco-profile assessments, aiming at obtaining a fully bio-based material with good performances and with low environmental impact, an additional target must be pursued, that is maximization of the content of the more eco-friendly PLA. However, to fully exploit the superior high temperature mechanical performances of PA11, it must represent a continuous phase in the blend. According to recent results obtained by Stoclet et al., such a condition is verified at 40% wt. of PA11 [38]. Therefore, nanoparticles have been added to PLA/PA11 blends in order to promote stable co-continuous morphologies at lower content of PA11, exploiting the ability of nanoparticles to guide the space arrangements of polymer phases.

Various research groups, and our group as well, have found that nanoparticles added to immiscible polymer blends are effective in inducing co-continuity when gathered inside the minor blend constituent and/or at the polymer/polymer interface [39-45]. In particular, it has been reported that nanoparticles localized inside the minor phase increase its bulk elasticity and viscosity, thus slowing down the droplet shape relaxation process. When localized at the interphase, the filler may also act as a compatibilizing agent, reducing the effective interfacial tension, and/or it may mechanically slow down the relaxation dynamics of the interface. As a consequence, coarse and elongated domains with irregular contours, unable to relax or break up, can interconnect during melt blending, eventually giving rise to a continuous structure. Despite the general agreement in recognising their importance, the roles of bulk rheology, interfacial rheology and interfacial tension are still not well established. The selection of different kinds of nanoparticles allowed to investigate these issues in detail. Specifically, we have chosen three fillers inclined to enrich PA11 phase: organo-modified montmorillonite (OMMT), organo-modified sepiolite (MS) and carbon nanotubes (CNTs). OMMT and MS share similar surface chemistry, but they differ in terms of shape. OMMT are flexible, plate-like nanoparticles, while MS are stiff, needle-like rods [46]. CNTs were deliberately selected because of their marked self-networking ability, which enables them to alter the rheological properties of the hosting polymer at very low particle loadings.

The selective positioning of the three different fillers inside the PA11 phase has effectively promoted its phase continuity. The comparative analysis of the effects of the selected fillers allowed to clarify the mechanisms involved in nanoparticles-induced co-continuity in

immiscible polymer blends. In particular, a cross checking of the experimental data obtained from morphological, dynamical mechanical and rheological analyses revealed that simply kinetically arresting the melt state relaxation dynamics of the filled polymer phase through the aggregation of nanoparticles into a space-spanning elastic network may be not sufficient to promote co-continuity and other mechanisms may take part, concurrently and/or alternatively. A critical role seems to be played by the ability of the selected fillers to differently affect the polymer-polymer interfacial features, and in particular the interfacial tension. The stronger reduction of the latter induced by OMMT or MS addition to the blend with respect to CNTs addition could be responsible of the major stability against break up and shape relaxation process of the elongated and irregularly-shaped domains of filled PA11, with a rheological gel-like behavior. The merging of these structures during melt mixing eventually results into co-continuity.

1.2.2. Structure of the thesis and main results

The present thesis is structured in two parts, each one with its own aim.

Part 1 :Heat-resistant fully bio-based nanocomposite blends based on Poly(lactic acid)

This section has been dedicated to designing a fully bio-based blend with PLA as the dominant component with improved high temperature creep resistance. The poor mechanical properties of the amorphous PLA above its glass transition have been corrected by blending it with the semicrystalline and bio-based PA11, and promoting the continuity of the latter phase through the addition of small amounts of OMMT. The selective positioning of the filler inside the PA11 and at the PLA/PA11 interface has been exploited to convert the drop-matrix morphology of a blend at 70 wt% of PLA into a stable co-continuous one. The OMMT-rich PA11 framework interpenetrates the major PLA phase, effectively contributing to bear stress. As a result, the nanocomposite blend keeps its structural integrity up to $\sim 160^{\circ}\text{C}$, i.e. about 100°C above the PLA glass transition. Additionally, on the basis of the analysis of the tensile properties at room temperature, optimized formulations with a better compromise between high- and low-temperatures mechanical properties have been sought.

Part 2 : Nanoparticle-induced co-continuity in immiscible polymer blends – A comparative study using Cloisite, Sepiolite, Carbon Nanotubes

The aim of this section was to investigate the underlying mechanisms of nanoparticles-induced co-continuity in immiscible polymer blends through a comparative study using three different fillers added to the PLA/PA11 blend (70/30 wt/wt). Specifically, we selected a modified cloisite, a modified sepiolite, and carbon nanotubes. Morphological and dynamic-mechanical analyses show that the three fillers selectively distribute inside the PA11 minor phase and are all able to convert the drop-matrix morphology of the blend into a stable and highly co-continuous one, provided that a critical nanoparticles loading is exceeded. Among the possible underlying mechanisms the roles played by (i) bulk rheology of the filled PA11 phase, (ii) self-networking propensity of nanoparticles, and (iii) interfacial properties of the blend, have been critically analyzed in relation to the specific chemistry and geometrical features of the nanoparticles.

1.3. REFERENCES

- [1] *Polymer blends and composites from renewable resources*; Yu L., Dean K., Li L.; Prog. Polym. Sci. 31 (2006) 576-602.
- [2] EN13432, ASTM 6400 or GreenPla in Japan-See ADEME website for more information about biodegradable plastics:
<http://www2.ademe.fr/servlet/getDoc?id=11433&m=3cid=96>
- [3] *Product overview and market projection of emerging bio-based plastics*; Shen L., Haufe J., Patel M.K.; PRO-BIP (2009).
- [4] Techno-economic feasibility of large-scale production of bio-based polymers in Europe. Report No. EUR No: 22103 EN, Catalogue (OPECE): LF-NA-22103-EN-C; Crank M., Patel M.K., Marsheider-Weidemann F., Schleich J., Husing B., Angerer G; (2005)
- [5] The future belongs to plastics and plastics belong to the future; Cadogan D., ECPI, Plasttekniske Dager, Oslo, 8-9 November (2006).
- [6] NatureWorks LLC, NatureWorks LLC Announces World's First Greenhouse-Gas-Neutral Polymer. (2005).
- [7] Metabolix, Metabolix Announces Results of Life Cycle Assessment for Mirel Bioplastics. (2007).
- [8] *Biodegradable Multiphase Systems Based on Plasticized Starch: A Review*; Avérous L.; Journal of Macromolecular Science, Part C: Polymer Reviews, 44 (3), (2004) 231-274
- [9] *Biodegradable polymer and their layered silicate nanocomposites: in greening the 21st century materials world*; Ray S.S., Bousmina M.; Progr. Mat. Sci. 50 (2005) 962-1079.
- [10] *Nano-biocomposites: biodegradable polyester/nanoclay systems*; Bordes P., Pollet E., Averous L.; Progr. Polym. Sci. 34 (2009) 125-155.
- [11] *Reactive Compatibilization of Biodegradable Poly(lactic acid)/Poly(ϵ -caprolactone) Blends with Reactive Processing Agents*; Harada M., Iida K., Okamoto K., Hayashi H., Hirano K.; Polym Eng. Sci. (2008) 1360-1368.
- [12] *The Effect of Crosslinking on the Mechanical Properties of Poly(lactic acid)/Polycaprolactone Blends*; Semba T., Kitagawa K., Ishiaku U. S., Hamada H.; J. Appl. Polym. Sci. 101, (2006) 1816-1825.

- [13] *Morphology and properties of compatibilized polylactide/thermoplastic starch blends*; Huneault M. A., Li H.; *Polymer* 48 (2007) 270-280.
- [14] *Thermal Properties and Morphology of Biodegradable PLA/Starch Compatibilized Blends*; Jang W. Y., Shin B. Y., Lee T. J., Narayan R.; *J. Ind. Eng. Chem.* 13 (3) (2007) 457-464.
- [15] *Reactive Blending of Biodegradable Polymers: PLA and Starch*; Jun C. L.; *J. Polym. Env.* 8 (1) (2000).
- [16] *Preparation of Modified Starch-Grafted Poly(lactic acid) and a Study on Compatibilizing Efficacy of the Copolymers in Poly(lactic acid)/Thermoplastic Starch Blends*; Wootthikanokkhan J., Kasemwananimit P., Sombatsompop N., Kositchaiyong A., Isarankura na Ayutthaya S., Kaabbuathong N.; *J. Appl. Polym. Sci* 126 (2012) E388-E395.
- [17] *Reactive compatibilization of PA12/plasticized starch blends: Towards improved mechanical properties*; Teyssandier F., Cassagnau P., Gérard J.F., Mignard N.; *European Polymer Journal* 47 (2011) 2361-2371.
- [18] *Morphologies and properties of plasticized starch/polyamide compatibilized blends*; Landreau E., Tighzert L., Bliard C., Berzin F., Lacoste C.; *European Polymer Journal* 45 (2009) 2609-2618.
- [19] *Polymer nanotechnology: Nanocomposites*; Paul D.R., Robeson L.M.; *Polymer* 49 (2008) 3187-3204.
- [20] *Nanoscale particles for polymer degradation and stabilization – Trends and future perspectives*. Kumar A.P., Depan D., Tomer N.S., Singh R. P.; *Progr Polym Sci* 34 (2009) 479-515.
- [21] *A review on polymer-layered silicate nanocomposites*; Pavlidou S., Papaspirides C.D.; *Progr Polym Sci* 33 (2008) 1119-1198.
- [22] *Nanocomposites: Stiffer by design*; Manias E., *Nat. Mater.* 6 (9) (2007)
- [23] *Uneven distribution of nanoparticles in immiscible fluids: Morphology development in polymer blends*; Fenouillot F., Cassagnau P., Majeste J.-C.; *Polymer* 50 (2009) 1333-1350.
- [24] *Formation of Co-continuous structures in melt-mixed immiscible polymer blends*; Potschke P. and Paul D.R.; *Journal of Macromolecular Science-Polymer Reviews* C43 (1) (2003) 87-141.

- [25] *Research Progress in Toughening Modification of Poly(lactic acid)*; Liu H., Zhang J.; J Polym. Sci. Part b: Polym. Physics 49 (2011) 1051-1083.
- [26] *Poly(lactic acid) modifications*; Rasal R.M., Janorkar A.M., Hirt D.E. Prog. Polym. Sci. 35 (2010) 338-356.
- [27] *Effect of molecular weight and crystallinity on poly(lactic acid) mechanical properties*; Perego G, Cella G. D., Bastioli C.; Polymer 59 (1996) 37-43.
- [28] *Improving mechanical performance of injection molded PLA by controlling crystallinity*; Harris A. M., Lee E. C.; J. Appl. Polym. Sci. 107 (2008) 2246-2255.
- [29] *Physical and mechanical properties of poly(L-lactic acid) nucleated by dibenzoylhydrazide compound*; Kawamoto N., Sakai A., Horikoshi T., Urushihara T., Tobita E.; J. Appl. Polym. Sci. 103 (2007) 244-250.
- [30] *Effect of nucleation and plasticization on the crystallization of poly(lactic acid)*; Li H., Huneault M. A.; Polymer 48 (2007) 6855-6866.
- [31] *New Polylactide/Layered Silicate Nanocomposites. 1. Preparation, Characterization, and Properties*; Ray S. S., Maiti P., Okamoto M., Yamada, Ueda K.; Macromolecules 35 (2002) 3104-3110.
- [32] *New Polylactide/Layered Silicate Nanocomposites. 3. High-Performance Biodegradable Materials*. Ray S. S., Yamada K., Okamoto M., Ogami A., Ueda K.; Chem. Mater. 15 (2003), 1456-1465.
- [33] *Biodegradable polylactide and its nanocomposites: opening a new dimension for plastics and composites*; Ray S. S., Okamoto M.; Macromol Rapid Commun 24 (2003) 815-40.
- [34] *Structure-properties of super-tough PLA alloy with excellent heat resistance*; Hashima K., Nishitsuji S., Inoue T.; Polymer 51 (2010) 3934-3939.
- [35] *Application of Eco-profile methodology to Polyamide 11*; Devaux J.-F., Pees B.
- [36] *Morphologies and properties of plasticized starch/polyamide compatibilized blends*; Landreau E., Tighzert L., Bliard C., Berzin F., Lacoste C.; European Polymer Journal 45 (2009) 2609-2618.
- [37] *Processing technologies for poly(lactic acid)*; Lim L.T., Auras R., Rubino M.; Progr. Polym. Sci. 33 (2008) 820-852.
- [38] *Morphology, thermal behavior and mechanical properties of binary blends of compatible biosourced polymers: Polylactide/Polyamide 11*; Stoclet G., Seguela R., Lefebvre J.-M.; Polymer 52 (2011) 1417-1425.

- [39] *Co-continuous Polyamide 6 (PA6)/Acrylonitrile-Butadiene-Styrene (ABS) Nanocomposites*; Li Y., Shimizu H.; *Macromol. Rapid Commun.* 26 (2005) 710-715.
- [40] *The role of organoclay in promoting co-continuous morphology in high-density poly(ethylene)/poly(amide) 6 blends*; Filippone G., Dintcheva N.Tz., Acierno D., La Mantia F.P.; *Polymer* 49 (2008) 1312-1322.
- [41] *Using organoclay to promote morphology refinement and co-continuity in high-density polyethylene/polyamide 6 blends-Effect of filler content and polymer matrix composition*; Filippone G., Dintcheva N.Tz., Acierno D., La Mantia F.P.; *Polymer* 51 (2010) 3956-3965.
- [42] *Kinetically Trapped Co-continuous Polymer Morphologies through Intraphase Gelation of Nanoparticles*; Li L., Miesch C., Sudeep P. K., Balazs A. C., Emrick T., Russell T. P., and Hayward R. C.; *Nano Lett.* 11 (2011) 1997-2003.
- [43] *Compatibilizing Bulk Polymer Blends by Using Organoclays*; Si M., Araki T., Ade H., Kilcoyne A. L. D., Fisher R., Sokolov J. C., and Rafailovich M. H.; *Macromolecules* 39 (2006) 4793-4801.
- [44] *Role of Interface Rheology in Altering the Onset of Co-Continuity in Nanoparticle-Filled Polymer Blends*; Filippone G., Romeo G., Acierno D.; *Macromol. Mater. Eng.* 296 (2011) 658-665.
- [45] *Clustering of Coated Droplets in Clay-Filled Polymer Blends*; Filippone G., Acierno D.; *Macromol. Mater. Eng.* 297 (2012) 923-928.
- [46] *Sepiolite needle-like clay for PA6 nanocomposites: An alternative to layered silicates?*; Bilotti E., Zhang R., Deng H., Quero F., Fischer H.R., Peijs T.; *Composites Science and Technology* 69 (2009) 2587-2595.

PART 1

Heat Resistant Fully Bio-based Nanocomposite Blends based on Poly(lactic acid)

2.1. INTRODUCTION

Poly(lactic acid) (PLA) is a biodegradable thermoplastic polymer, entirely derived from renewable plant sources, such as starch and sugar. It is a linear aliphatic polyester that can exist in optically active D- or L-enantiomers. High molecular weight PLA is generally synthesized through ring-opening polymerization of lactide (the dimer of lactic acids) (Figure 2.1) [1, 2].

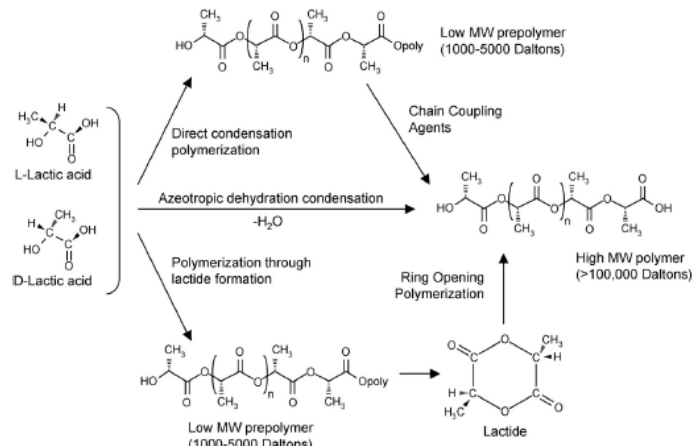


Fig. 2.1: Synthesis of PLA from L- and D-lactic acid [1, 2].

Due to the optical activity of lactic acid, lactide can be found in three different versions, i.e., D, D-lactide, L, L-lactide, and D, L-lactide (meso-lactide) (Figure 2.2) [2].

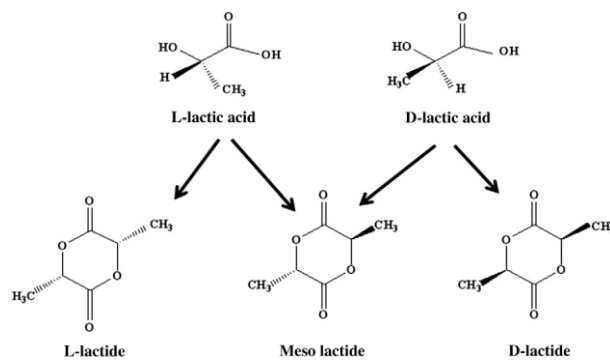


Fig. 2.2: Stereoforms of lactides [2].

Commercial grades PLA are copolymers of Poly(L-lactic acid) (PLLA) and Poly(D, L-lactic acid) (PDLLA), which are produced from L-lactides and D, L-lactides, respectively. The optical purity of PLA has many profound effects on the structural, thermal, barrier and mechanical properties of the polymer. PLA polymers with L-content greater than ~90% tend

to be semicrystalline, whereas those with lower optical purity are amorphous. Moreover, the melting temperature, T_m , glass transition temperature, T_g , and crystallinity degree, χ , all decrease with decreasing L-isomer content. Table 2.1 shows the T_g and T_m of different PLA polymers produced with different ratios of copolymers [1].

Table 2.1: Primary transition temperatures of selected PLA copolymers [1].

Copolymer ratio	Glass transition temperature (°C)	Melting temperature (°C)
100/0 (L/D,L)-PLA	63	178
95/5 (L/D,L)-PLA	59	164
90/10 (L/D,L)-PLA	56	150
85/15 (L/D,L)-PLA	56	140
80/20 (L/D,L)-PLA	56	125

Advances in the polymerization technology have significantly reduced the production cost and have contributed to make PLA economically competitive with petroleum-based polymers. PLA has attracted increasing interest in various markets, such as packaging, textile, and automotive industries, as very promising eco-friendly alternative to traditional petroleum-based commodity polymers. Despite its numerous advantages such as high strength and high modulus (comparable with PET mechanical properties), the low mechanical resistance at high temperature is limiting the expansion and diversification of its possible applications.

In particular, the slow crystallization rate of PLA generally results in amorphous articles, which lose their mechanical properties soon as the glass transition temperature, $T_g=55\div 60^\circ\text{C}$, is approached.

In fact, at temperature higher than T_g only the PLA crystalline phase can confer useful mechanical properties. Various strategies have been proposed to improve the typical low crystallization rates and the final crystallinity degree of PLA.

Crystallization of PLA articles can be induced by annealing at temperatures higher than T_g and below the melting point [3]. However, a post-processing step to increase PLA crystallinity, like annealing, may not be economically and/or technically affordable.

Another strategy to increase the crystallinity of PLA is by incorporating nucleating agent in the polymer during extrusion. In this contest, talc and ethylene bis-stearamide (EBS) were found to be effective nucleating agents. However, post-annealing processing step of both nucleated and neat PLA materials was necessary to increase the crystallinity of PLA to its maximum level of 42% and the addition of nucleating agents was useful only in accelerating the annealing process [4].

In another study, a series of organic compounds having hydrazide end-groups were evaluated in terms of their nucleating abilities. Best results, obtained with benzoylhydrazide compounds, showed increased crystallization temperature upon cooling and led to fully crystallized samples at moderate cooling rates (-20°C/min) [5]. Unfortunately, these compounds are not readily available as they have only been synthesized at the laboratory scale.

Li and Huneault found that adding nucleating agents, such as talc, together with plasticizers, such as Poly(ethylene glycol) (PEG), has a synergistic effect on PLA crystallization kinetics, due to improved chain mobility and the enhanced nucleating ability. In particular, the crystallization rate of the developed formulations was sufficient to obtain fully crystallized parts in an injection molding cycle and, in all cases, the crystallized PLA formulations showed higher temperature resistance than the unmodified ones. This required, however, the use of hot molds in the 70-100°C range [6].

Another well-established method for the improvement of the PLA thermal and mechanical properties is the addition of nanoparticles. In this context, Shina Ray and Okamoto prepared a series of PLA/organically modified layered silicates (OMLS) nanocomposites by melt extrusion, wherein silicate layers of OMLS was either intercalated, intercalated-and-flocculated, partly exfoliated, or a mixture of the three previous forms. Despite the low amounts of filler, all the PLA nanocomposites exhibited enhanced properties. These improvements include rate of crystallization and, consequently, mechanical properties both at low and high temperature. However, also in this case high-temperature resistant PLA formulations are obtained only after a post-annealing processing step, made faster by the nucleating ability of the nanoparticles [7].

Blending with high temperature resistant polymers is another possible strategy to develop PLA-based formulations with improved heat resistance.

Hashima et al. developed a super-tough PLA alloy with good heat resistance by blending with (i) the tough hydrogenated styrene-butadiene-styrene block copolymer (SEBS), (ii) a small amount of the reactive compatibilizer poly(ethylene-co-glycidyl methacrylate) (EGMA) and (iii) the ductile and heat-resistant polycarbonate (PC). An effective improvement of the material heat resistance is obtained when the PC content is raised up to 40 wt.%, *i.e.* when the elongated PC domains become a somewhat continuous inside the blend [8].

Zhang et al. designed fully biodegradable and bio-renewable ternary blends from PLA, poly(3-hydroxybutyrate-co-hydroxyvalerate) (PHBV), and poly(butylene succinate) (PBS)

with a good balance of properties. The judicious choice of the blend compositions, in fact, resulted in specific morphologies, that in turn provided a wide variety of mechanical and thermal performances. In particular, the thermal resistance of PLA was effectively improved in the blends at 60 %wt. of PHBV, *i.e.* the blends where the semi-crystalline PHBV phase is the matrix [9].

Aiming at improving PLA thermo-mechanical properties, Stoclet et al. have recently blended it with polyamide 11 (PA11), a bio-based yet not biodegradable polymer [10]. Due to its semi-crystalline feature, PA11 exhibits high temperature resistance, which suggests its use to correct the PLA softness above its T_g . In addition, the relatively low processing temperature of PA11 allows to minimize the thermo-mechanical degradation of PLA which usually occurs during melt blending [1]. To fully exploit the superior high temperature mechanical performances of PA11, it must represent a continuous phase in the blend. Stoclet and co-workers reached such a condition at 40 wt.% of that component. Our research activity has been aimed at designing a blend with high content of the more eco-sustainable PLA, yet preserving the continuity of PA11, to obtain a heat resistant fully bio-based and eco-friendly formulation suitable for a wider variety of technological applications. This goal has been pursued through the addition of nanoparticles. In fact, during the last years it has been reported that anisotropic nanofillers can be used not only as a mere reinforcement but also as a medium to guide the nano- and microstructure of multiphase polymeric systems. When nanoparticles are combined with an immiscible polymer blend, they are inclined to enrich specific regions of the blend, e.g. one of the phases or the interface, depending on (i) their affinity with each polymeric component, (ii) the processing conditions and (iii) the chemical/physical material properties [11]. Controlling the preferential localization of the nanoparticles into specific regions of the material may be crucial to design the blend morphology and, consequently, to optimize the final performances. In particular, the uneven distribution of nanofillers inside specific regions of the blends can either produce a drastic reduction on the dimensions of the minor phase [12-18] or can assist the unexpected formation of co-continuous morphologies [19-21]. Co-continuity exists within a narrow range of compositions or, outside this range, it can be promoted by using targeted expedients during the mixing process. Adding nanoparticles to polymer blends often shifts the onset of continuity to lower content of the minor phase and/or enlarges the co-continuous region, stabilizing the resultant interpenetrated morphology. According to more recent results, co-continuity at low contents of either phase can be promoted if platelet-like nanoparticles

(organoclay) gather inside the minor blend constituent [19-21] and at the polymer-polymer interface [22, 23]. As a matter of fact, the increasing elasticity of the clay-rich minor phase slows down the shape relaxation process and coarse and elongated domains can interconnect giving rise to a continuous structure. Additionally, the clay localized at interphase on one hand promotes the clustering of coated droplets and on the other hand slows down the melt state relaxation dynamics of the interface.

For these reasons, we have selected as filler for our PLA/PA11 blends a commercially available organomodified montmorillonite (OMMT), which is inclined to enrich the heat resistant PA11 phase and the interfacial region. In such a way the drop-matrix morphology of a sample at 70 wt.% of PLA was converted into a stable co-continuous one, in which the OMMT-rich PA11 forms a continuous framework that interpenetrates the PLA. The macroscopic thermo-mechanical behavior clearly benefits from such a microstructure, and a remarkable increase of both the rubbery modulus and creep resistance has been achieved. Specifically, the material resists up to $\sim 160^{\circ}\text{C}$, i.e. more than 100°C above the temperature at which PLA loses its structural integrity. Thermal analyses show that neither blending with PA11 nor adding of filler is able to promote crystallization of PLA phase, confirming that the enhancement of high temperature mechanical properties is exclusively due to the morphology changes induced by the OMMT.

Looking for optimized formulations, the room temperature tensile properties have been investigated to critically test the degree of embrittlement of the material upon addition of nanoparticles. We show that an increase of toughness can be achieved by reducing the OMMT amount at the expense of the high temperature creep resistance, which, in any case, remains much higher than that of pure PLA.

2.2. MATERIALS AND METHOD

2.2.1. Materials and blends preparation.

The PLA (2002D by NatureWorks) has density $\rho=1.24$ g/cm³ at 25°C and melt flow index MFI=6 g/10' (210°C/2.16 kg). The PA11 (Nylon 11 by Sigma Aldrich) has $\rho=1.026$ g/cm³ at 25°C, T_g=46°C and T_m=198°C. The filler is an organomodified montmorillonite (OMMT, Cloisite 30B from Southern Clay Products) modified by 90 meq/100g of bis(2-hydroxyethyl) methyl tallow alkyl ammonium cations. The onset of thermal decomposition of the organic modifier in Cloisite 30B is higher than the temperature set for the melt compounding, and this should result in a more uniform dispersion of filler inside the polymer matrix [24].

Before melt processing, the polymers and the filler were dried at 80°C for 12 h in a vacuum oven. A DSM Xplore micro co-rotating twin-screw extruder was used to compound the materials, which were extruded in a single step extrusion under nitrogen atmosphere at $T=215^\circ\text{C}$ and screw speed 80 rpm, corresponding to average shear rates of order of ~ 50 s⁻¹. The residence times, carefully controlled owing to an integrated back-flow channel, were set to ~ 1 min for each blend. The neat polymers used as reference materials were processed using the same conditions. Preliminary investigations indicate that the previous conditions represent a good compromise between filler dispersion and thermo-mechanical stability of the polymer matrices. The blend compositions are summarized in Table 2.2.

Table 2.2. Compositions of samples.

Sample	PLA/PA11 [wt/wt]	OMMT [phr]
PLA	100/0	-
PLA-C3	100/0	3
PLA90	90/10	-
PLA90-C3	90/10	3
PLA80-C3	80/20	3
PLA70	70/30	-
PLA70-C3	70/30	3
PLA70-C6	70/30	6
PLA50	50/50	-
PLA50-C6	50/50	6
PA11	0/100	-
PA11-C3	0/100	3
PA11-C6	0/100	6
PA11-C9	0/100	9

The extruded materials were granulated, dried again and compression-molded into rectangular bars, disks and thin sheets for the subsequent analyses by using a laboratory press (LP-20B by Lab. Tech. Eng. Company Ltd.). The materials were compressed at $T=215^{\circ}\text{C}$ under a pressure $P=40$ MPa for 5 min, then cooled down to room temperature at about $30^{\circ}\text{C}/\text{min}$. The neat polymers used as reference materials were processed using the same conditions.

2.2.2 Characterization methods

Contact angle measurements were taken at room temperature using a digital camera (Best Scientific, U.K.) with microvideo zoom lens. Static contact angles of two test liquids (distilled water and glycerol) were measured by depositing a drop of 3-5 mL on the sample surface and the values were estimated as the tangent to the drop at the intersection between the sessile drop and the surface, using MB ruler software. To avoid solvent evaporation, images were taken within 30 s of drop deposition. The reported contact angle values are the average of at least five measurements at different spots of the surface.

Wide-angle X-ray diffractometry (WAXD) was performed at room temperature on the compression-molded samples using a Siemens D-500 X-ray diffractometer, with $\text{CuK}\alpha$ radiation of wavelength of 1.54 \AA . The scanning rate was $10^{\circ} \text{ min}^{-1}$. The interlayer spacing between the silicate layers of the OMMT, d_{001} , was computed by applying the Bragg's condition to the low angle peak ($2^{\circ} < 2\theta < 4^{\circ}$) of the scattering intensities.

The morphology of the filled blends on nano-scale was observed through transmission electron microscopy (TEM) using a Philips EM 208 TEM with 100 keV accelerating voltage. The specimens were in the form of thin slices (thickness ~ 150 nm) microtomed with diamond knife at room temperature from the compression-molded samples. The space arrangement of the polymer phases on micro-scale was investigated through scanning electron microscopy (SEM) using a SEM Leica Stereoscan 420. The inspected surfaces, sputtered with gold, were obtained through brittle fracture in liquid nitrogen of compression-molded samples.

Differential scanning calorimetry (DSC) was performed using a TA Instruments Q20 DSC. The samples were heated from 20°C to 210°C , kept for 5 min at 210°C , cooled down to 20°C , and then heated again up to 210°C . The heating and cooling cycles were all carried out at $10^{\circ}\text{C} \text{ min}^{-1}$ under nitrogen atmosphere. The degree of crystallinity was computed as $\chi = \Delta H_m / \Delta H_{m0}$, where ΔH_m is the melting enthalpy of the second heating scan (in case normalized to the content of the considered phase in the blend) and ΔH_{m0} is the melting enthalpy of a perfect crystal of m .

Dynamic-mechanical analyses (DMA) were carried out using a Triton 2000 DMA (Triton technology, UK). Specimens in the form of rectangular bars ($1.2 \times 12 \times 15 \text{ mm}^3$) were heated at 2°C min^{-1} from $\sim 10^\circ\text{C}$ to 140°C , and the elastic (E') and viscous (E'') flexural moduli were recorded as a function of temperature. The tests were performed in single cantilever bending mode at a frequency $\omega=1 \text{ Hz}$ and total displacement of 0.02 mm , which is small enough to be in the linear regime. Creep analyses were carried out on rectangular bars ($3 \times 10 \times 50 \text{ mm}^3$) in three point bending mode using the same DMA apparatus. A load of 0.455 MPa was applied at the center of the specimen supported near its ends while heating at 2°C min^{-1} from room temperature up to 160°C . The sample deflection was recorded as a function of the temperature.

The room temperature tensile mechanical properties were measured using an Instron Machine Model 3360 with a load cell of 5 kN according to ASTM test method D882. Samples in the form of thin strips with uniform width of 10 mm and total length of 150 mm (10 mm of effective length) were cut out from $\sim 0.2 \text{ mm}$ thick compression-molded samples. The specimens were strained at a constant crosshead speed of 50 mm min^{-1} , and the Young's modulus and properties at break were recorded. The reported data represent average values computed from a minimum of five independent measurements.

2.3. RESULTS AND DISCUSSION

2.3.1. Morphological Analysis

The localization of nanoparticles in polymer blends should be linked to the balance of interactions between the surface of the particles and the polymer components. As for low viscosity fluid emulsions, the knowledge of the polymer/polymer and polymer/filler interfacial tensions is in principle sufficient to predict the preferential location of the filler in a polymer blend. This may suggest that the final localization of filler in an immiscible blend system could be designed through thermodynamic approaches.

According to the Young's equation the location of a filler at equilibrium state can be estimated through the wetting coefficient ω_a [25]:

$$\omega_a = \frac{\sigma_{\text{clay-B}} - \sigma_{\text{clay-A}}}{\sigma_{A-B}} \quad (1)$$

where $\sigma_{i,j}$ is the interfacial energy between i and j .

If $\omega_a > 1$ (resp. $\omega_a < -1$), the filler locates in polymer A (resp. B); if instead $-1 < \omega_a < 1$, then the filler preferentially locates at the interface between both polymers.

The interfacial energies can be calculated starting from the surface energies σ_i and their dispersive, σ_i^d , and polar, σ_i^p , components using the harmonic-mean equation (2) [26]:

$$\sigma_{12} = \sigma_1 + \sigma_2 - 4 \left(\frac{\sigma_1^d \sigma_2^d}{\sigma_1^d + \sigma_2^d} + \frac{\sigma_1^p \sigma_2^p}{\sigma_1^p + \sigma_2^p} \right) \quad (2)$$

Contact angle measurement is a traditional procedure used for the assessment of the surface energy of solids [26]. The relation between the contact angle and surface energy is described by the Owens-Wendt method [27]:

$$\sigma_l(1 + \cos \theta) = 2(\sigma_s^d \sigma_l^d)^{\frac{1}{2}} + 2(\sigma_s^p \sigma_l^p)^{\frac{1}{2}} \quad (3)$$

where σ_l and σ_s are the surface energy of the probe liquid and the solid, σ_l^d , σ_s^d , σ_l^p and σ_s^p are the dispersive and polar components of the liquid and the solid, respectively, and θ is the contact angle. If the contact angles of at least two liquids with known σ_l^d and σ_l^p parameters are measured on a solid surface, the σ_s^d and σ_s^p parameters as well as the surface energy of that solid σ_s can be calculated using equation (3) and knowing that $\sigma_i = \sigma_i^d + \sigma_i^p$.

The measured contact angles, the computed surface parameters for PLA and PA11 and the surface parameters of OMMT are reported in Table 2.3. The literature values of the two test liquids are: $\sigma^d=21.8 \text{ mJ/m}^2$ and $\sigma^p=51 \text{ mJ/m}^2$ for water; $\sigma^d=37 \text{ mJ/m}^2$ and $\sigma^p=26.4 \text{ mJ/m}^2$ for glycerol [28]. The surface tension of PLA and PA11 were extrapolated at $T=215^\circ\text{C}$, i.e. at the temperature of melt blending, starting from the computed values of σ_i at 25°C and assuming linear dependence of the surface tension with temperature using a temperature coefficient of -0.06; the polar component, estimated supposing temperature independence, is shown as well. The data for Cloisite 30B are experimental values reported in literature [24].

Table 2.3: Measured contact angles and computed surface energies for PLA and PA11 at 25°C ^(a) and 215°C ^(b). The data for Cloisite 30B are experimental values from [24].

Material	Contact Angle °		Surface Energy mJ/m ²		
	Water	Glycerol	σ	σ^d	σ^p
PLA	63.5	64.1	38.5 ^{a)}	7.9 ^{a)}	30.5 ^{a)}
			27.1 ^{b)}	5.6 ^{b)}	21.5 ^{b)}
PA11	69.5	53.5	41.8 ^{a)}	31.4 ^{a)}	10.4 ^{a)}
			30.4 ^{b)}	22.8 ^{b)}	7.5 ^{b)}
Cloisite 30B			34	22.5	11.5

Although the assumptions made to compute the data of Table 2.3 may bring about non-negligible errors, the values of σ_i at high temperature can be used for an approximate estimation of the wetting coefficients of the studied systems during melt compounding.

Table 2.4 shows the interfacial tensions between the constituents, computed using the harmonic mean equation (2), and the resultant wetting coefficient, calculated with Young's equation (1).

Table 2.4. The calculated values of interfacial energies and wetting coefficient.

Sample	σ_{i-j} [mJ m ⁻²]	ω_a
PLA-Clay	13.22	
PA11-Clay	0.83	
PLA-PA11	17.17	
PLA-PA11-Clay		-0.72

Wettability considerations indicate that, at thermodynamic equilibrium, the filler preferentially enriches the interfacial region. Additionally, the proximity of the ω_a value to -1 suggests that, when the interface is saturated, a portion of the organoclay preferentially locates inside the PA11 phase. However, the equilibrium state of phase morphology may not be reached during mixing of polymer melt because of their very high viscosity. Furthermore, the filler distribution also depends on the sequence of addition of the components [11]. Consequently, a careful ex-post morphological study is necessary to assess the actual spatial distribution of the organoclay inside the blend. TEM investigations were performed for this purpose, and two micrographs at different magnification are shown in Figure 2.3 for the sample PLA90-C3, which is diluted enough to exhibit drop-matrix morphology.

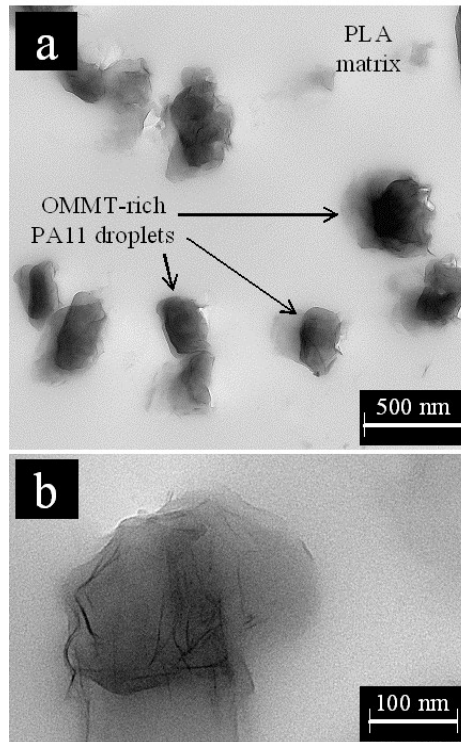


Fig. 2.3: (a) TEM micrograph of the sample PLA90-C3. A magnification of a OMMT-rich PA11 droplet is shown in (b)TEM micrographs of the sample PLA90-C3.

Organoclays in a polymer matrix appear as dark features because of their high electronic density. On the contrary, unless using specific staining agents, polymer phases are usually difficult to be distinguished in TEM micrographs. The filler appears unevenly distributed on microscale, being predominantly confined inside micron-sized domains representing the PA11 droplets. The magnification of one of such OMMT-rich domains reveals that the silicate layers are in the form of randomly oriented, crumpled tactoids (Figure 2.3.b). Noteworthy, thin platelet stacks seem to locate at the drop-matrix interface, supporting the predictions of wettability calculations.

Additionally, WAXD analyses (Figure 2.4) indicates the loss of the ordered lamellar structures of the pristine filler during melt blending.

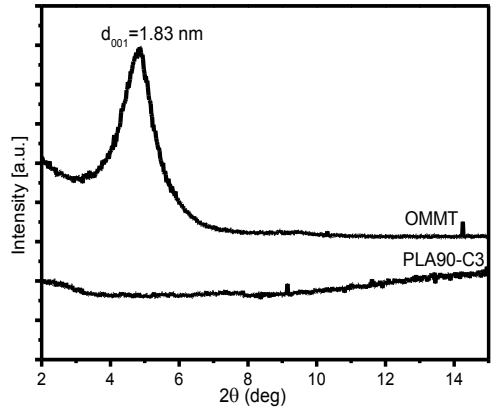


Fig. 2.4. WAXD patterns of the pristine OMMT and the sample PLA90-C3.

The selective positioning of the OMMT inside the PA11 and at the interface is relevant to our purpose, that is to promote the continuity of that heat resistant constituent in the blends. The impact of the uneven distribution of the filler on the space arrangement of the polymer phases on micro-scale is shown in Figure 2.5, where representative SEM micrographs are reported.

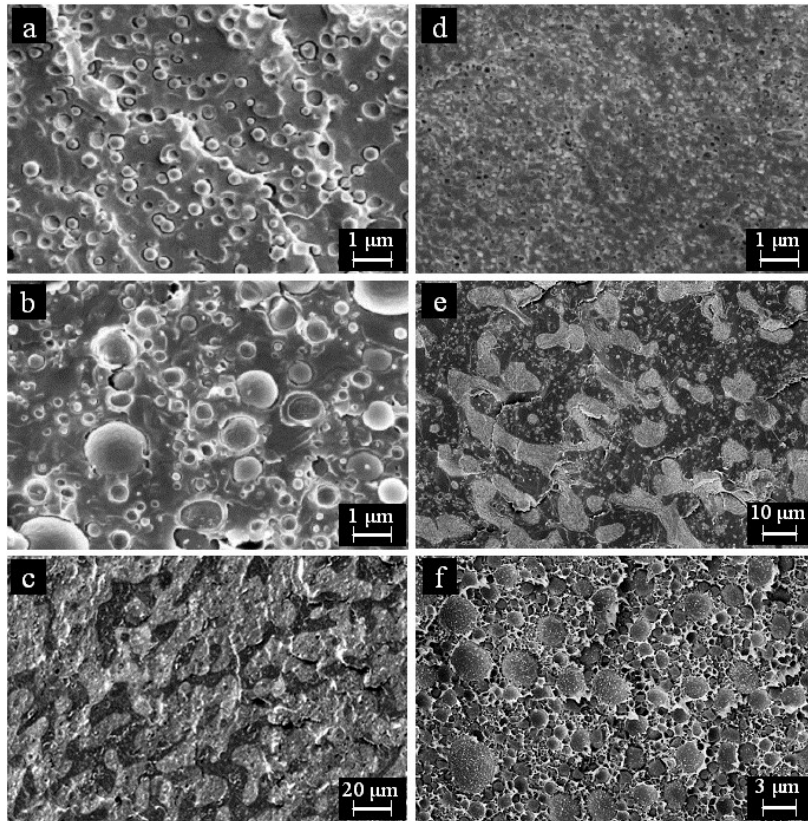


Fig. 2.5. SEM micrographs of the samples PLA90 (a), PLA70 (b), PLA50 (c), PLA90-C3 (d), PLA70-C3 (e), and PLA50-C6 (f).

The unfilled samples PLA90 and PLA70 exhibit drop-matrix morphology, with roughly spherical PA11 droplets suspended in the PLA matrix. Increasing the PA11 content from 10 to 30 wt.% results in a growth of the average drop size. The microvoids surrounding the minor phase inclusions and the holes due to the removal of the droplets during the fracture suggest a scarce interfacial adhesion. When the PA11 content is raised up to 50 wt.% a co-continuous morphology forms: bright and dark domains of several tens of microns in size are clearly interpenetrated; the former are constituted by the PA11 phase, which higher ductility results in the formation of lighter nanofibrils during the sample fracture.

The impact of the filler depends on the amount of the host PA11 phase. The diluted sample PLA90-C3 keeps a drop-matrix morphology as its unfilled counterpart, but the average droplet size significantly decreases. Such a result is not unprecedented. Coalescence suppression is often proposed as the dominant mechanism on the basis of the morphology refinement in organoclay-filled polymer blends [18, 29]. Coarsening is hindered because of the platelet-like structure of the filler, which acts as physical barriers preventing the coalescence of colliding droplets during melt mixing. Changes in the viscoelastic properties of the polymer phases related to the uneven filler distribution may also contribute in reducing the critical conditions for droplets break up [30].

Moreover, interface-located platelets may enhance the interfacial adhesion, thus stabilizing fine morphologies [31]. In our case, however, the scarce interfacial adhesion emerged from the visual inspection of the SEM micrographs suggests that the latter effect may play a minor role.

Most relevant morphological changes occur for the sample PLA70-C3. The brighter PA11 phase appears in the form of coarse domains with elongated and irregular shape. Such structures, which coexist with a multitude of tiny spherical PA11 droplets, interpenetrate the PLA major phase. This finding is in line with our purpose: the selective localization of the OMMT promotes the continuity of the PA11 phase in spite of its low content. Actually, similar nanoparticles induced co-continuity in immiscible polymer blends has been observed on many other ternary systems [32-34]. Much has been reported regarding the mechanisms involved, such as the viscoelastic effect [35], the nanoparticles-induced compatibilizing effect when the fillers accumulate at the blend interface [15, 36, 37], the self-networking capability of nanoparticles [38-40], as well as the equilibrium of the fibril break-up and the droplet coalescence based on the viewpoint of microrheology [41]. Although system-specific, most of the previous mechanisms are ultimately ascribable to changes of the rheology of the systems

and/or to alterations of the properties of the blend interface. However, there is a lack of systematic studies aimed at critically analysing the role of the various phenomena possibly involved. Many relevant issues remain still open and we address at the next section of the present work for a detailed interpretation about the co-continuity development observed in our system upon the addition of nanoparticles. Specifically, we will discuss about the role played by the alterations of PA11 rheological properties caused by the selective distribution of nanoparticles in promoting co-continuity.

Besides promoting co-continuity, the filler also brings the phase inversion composition forward: the sample PLA50-C6 exhibits drop-matrix morphology, but this time PLA drops are suspended in the OMMT-rich PA11 matrix. A possible explanation is that the nanoparticles screen the PLA domains during melt mixing, preventing the merging step required to turn them into a continuous phase. The occurrence of other mechanisms cannot be excluded.

In the light of TEM and SEM investigations, a schematic picture of the morphology evolution of the virgin and filled blends is shown in Figure 2.6. Adding OMMT to the blends has a double effect: (i) it promotes a refinement of the drop-matrix morphology at low content of PA11, and (ii) it shifts the phase inversion composition towards lower amounts of PA11, making this phase already continuous at 30 wt.%.

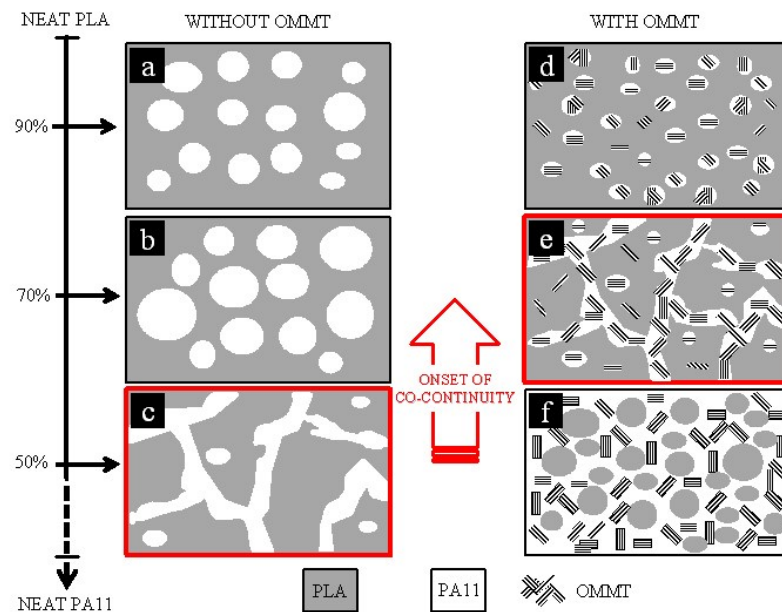


Fig. 2.6. Schematic illustration of the morphology evolution of the unfilled and filled blends as a function of composition as emerged from SEM and TEM analyses.

2.3.2. Crystallization behaviour.

Besides altering the blend microstructure, the filler may also affect the crystallization ability of the polymer phases. This is a critical issue, as crystallinity is a key parameter governing the mechanical performances of polymer systems. Figure 2.7 shows the DSC traces obtained during cooling and second heating scans for the neat and filled polymers and the virgin and filled blends. The corresponding calorimetric parameters are listed in Table 2.5.

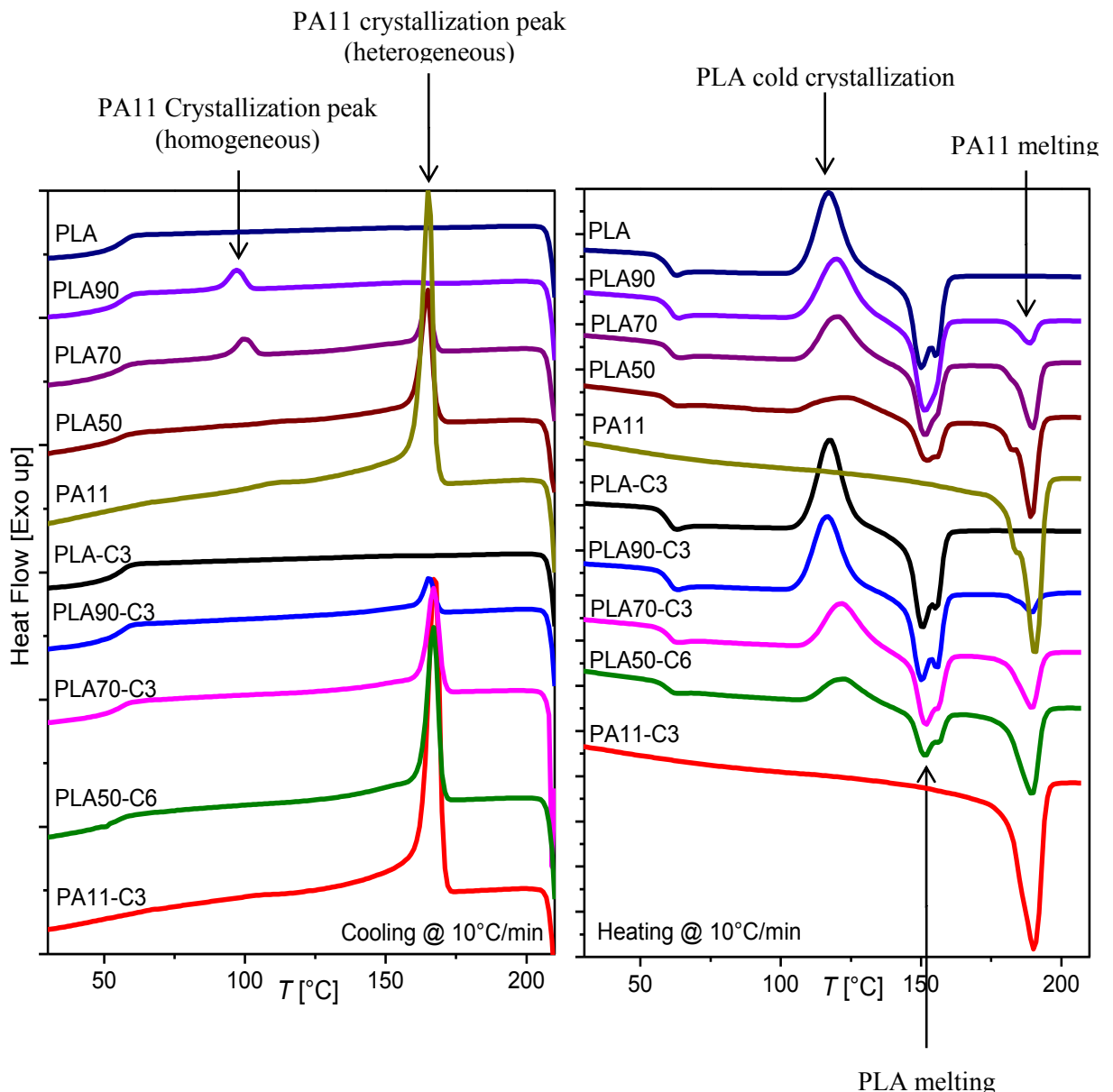


Fig. 2.7: DSC traces of the neat polymers and the unfilled and filled blends upon cooling (left) and heating (right) at 10°C min⁻¹

Table 2.5: Crystallization temperature (T_c) and enthalpy (ΔH_c), Cold Crystallization temperature (T_{cc}) and enthalpy (ΔH_{cc}), Melting temperature (T_m) and enthalpy (ΔH_m) for the samples as in Figure 2.7. The degree of crystallinity (χ_{PA11}) is the mass percentage crystallinity of PA11 calculated by $\chi_{PA11}=100 \times \Delta H_{m(PA11)} / 200m$, where $\Delta H_{m(PA11)}$ is the measured melting enthalpy of PA11 phase from the second heating scan, 200 J/g was taken as the enthalpy of melting for PA11 perfect crystal [58], m is the weight fraction of PA11 in the blends.

Sample	Component	Cooling @ -10°C/min		Second Heating @ 10°C/min				χ_{PA11} [%]
		T_c peak(s) [°C]	ΔH_c [J/g]	T_{cc} [°C]	T_m peak(s) [°C]	ΔH_{cc} [J/g]	ΔH_m [J/g]	
PLA		-	-	117.4	150.2; 155.5	26.4	26.3	-
PLA-C3		-	-	117.6	150.5; 154.8	27.1	26.5	-
PLA90	PLA	-		120.3	151.3; 155	22.3	23.3	-
	PA11	157.6; 96.7	0.65; 3.1	-	189	-	3.8	19
PLA90-C3	PLA	-	-	116.9	150.3; 155.7	23.1	25.4	-
	PA11	165.4	4.9	-	189.8	23.1	4.9	25.2
PLA70	PLA	-	-	121	151.4; 156	17.1	17	-
	PA11	164.7; 99.2	9.17; 2.87	-	182.5; 189.9	-	12	20
PLA70-C1	PLA	-	-	115	149.2; 156	19.9	21.8	-
	PA11	167	13	-	183.1; 188.5	-	13	22
PLA70-C3	PLA	-	-	122.2	151.7; 156	19.3	17	-
	PA11	167	12	-	189.5	-	12	21
PLA70-C6	PLA	-	-	120.3	151.2; 156.4	18.2	17	-
	PA11	166.3	12	-	189.2	-	12	21.3
PLA50	PLA	-	-	124.5	151.9; 156.3	10.8	9.5	-
	PA11	164.8	18	-	182; 189.3	-	18	18
PLA50-C6	PLA	-	-	122.6	151.3; 156.6	8.5	9.3	-
	PA11	167	19	-	189.5	-	19	20.2
PA11		165.3	33.5	-	183.6; 190.6	-	33.5	16.7
PA11-C3		167.5	38	-	190.3	-	38	19.6

The PA11 is a typical semicrystalline polymer, with crystallization temperature $T_c \sim 170^\circ\text{C}$ and melting temperature $T_m \sim 180 \div 194^\circ\text{C}$; the double melting peak reflects the peculiar polymorphism of this polymer [42, 43]. PLA remains amorphous when cooled down from the

melt, but it is able to crystallize upon heating (cold crystallization) at $T_c \sim 105^\circ\text{C}$; the resulting crystalline phase melts down at $T_m \sim 140\div 160^\circ\text{C}$ with a double peak. The double melting peak of PLA is usually assigned to a melting recrystallization phenomenon during the heating scan, due to unstable defective crystals [44].

Concerning the impact of the filler on pure polymers, it has no effects on the crystallization ability of PLA neither upon cooling nor upon heating. Differently, the organoclay acts as a nucleating agent for PA11 as indicated by the clear increase of crystallization enthalpy and the occurrence of the corresponding peak at higher temperature.

Regarding the crystallization behavior of the unfilled blends, Figure 2.7 and Table 2.5 shows that PLA90 and PLA70 blends exhibited two crystallization peaks, both related to the PA11 phase. The occurrence of the multiple crystallization peaks of the minor phase PA11 is attributed to the confined crystallization or fractionated crystallization phenomenon, which happens when the number of droplets of the minor phase is higher than the number of heterogeneities that act as nuclei and this changes the nucleation mechanism from predominantly heterogeneous to predominantly homogeneous. The generation of homogeneous nuclei in heterogeneity-free droplets needs a very large degree of supercooling and crystallization temperature depression of $70\text{-}80^\circ\text{C}$ has been reported. The PLA90 blend displays a greater low temperature crystallization peak compared with the high temperature one because of a finer blend morphology than PLA70 blend. Conversely, the PLA50 blend displays a unique thermal event around the bulk crystallization temperature of PA11. This result can be indirectly considered a confirmation of the coarse and co-continuous morphology of the PLA50 blend because for such a microstructure nucleation can trigger crystal growth within the total volume occupied by crystallizable polymer chains.

The above observations are not unprecedented since they have been recorded for various other immiscible polymer blends [45-49] and even in PLA/PA11 blends [10].

The role of filler on the crystallization behavior of ternary systems depends strongly on its localization. TEM observations revealed the preferential localization of the filler inside the PA11 phase. This is consistent with the clear increase of the crystallization enthalpy and the crystallinity degree of the PA11 phase in the filled blends with respect to their unfilled counterparts, which indicates the nucleating action of the filler. Additionally, Figure 2.7 and Table 2.5 indicates that the confined crystallization of the PA11 droplets in PLA90 and PLA70 blends is suppressed upon the addition of organoclay. This suggests that the organoclay has a heterogeneous nucleation effect on PA11 phase [50].

The crystallinity of PLA phase upon cooling remains unchanged also in the ternary blends and this suggests that the blend morphology represents the key parameter governing the mechanical performances of the system.

3.3. Thermo-mechanical behaviour.

The elastic modulus at $\omega=1$ Hz is reported in Figure 2.8.a as a function of temperature for the neat polymers and the unfilled blends at different composition.

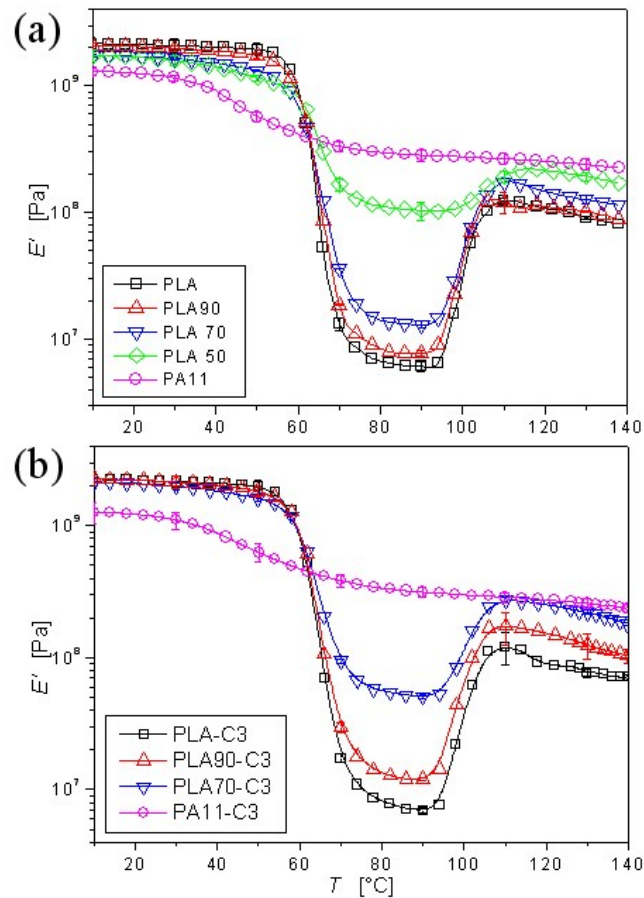


Fig. 2.8. (a) Elastic modulus of the neat polymers and the unfilled blends and (b) the OMMT-filled samples. The error bars are the standard deviations estimated on three independent tests.

The glass transition of the amorphous PLA at $\sim 60^\circ\text{C}$ causes a drop of the modulus of ~ 3 decades. When the temperature approaches 100°C , E' raises upon heating due to cold crystallization (see Figure 2.7). Differently, the modulus of PA11 decreases by only 2/3 of decade at $T_g \sim 50^\circ\text{C}$ because of the bearing contribution of the crystalline phase. Making the PA11 phase continuous in the blends is thus expected to enhance the creep resistance of PLA.

Hereafter we focus on the rubbery modulus in the range $T=60\div 100^{\circ}\text{C}$, i.e. where the drastic softening of PLA limits its usage in a variety of possible applications.

The moduli of the unfilled blends lie between those of the neat constituents. In agreement with the SEM observations, the amorphous PLA governs the blend response when it represents the continuous phase, namely in the samples PLA90 and PLA70. The stiff but isolated PA11 drops are ineffective as reinforcement above the glass transition of the PLA matrix. A substantial increase of E' is instead attained in the sample PLA50, in which the continuous PA11 phase efficiently contributes to bear the stress.

The T -dependence of the elastic modulus of selected filled samples is reported in Figure 2.8.b. A slight increase of E' in the range of interest is observed for the sample with drop-matrix morphology PLA90-C3. Keeping in mind the selective positioning of the filler, its nucleating action, and considering the scarce interfacial adhesion gathered from a visual inspection of SEM micrographs, such a growth is primarily ascribed to the enhanced modulus of the OMMT-rich PA11 droplets. The effect of the filler is much more significant for the sample PLA70-C3: it originates not only from the mere reinforcing action of the OMMT, but also from the ability of the latter to promote the continuity of the host PA11 phase. As a result, the rubbery modulus of the filled blend approaches that of the co-continuous PLA50 sample despite the much lower content of PA11.

The filler-induced changes in the blend microstructure are even more evident when the high temperature creep resistance is tested. The sample deflection under constant load is shown in Figure 2.9.a as a function of T for the neat polymers and the samples PLA70 and PLA70-C3.

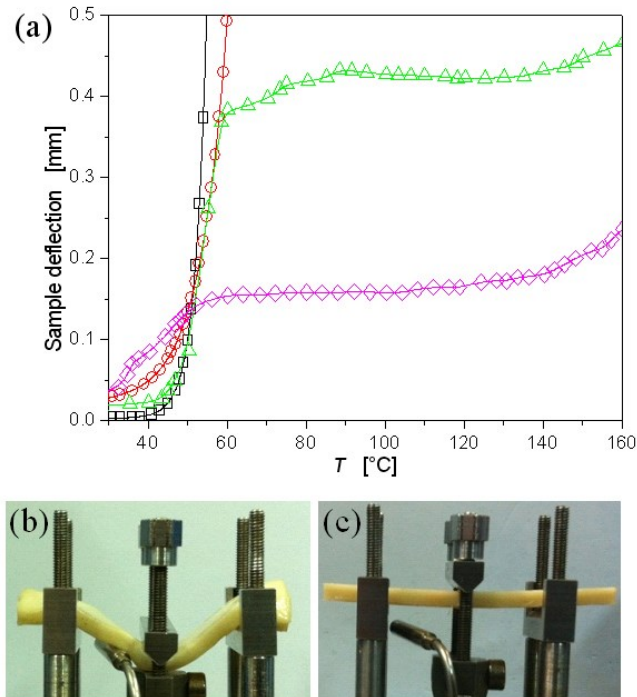


Fig. 2.9: (a) Sample deflection recorded during creep tests for the sample PLA (squares), PA11 (diamonds), PLA70 (circles) and PLA70-C3 (triangles). The pictures show the samples PLA70 (b) and PLA70-C3 (c) at the end of the test, that is after the temperature had reached $\sim 160^{\circ}\text{C}$.

In the glassy state the PA11 stiffness is somewhat lower than that of the PLA. Above the T_g , however, the deformation rate of PA11 slows down while heating and eventually stops due to the crystalline phase, which constrains the mobility of the amorphous phase. The reinforcing action of crystallites vanishes when the T_m of PA11 is approached. The behaviour of the drop-matrix sample PLA70 retraces that of its PLA major phase. Conversely, the plateau in the curve of the sample PLA70-C3 reflects the presence of the continuous structure of filled PA11 that interpenetrates PLA. The stress-bearing ability of the three-dimensional OMMT-rich PA11 network can be clearly appreciated in Figure 2.9.b, where the pictures of the samples PLA70 and PLA70-C3 soon after the end of the creep tests are shown. The sample PLA70 collapses soon after the T_g is approached, whereas the filled blend PLA70-C3 keeps its structural integrity up to $\sim 160^{\circ}\text{C}$ thanks to the continuous framework of filled PA11. We stress that the latter result cannot be ascribed to the crystallization ability of the PLA phase upon the slow heating experienced during the creep tests. PLA cold crystallization, in fact, begins well above the T_g , i.e. after the sample has, in case, evidently deflected. We thus conclude that the enhanced creep resistance of the sample PLA70-C3 originates from the ability of OMMT to promote the continuity of the high-temperature resistant PA11 phase.

2.3.4. Optimizing the formulation – High vs. room temperature mechanical properties

Looking for optimized creep-resistant formulations, further mechanical analyses were performed on samples with different composition. In particular, we aim at maximizing the PLA content while preserving the high-temperature mechanical resistance. The results of additional creep tests are reported in Figure 2.10.a, where the sample deflection is shown as a function of temperature for the new formulations PLA80-C3, PLA70-C1 and PLA70-C6. The reference curve of the sample PLA70-C3 is reported for comparison.

The sample PLA80-C3 yields at about 50°C, i.e. soon after the polymers experience the glass transition. The OMMT cannot promote the continuity of the heat resistant PA11 phase in the blend at 80 wt.% of PLA. Conversely, all the curves of the filled samples at 30 wt.% of PA11 approach a plateau after the T_g of the matrices is exceeded. The value of such T -independent displacement inversely depends on the OMMT content. The sample PLA70-C1 results visibly deflected at the end of the creep test (Figure 2.10.b), whereas the sample PLA70-C6 keeps its shape up to ~160°C (Figure 2.10.c).

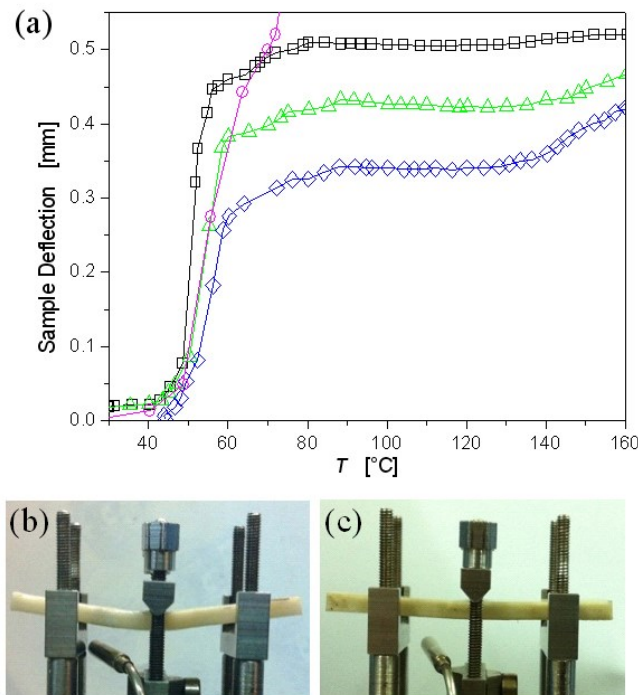


Fig. 2.10. (a) Sample deflection recorded during the creep tests for the blends PLA80-C3 (circles), PLA70-C1(squares), PLA70-C3 (triangles) and PLA70-C6 (diamonds). The pictures show the samples PLA70-C1 (b) and PLA70-C6 (c) soon after the end of the test.

We observe that maximizing the high-temperature creep resistance through OMMT may bring about an excessive material embrittlement at room temperature. This is shown in Figure 2.11,

where representative tensile stress-strain curves are shown for the neat polymers, the unfilled blend PLA70 and the filled samples PLA70-C1, PLA70-C3 and PLA70-C6; the average values of Young's modulus (E), tensile strength (TS), elongation at break (EB), and toughness (T) are summarized in Table 2.6.

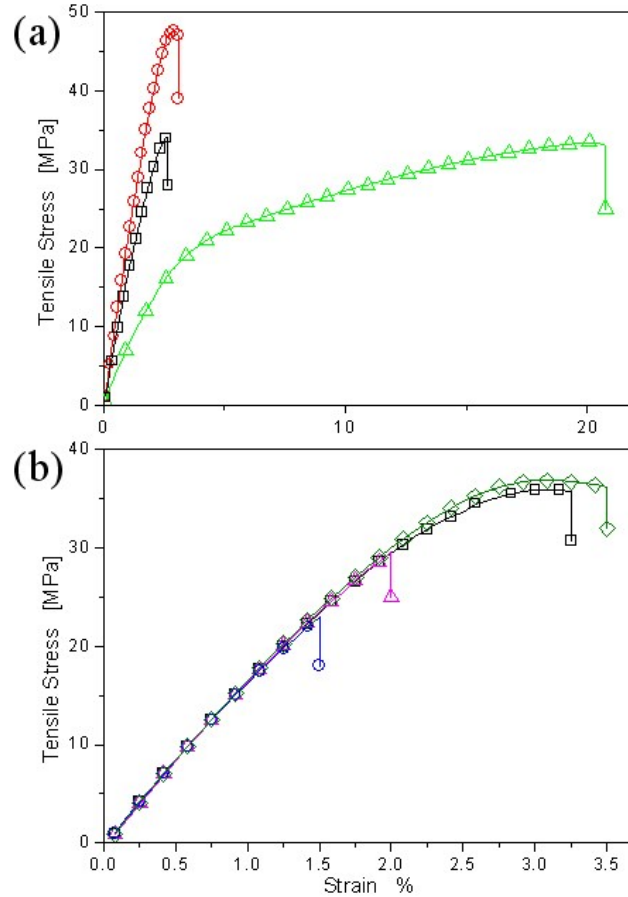


Fig. 2.11. Representative stress-strain curves. (a) PLA (circles), PA11 (triangles) and PLA70 (squares). (b) PLA70-C1 (diamonds), PLA70-C3 (triangles) and PLA70-C6 (circles); the reference curve of the sample PLA70 is reported as well (squares).

Table 2.6. Values of Young's modulus, tensile strength, elongations at break and toughness.

Sample	E [MPa]	TS [MPa]	EB [%]	T [MPa]
PLA	2060±111	49.7±2.3	3.4±0.2	0.92±0.1
PA11	761±16	29.7±2.8	20.7±2.2	4.7±0.9
PLA70	1644±72	35.6±3.2	3.3±0.8	0.72±0.32
PLA70-C1	1775±67	37.3±3.0	3.5±0.5	0.75±0.17
PLA70-C3	1725±53	29±2.8	2.1±0.2	0.31±0.06
PLA70-C6	1694±39	23.4±1.7	1.7±0.1	0.19±0.02

The neat PLA is a typical brittle polymer, with high modulus and tensile strength. Conversely, the PA11 exhibits high elongation at break and toughness. The values of E and TS of the unfilled blend PLA70 fall in between those of the constituents, whereas EB and, as a consequence, T , are governed by the PLA major phase. This is consistent with the drop-matrix morphology and the scarce interfacial adhesion of this sample. Adding only 1 phr of OMMT results in a general increase of the mechanical properties with respect to the unfilled blend. The filler has instead a detrimental effect at too high contents, when the presence of agglomerates of clay platelets is expected. Cracks generally initiate on and propagate within such clusters, worsening the quality of the stress transfer between polymer and filler and lowering the ultimate properties [51].

To summarize, as the case may be a compromise has to be sought between high and room temperature mechanical performances. The sample PLA70-C3 exhibits well balanced properties, but an increase of toughness can be achieved by reducing the OMMT amount at the expense of the high temperature creep resistance, which, in any case, remains much higher than that of pure PLA.

2.4. CONCLUSIONS

Aim of this section of the research activity has been the individuation of bio-based and eco-sustainable polymeric formulations, able to replace, totally or partially, conventional polymers in industrial sectors where petroleum-based plastics still dominate owing to their generally better mechanical and thermal properties.

Basing on the goal, we have designed a fully bio-based blend with the eco-friendly PLA as the dominant component with improved high temperature creep resistance. The poor mechanical properties of the amorphous PLA above its glass transition have been corrected by blending it with PA11, a semicrystalline bio-based polymer, and promoting the continuity of the latter phase through the addition of small amounts of OMMT. The selective positioning of the filler inside the PA11 and at the PLA/PA11 interface has been exploited to convert the drop-matrix morphology of a blend at

70 wt% of PLA into a stable co-continuous one. In such a way, a remarkable improvement of the high temperature mechanical performances has been achieved owing to the OMMT-rich PA11 framework, which interpenetrates the PLA, major phase, and contributes to bear stresses up to 160°C, i.e., 100°C above the PLA glass transition. Neither the mere reinforcing

action of the filler nor changes in the crystallinity of the polymeric blend constituents are responsible for the observed improvement. Looking for optimized formulations, we have found that reducing the PA11 content results in the loss of the high temperature creep resistance. On the other hand, increasing the OMMT content in the blend at 70 wt% of PLA may bring about an excessive material embrittlement at room temperature.

2.5. REFERENCES

- [1] *Processing technologies for poly(lactic acid)*; Lim L.T., Auras R., Rubino M.; *Progr. Polym. Sci.* 33 (2008) 820-852.
- [2] *Poly(lactic acid) modifications*; Rasal R. M., Janorkar A. M., Hirt D. E.; *Prog. Polym. Sci.* 35 (2010) 338-356.
- [3] *Effect of molecular weight and crystallinity on poly(lactic acid) mechanical properties*; Perego G, Cella G. D., Bastioli C.; *Polymer* 59 (1996) 37-43.
- [4] *Improving mechanical performance of injection molded PLA by controlling crystallinity*; Harris A. M., Lee E. C.; *J. Appl. Polym. Sci.* 107 (2008) 2246-2255.
- [5] *Physical and mechanical properties of poly(L-lactic acid) nucleated by dibenzoylhydrazide compound*; Kawamoto N., Sakai A., Horikoshi T., Urushihara T., Tobita E.; *J. Appl. Polym. Sci.* 103 (2007) 244-250.
- [6] *Effect of nucleation and plasticization on the crystallization of poly (lactic acid)*; Li H., Huneault M. A.; *Polymer* 48 (2007) 6855-6866.
- [7] *Biodegradable polylactide and its nanocomposites: opening a new dimension for plastics and composites*; Ray S. S., Okamoto M.; *Macromol. Rapid Commun.* 24 (2003) 815-840.
- [8] *Structure-properties of super-tough PLA alloy with excellent heat resistance*; Hashima K., Nishitsuji S., Inoue T.; *Polymer* 51 (2010) 3934-3939.
- [9] *Fully Biodegradable and Biorenewable Ternary Blends from polylactide, Poly(3-hydroxybutyrate-co-hydroxyvalerate) and Poly(butylene succinate) with Balanced Properties*; Zhang K., Mohanty A. K., Misra M.; *ACS Appl. Mater. Interfaces* 4 (2012) 3091-3101.
- [10] *Morphology, thermal behavior and mechanical properties of binary blends of compatible biosourced polymers: Polylactide/Polyamide11*; Stoclet G., Seguela R., Lefebvre J.-M.; *Polymer* 52 (2011) 1417-1425.
- [11] *Uneven distribution of nanoparticles in immiscible fluids: Morphology development in polymer blends*; Fenouillot F., Cassagnau P., Majestè J.-C.; *Polymer* 50 (2009) 1333-1350.
- [12] *Effects of organoclays on morphology and thermal and rheological properties of polystyrene and poly(methyl methacrylate) blends*; Gelfer M. Y., Song H. H., Liu L.,

- Hsia B. S., Chu B., Rafailovich M.; *J. Polym. Sci. Part B: Polym. Phys.* 41 (2003) 44–54.
- [13] *Compatibilization of Immiscible Poly(propylene)/Polystyrene Blends Using Clay*; Wang Y., Zhang Q., Fu Q.; *Macromol Rapid Commun* 24 (2003) 231-235.
- [14] *Effect of Organoclay Platelets on Morphology of Nylon-6 and Poly (ethylene-r an-propylene) Rubber Blends*; Khatua B. B., Lee D. J., Kim H. Y., Kim J. K.; *Macromolecules* 37 (2004) 2454-2459.
- [15] *Compatibilizing bulk polymer blends by using organoclays*; Si M., Araki T., Ade H., Kilcoyne A. L. D., Fisher R., Sokolov J. C., and Rafailovich M. H.; *Macromolecules* 39 (2006) 4793-4801.
- [16] *Morphological and rheological properties of polyamide 6/poly (propylene)/organoclay nanocomposites*; Chow W. S.; Mohd Ishak Z. A., Karger-Kocsis J.; *Macromol Mater Eng* 290 (2005) 122-127.
- [17] *Effect of clay on the morphology and properties of PMMA/poly (styrene-co-acrylonitrile)/clay nanocomposites prepared by melt mixing*; Lee M. H., Dan C. H., Kim J. H., Cha J., Kim S., Hwang Y., Lee C. H.; *Polymer* 47 (2006) 4359-4369.
- [18] *The role of organically modified layered silicate in the breakup and coalescence of droplets in PBT/PE blends*; Hong J. S., Namkung H., Ahn K. H, Lee S. J., Kim C.; *Polymer* 47 (2006) 3967-3975.
- [19] *Co-continuous Polyamide 6 (PA6)/Acrylonitrile-Butadiene-Styrene (ABS) Nanocomposites*; Li Y., Shimizu H.; *Macromol Rapid Commun* 26 (2005) 710-715.
- [20] *The role of organoclay in promoting co-continuous morphology in high-density poly(ethylene)/poly(amide) 6 blends*; Filippone G., Dintcheva N. T., Acierno D., La Mantia F. P.; *Polymer* 49 (2008) 1312-1322.
- [21] *Using organoclay to promote morphology refinement and co-continuity in high-density polyethylene/polyamide 6 blends-Effect of filler content and polymer matrix composition*; Filippone G., Dintcheva N. T., La Mantia F. P., Acierno D.; *Polymer* 51 (2010) 3956-3965.
- [22] *Role of Interface Rheology in Altering the Onset of Co-Continuity in Nanoparticle-Filled Polymer Blends*; Filippone G., Romeo G., Acierno D.; *Macromol Mater Eng* 296 (2011) 658-665.
- [23] *Clustering of Coated Droplets in Clay-Filled Polymer Blends*; Filippone G., Acierno D.; *Macromol Mater Eng* 297 (2012) 923-928.

- [24] *Thermal decomposition of alkyl ammonium ions and its effects on surface polarity of organically treated nanoclay*; Dharaiya D., Jana S. C.; *Polymer* 46 (2005) 10139-10147.
- [25] *Selective localization of carbon black in immiscible polymer blends: a useful tool to design electrical conductive composites*; Sumita M., Sakata K., Asai S., Miyasaka K., Nakagawa H.; *Polym. Bull.* 25 (1991) 265.
- [26] Wu S., “Polymer Interface and Adhesion”, Marcel Dekker Inc., New York 1982.
- [27] D. K. Owens, R. C. Wendt, *J. Appl. Polym. Sci.* 1969, 13, 1741.
- [28] *Polar interactions at liquid/polymer interfaces*; Alain Carrè; *J. Adhesion Sci. Technol.* 21 (10) (2007) 961-981.
- [29] *Effect of clay treatment on structure and mechanical behavior of elastomer-containing polyamide 6 nanocomposite*; Kelnar I., Khunova V., Kotek J., Kapralkova L.; *Polymer* 48 (2007) 5332-5339.
- [30] *Influence of elastic properties on drop deformation and breakup in shear flow*; Mighri F., Carreau P. J., Aiji A.; *J. Rheol.* 42 (1998) 1477-1490.
- [31] *Effect of clay on the morphology of binary blends of polyamide 6 with high density polyethylene and HDPE-graft-acrylic acid*; Fang Z., Xu Y., Tong L.; *Polym. Eng. Sci.* 47 (2007) 551-559.
- [32] *Novel morphologies of poly (phenylene oxide)(PPO)/polyamide 6 (PA6) blend nanocomposites*; Li Y., Shimizu H.; *Polymer* 45 (2004) 7381-7388.
- [33] *Selective localization of nanofillers: effect on morphology and crystallization of PLA/PCL blends*; Wu D., Lin D., Zhang J., Zhou W., Zhang M., Zhang Y., Wang D., Lin B.; *Macromol. Chem. Phys.* 212 (2011) 613–626.
- [34] *Effect of Organoclay on the Morphology and Properties of Poly (propylene)/Poly [(butylene succinate)-co-adipate] Blends*; Ray S. S., Bandyopadhyay J., Bousmina M.; *Macromol. Mater. Eng.* 292 (2007) 729-747.
- [35] Paul DR, Barlow JW. *J Macromol Sci Rev Macromol Chem* 1980;C18:109-68.
- [36] Goffin AL, Raquez JM, Duquesne E, Siqueira G, Habibi Y, Dufresne A, et al. *Polymer* 2011;52:1532e8.
- [37] Gubbels F, Jerome R, Vanlathen E, Deltour R, Blacher S, Brouers F. *Chem Mater* 1998;10:1227e35.
- [38] *Carbon black self-networking induced co-continuity of immiscible polymer blends*; Wu G., Li B., Jiang J.; *Polymer* 51 (2010) 2077-2083.

- [39] *Morphology evolution of immiscible polymer blends as directed by nanoparticle self-agglomeration*; Cai X., Li B., Pan Y., Wu G.; *Polymer* 53 (2012) 259-266.
- [40] *Kinetically Trapped Co-continuous Polymer Morphologies through Intraphase Gelation of Nanoparticles*; Li L., Miesch C., Sudeep P. K., Balazs A. C., Emrick T., Russell T. P., and Hayward R. C.; *Nano Lett.* 11 (2011) 1997-2003.
- [41] Steinmann S, Gronski W, Friedrich C. *Polymer* 2002;43:4467e77.
- [42] *Influence of annealing on structure of Nylon 11*; Zhang Q., Mo Z., Liu S., Zhang H.; *Macromolecules* 33 (2000) 5999-6005.
- [43] *Crystal transitions of Nylon 11 under drawing and annealing*; Zhang Q. X., Mo Z. S., Zhang H. F., Liu S. Y., Cheng S. Z. D.; *Polymer* 42 (2001) 5543-5547.
- [44] *Thermal analysis of the double-melting behavior of poly (L-lactic acid)*; Yasuniwa M., Tsubakihara S., Sugimoto Y., Nakafuku C.; *J Polym Sci Polym Phys* 42 (2004) 25-32.
- [45] Frensch H., Harnischfeger P., Jungnickel B; *ACS Symp Series* 395 (1989) 101.
- [46] Robitaille C., Prud'homme J.; *Macromolecules* 16 (1983) 665-71.
- [47] *Confined crystallization phenomena in immiscible polymer blends with dispersed micro- and nanometer sized PA6 droplets, part 3: crystallization kinetics and crystallinity of micro- and nanometer sized PA6 droplets crystallizing at high supercoolings*; Tol R. T., Mathot V. B. F., Groeninckx G.; *Polymer* 46 (2005) 2955-65.
- [48] *Crystallization of polyamide confined in sub-micrometer droplets dispersed in a molten polyethylene matrix*; Sanchez M. S., Mathot V., van den Poel G., Groeninckx G., Bruls W.; *J Polym Sci. Polym Phys* 44 (2006) 815-25.
- [49] *Toughening of Biodegradable Polylactide/Poly(butylene succinate-co-adipate) Blends via in Situ Reactive Compatibilization*; Ojijo V., Ray S. S., Sadiku R.; *ACS Appl. Mater. Interfaces* 4 (2012) 2395-2405.
- [50] *Fractionated crystallization in PA6/ABS blends: Influence of a reactive compatibilizer and multiwall carbon nanotubes*; Bose S., Bhattacharyya A. R., Kodgire P. V., Misra A.; *Polymer* 48 (2007) 356.
- [51] *Structural and mechanical properties of polymer nanocomposites*; Tjong S. C.; *Mater. Sci. Eng. R.* 53 (2006) 173-197.

PART 2

Nanoparticle-induced co-continuity in immiscible polymer blends – A comparative study using Cloisite, Sepiolite, Carbon Nanotubes

3.1. INTRODUCTION

Blending polymer is a well-established route to develop new materials with favourable combinations of properties. Most polymer pairs are thermodynamically immiscible because of the typically low mixing entropy of macromolecular materials. For low amounts of either of the phases immiscibility results in a globular morphology, with spherical droplets of the minor phase suspended in the majority component. The properties of such blends typically range between those of the pure constituents, but in many cases the presence of the dispersed phase can drastically worsen the performances of the pure matrix. As the content of the minor component is raised up to a critical value, the morphology changes into co-continuous. The interpenetration of the phases that characterizes this particular morphology may result in a synergistic combination of the properties of the blend constituents, providing improved mechanical properties, heat resistance, and electrical and thermal conductivity [1-3]. In case of unfilled systems, the range of compositions where co-continuity occurs uniquely depends on the ratio between the viscosities of the blend constituents. Deviations from this general rule can take place in the presence of nanoparticles, which can be hence profitably exploited to induce co-continuity. As an example of the possible technological implications, in the previous section of the thesis we have shown that the self-supporting ability of a blend rich in poly(lactic acid) (PLA) can be increased by more than 100°C above the T_g by promoting the continuity of the minor phase of polyamide 11 (PA11), a bio-based polymer with high heat deflection temperature (HDT), through the addition of small amounts of an organo-modified clay [4]. Nanoparticle-induced co-continuity in immiscible polymer blends has been previously observed in many systems, having been ascribed to different possible mechanisms. The empiric relations and theories usually employed to predict the phase inversion composition in unfilled blends are known to fail when applied to nanofilled systems [5-7]. Starting from geometrical considerations, Willemsse et al. derived an empirical relationship for co-continuity in unfilled blends in which the minor phase consists of elongated structures [8]. The latter form during melt mixing, and their stability depends on a balance between the polymer-polymer interfacial tension (σ_{ij}), which drives the elongated domains to retract back to a spherical shape or to fragment into small droplets, and the rheological stresses related to the morphological evolutions. This equilibrium is certainly altered upon addition of nanoparticles, which affect both the interfacial tension and flow behaviour. However, the underlying mechanisms are still far from being understood. It has been reported that a major

role is played by rheology. In case of selective positioning within either of the polymers, the increased elasticity and viscosity could slowdown both the shape relaxation and break up processes, stabilizing irregularly-shaped domains of the minor phase [9-11]. The kinetic trapping of the filled phase may eventually result into stable co-continuous morphologies [12-14]. The self-networking capability of the filler is believed to be crucial [15-17], but many issues remain unresolved. Among others, the relevance of the nanoparticles located at the polymer-polymer interface has been seldom systematically investigated. Theoretical [18] and experimental [19-22] studies suggest a compatibilizing action of the interfacially-adsorbed particles. A significant reduction of the average size of the minor phase of blends with drop-matrix morphology is usually reported as the evidence of compatibilization, but coalescence suppression by shielding mechanism could generate the same effect without actually affecting the interfacial tension [23-24]. Such an effect, however, would not be useful for the purpose of promoting co-continuity. A lowering of σ_{ij} is rather needed, so as to stabilize elongated domains of the minor phase. Using extensional force measurements, Han and co-workers found a decrease of σ_{ij} in the presence of interfacially-adsorbed clay particles [25]. Si et al. noticed that the same kind of filler ensures an increased miscibility, as evidenced by the collapse of the T_g values of the blend constituents into one [26]. On the other hand, micropipette tensiometry experiments by Vignati et al. showed an essential independence of σ_{ij} on the concentration of spherical particles, the compatibilizing ability being mainly ascribed to steric hindrance or surface rheology effects [27]. The role of the latter has been investigated by Filippone et al., who found that interfacially-adsorbed plate-like nanoparticles are more effective than spherical fillers in altering the surface rheology of immiscible blends [28]. Well adapting to the polymer-polymer interface, organo-modified clays can generate variations in the mean curvature of the drop surface even in case of partial coverage [29]. Additionally, clustering phenomena of clay-coated droplets could possibly contribute to some extent to the lowering of the onset of co-continuity [30].

Despite the general agreement in recognising their importance, the roles of bulk rheology, interfacial rheology and interfacial tension are still not well established. Among others, two issues need to be examined more in depth: how effective is to promote co-continuity by kinetically arresting the relaxation dynamics of the bulk polymer phases by means of nanoparticles? And, if so, is the self-networking ability of the particles the only relevant parameter? In this paper we deal with these issues through a comparative study on a blend of PLA and PA11 (PLA/PA11 70/30 wt/wt) filled with different kinds of nanoparticles inclined

to enrich the minor PA11 phase. Specifically, we used organo-modified montmorillonite (OMMT), organo-modified sepiolite (MS) and multi-walled carbon nanotubes (CNTs). OMMT and MS share similar surface chemistry, but they differ in terms of shape. With respect to flexible, plate-like OMMT nanoparticles, the use of stiffer, needle-like rods such as MS could reveal more effective for the purpose of inducing co-continuity. CNTs were instead selected because of their marked self-networking ability, which makes them able to alter the rheological properties of the hosting polymer at very low particle loadings. Morphological, rheological and dynamic-mechanical analyses demonstrate that the three kinds of filler are all able to induce the transition from drop-matrix to co-continuous morphology. However, the cross-check of the experimental data reveals that simply slowing down the melt state relaxation dynamics of the minor phase may be not sufficient to promote co-continuity. The effect of the geometrical features of the particles is discussed, as well as their ability to affect the interfacial tension. In particular, the lowering of the latter seems playing a crucial role, stabilizing irregularly-shaped domains whose merging eventually results into co-continuity.

3.2. MATERIALS AND METHODS

3.2.1. *Materials and blends preparation*

The PLA used in this study is a commercial product supplied by NatureWorks with the trade name PLA 2002D. According to the material datasheet, it has density $\rho=1.24 \text{ g/cm}^3$ at $T=25^\circ\text{C}$, glass transition temperature $T_g\approx 60^\circ\text{C}$ melt flow index MFI=6 g/10' ($210^\circ\text{C}/2.16 \text{ kg}$) and D-LA enantiomer content of about 4%. The PA11, purchased from Sigma Aldrich, has $\rho=1.026 \text{ g/cm}^3$ at $T=25^\circ\text{C}$, $T_g=46^\circ\text{C}$ and melting temperature $T_m=198^\circ\text{C}$.

As filler we used three different kinds of nanoparticles. The OMMT was supplied by Southern Clay Products with trade name of Cloisite 30B. It is a platelet-like clay modified by 90 meq/100 g of bis(2-hydroxyethyl) methyl tallow alkyl ammonium cations with $\rho=2.8 \text{ g/cm}^3$. MS was supplied by Tolsa SA (Spain). It is a needle-like clay modified with benzyl dimethyl hydrogenated tallow ammonium salt. The density is $\rho=2.2 \text{ g/cm}^3$ and the BET surface area is $75 \text{ m}^2/\text{g}$. The characteristic average dimensions of the individual sepiolite nano-fibres are approximately 1-2 μm in length and 20-30 nm in diameter. Multi-walled CNTs (MWCNTs) were supplied by Nanocyl SA (Belgium) with trade name Nanocyl[®] 7000. The main features are: purity >95%, diameter 10 nm, length of 1.5 μm , surface area of 250-300 m^2/g and $\rho=1.75 \text{ g/cm}^3$.

The unfilled and nano-filled blends were prepared by compounding the constituents in a DSM Xplore micro 15 co-rotating twin-screw extruder equipped with conical co-rotating screws having a length $L=150$ mm, length-over-diameter ratio $L/D=18$ and a net capacity of 12 g. The polymers and the fillers, dried overnight under vacuum at $T=80^{\circ}\text{C}$, were simultaneously loaded inside the mixing apparatus. The extrusions were performed under gaseous nitrogen at $T=215^{\circ}\text{C}$ and screw speed 80 rpm, corresponding to average shear rates of $\sim 50\text{ s}^{-1}$. The residence times, carefully controlled owing to an integrated back-flow channel, were set to ~ 1 min for each blend. The designations and compositions of the prepared samples are summarized in Table 3.1.

Table 3.1: Compositions of samples.

Sample	Composition [PLA/PA11 + filler wt/wt]	Sample Code
PLA/PA11	100/0; 0/100; 70/30	PLA; PA11; PLA70
PLA/PA11 + OMMT	100/0 + x; 0/100 + x; 70/30 + x	PLA-Cx; PA11-Cx; PLA70-Cx
PLA/PA11 + MS	100/0 + y; 0/100 + y; 90/10 + y; 70/30 + y	PLA-Sy; PA11-Sy; PLA90-Sy; PLA70-Sy
PLA/PA11 + CNTs	0/100 + z; 90/10 + z; 70/30 + z	PA11-Nz; PLA90-Nz; PLA70-Nz

The extruded materials were granulated, dried again and compression-molded using a Collin P300E hydraulic hot press. Rectangular bars and disks were shaped at $T=215^{\circ}\text{C}$ under a pressure $P\approx 40$ MPa for 5 min, then the samples were cooled down to room temperature at about $30^{\circ}\text{C min}^{-1}$. The neat polymers used as reference materials were processed using the same conditions.

3.2.2. Characterization methods

The morphology of the filled blends at nano-scale was inspected through transmission electron microscopy (TEM) using a Philips EM 208 TEM with 100 keV accelerating voltage. The specimens were in the form of thin slices (thickness ~ 150 nm) microtomed with diamond knife at room temperature from the compression-molded samples. The space arrangement of the polymer phases at micro-scale was investigated through scanning electron microscopy (SEM) using a Jeol JSM-6300F SEM. The inspected surfaces, sputtered with gold, were obtained through brittle fracture in liquid nitrogen of compression-moulded samples.

Rheological analyses were carried out using a stress-controlled rotational rheometer (AR-G2 by TA Instruments) in parallel plate geometry (plate diameter 25 mm). Frequency scans at 215°C were performed from $\omega=10^2$ down to 10^{-1} rad s^{-1} to get the elastic (G') and viscous (G'') shear moduli in the linear regime. The latter was preliminarily estimated through strain scan experiments. Since changes in the rheological properties occurred during testing, a

sequence of four consecutive frequency scans was performed on each sample, and the moduli at time-zero, i.e. in conditions near those of the samples used in the thermo-mechanical characterization, were extrapolated as described in the Appendix.

Dynamic-mechanical analyses (DMA) were carried out using a DMA Q800 (TA Instruments). Specimens in the form of rectangular bars ($3 \times 13 \times 35 \text{ mm}^3$) were heated at 2°C min^{-1} from $\sim 25^\circ\text{C}$ to 140°C , and the elastic (E') and viscous (E'') flexural moduli were recorded as a function of temperature. The tests were performed in single cantilever bending mode at a $\omega=1 \text{ Hz}$ and strain amplitude of 0.1 %, which is small enough to be in the linear regime.

The electrical conductivity of CNTs-filled samples in the form of rectangular bars ($1.7 \times 3.8 \times 20 \text{ mm}^3$) was measured by a two-point measurement using a picoammeter (Keithley 6485) and a DC voltage source (Agilet 6614C). Silver paste coating was used to ensure good contact with the electrodes of the electrometer. At least three specimens for each composite were tested, and average value was reported.

Contact angle measurements were performed for the assessment of the surface energies [31]. In particular, static contact angles of two test liquids, namely distilled water and glycerol, were measured at room temperature using a digital camera (Best Scientific, U.K.) with microvideo zoom lens and a MB ruler software. A drop of the test liquid of 3-5 mL was deposited on the sample surface, and the value of contact angle θ was estimated from the tangent to the drop at the intersection between the sessile drop and the surface. To avoid solvent evaporation, images were taken within 30 s of drop deposition. Then, the surface energies of the samples (σ) and their polar (σ^p) and dispersive (σ^d) components were computed using the Owens-Wendt relation [32]:

$$\sigma_l(1 + \cos \theta) = 2\left(\sigma_s^d \sigma_l^d\right)^{\frac{1}{2}} + 2\left(\sigma_s^p \sigma_l^p\right)^{\frac{1}{2}} \quad (1)$$

where the subscripts l and s stand for *liquid* and *solid*, respectively. The literature values of the two test liquids are $\sigma^d=21.8 \text{ mJ/m}^2$ and $\sigma^p=51 \text{ mJ/m}^2$ for water, and $\sigma^d=37 \text{ mJ/m}^2$ and $\sigma^p=26.4 \text{ mJ/m}^2$ for glycerol [33]. Once the surface tensions were collected, the values of interfacial tension were computed using the geometric equation:

$$\sigma_{ij} = 2\left(\sigma_s^d \sigma_l^d\right)^{\frac{1}{2}} + 2\left(\sigma_s^p \sigma_l^p\right)^{\frac{1}{2}} \quad (2)$$

3.3. Results and Discussion

3.3.1. Selective confinement of the nanoparticles in the PA11 phase

The localization of nanofillers in an immiscible polymer blend prepared by melt mixing is the result of a complex interplay between thermodynamic aspects and kinetics factors. Many physical and processing parameters are involved, such as absolute viscosity and viscosity ratio of the polymers, interfacial tension among the polymers and the particles, compounding procedure, mixing time, etc [34]. As a consequence, predicting the final localization of nanoparticles in polymer blends can be a difficult task, and ex-post morphological analysis are usually performed to assess the actual uneven distribution of the filler. Here we performed electron microscopy on samples diluted enough to easily distinguish the polymer phases and detect the nanoparticles.

Our previous analysis on OMMT-filled PLA/PA11 blends showed that the selected organo-clay locates inside the polyamide phase and at the PLA-PA11 interface. Additionally, both morphological and WAXD analysis revealed a good degree of exfoliation and the loss of the ordered lamellar structures of the pristine OMMT. As shown in Figure 3.1 for the ternary sample PLA90-S1.5, a similar uneven distribution is noticed in the ternary system containing MS.

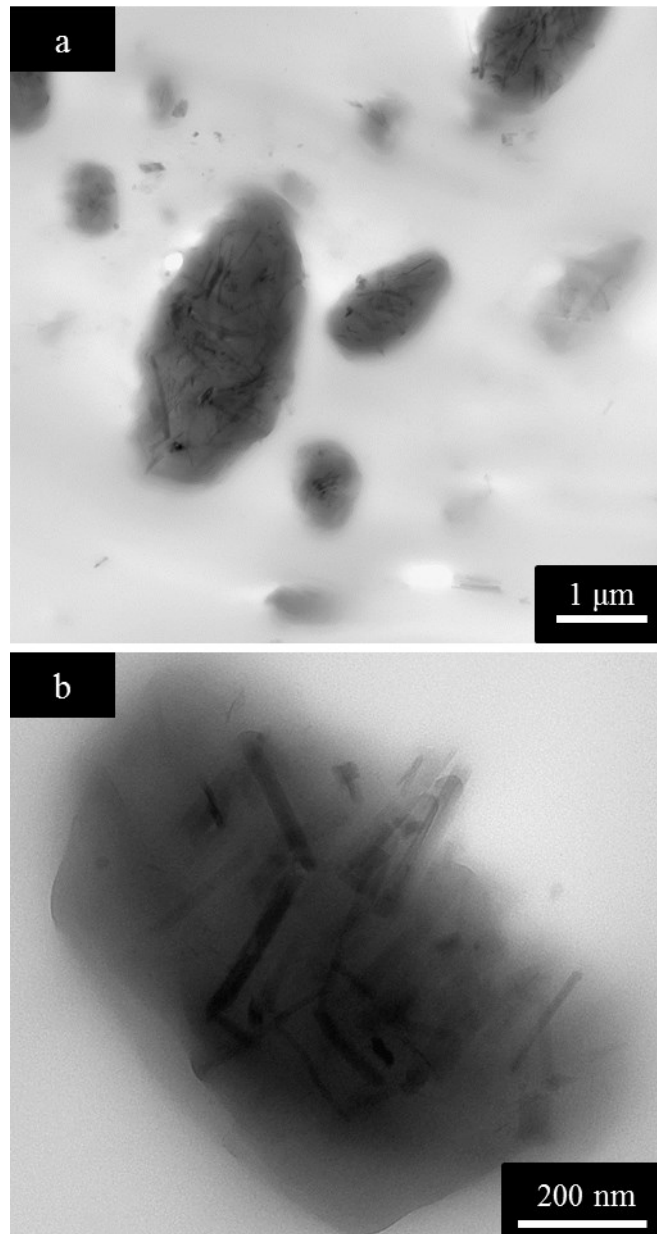


Fig. 3.1: (a) TEM micrograph of the sample PLA90-S1.5. A magnification of a MS-rich PA11 droplet is shown in (b)

The blend exhibits drop-matrix morphology. The typical size of the PA11 dark domains is below 1 μm. Randomly oriented bundles or single MS needles appear predominantly confined inside the PA11 drops, while almost no particles can be noticed within the PLA phase.

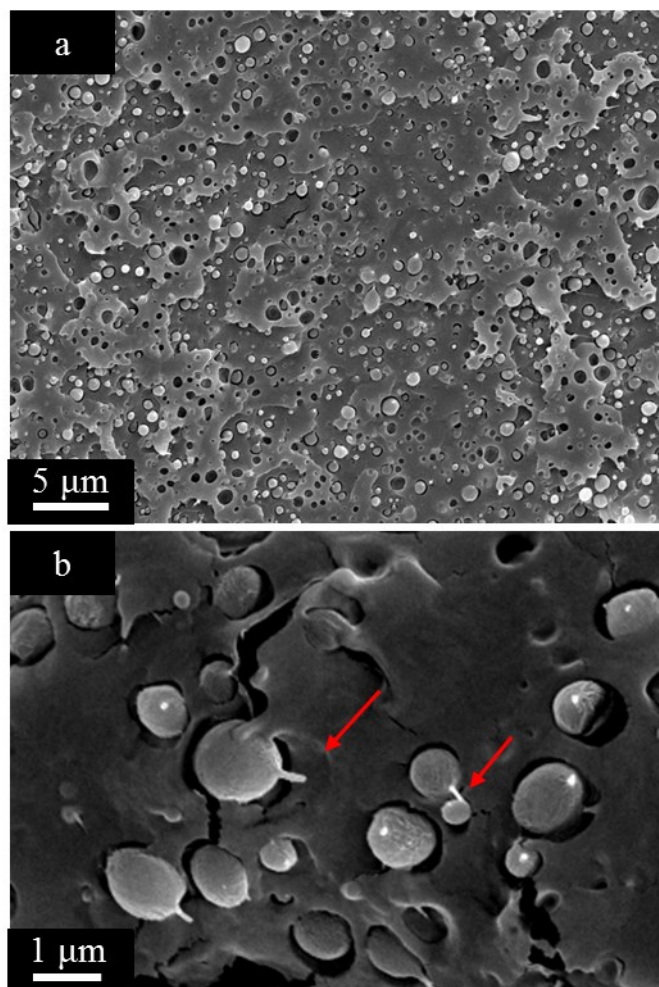


Fig. 3.2: SEM micrographs of the sample PLA90-S1.5 at different magnifications. The arrows indicate part of MS.

The space arrangement of the polymer phases is shown in Figure 3.2, where a representative SEM micrograph of the sample PLA90-S1.5 is reported. MS rods piercing the surface of the PA11 domains can be noticed at high magnifications. This is not surprising, as the length of the MS nanoparticles is generally greater than the average size of the PA11 droplets.

3.3.2. Nanoparticle-induced co-continuity

OMMT- and MS-based blends

In our previous study on the OMMT-filled PLA/PA11 blends we found that the microstructure of a blend at 30 wt.% of PA11 changes from drop-matrix to co-continuous upon addition of small amounts of OMMT. In this section we show that, provided a critical nanoparticle loading is exceeded, a similar morphological transition takes place irrespective

of filler nature. First we focus on the ternary systems containing OMMT and MS, which share similar surface chemical characteristics but differ in terms of geometrical features.

The SEM images of the blend at 30 wt.% of PA11 filled with various amounts of OMMT and MS are shown in Figure 3.3.

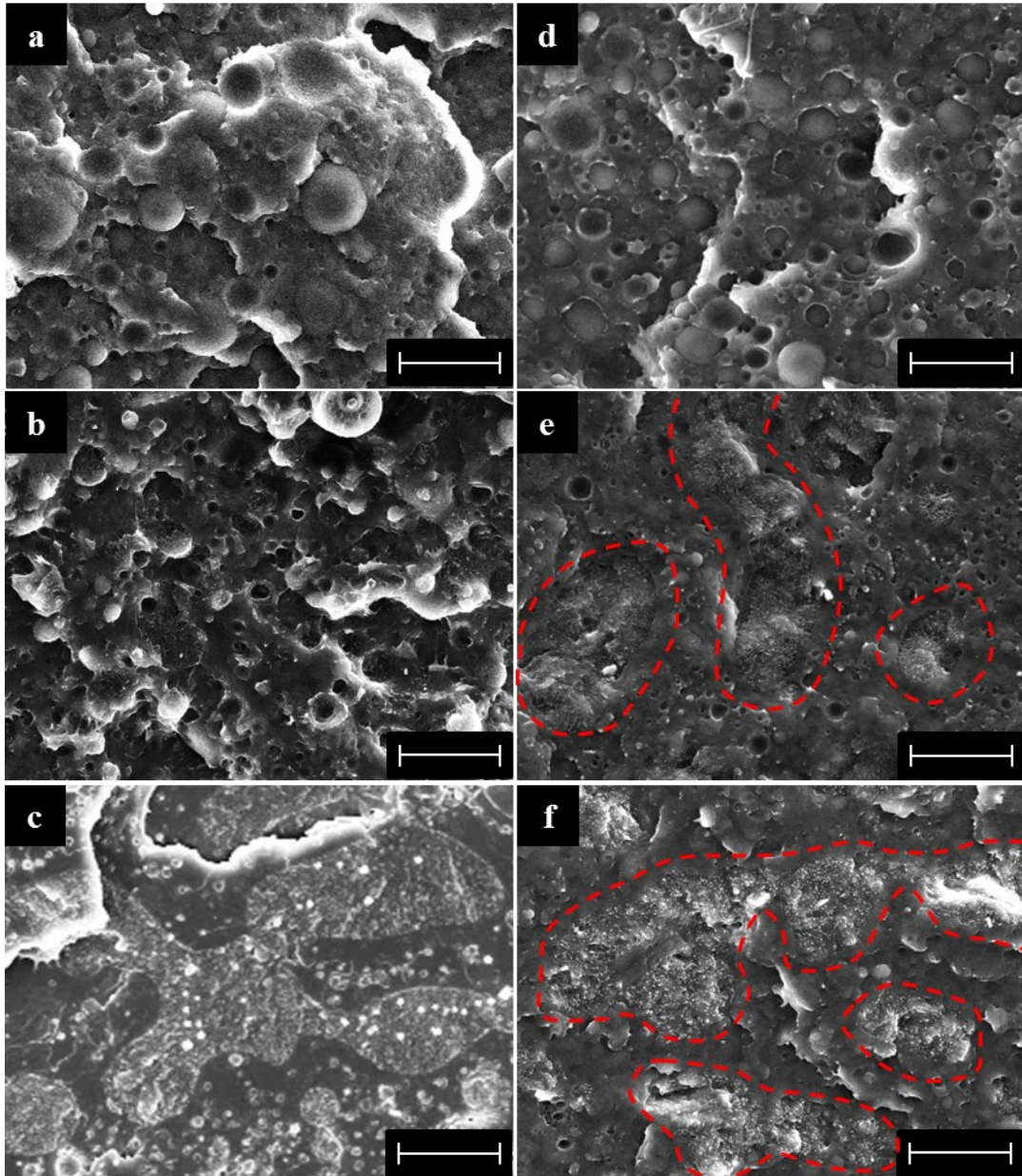


Fig. 3.3: SEM micrographs of the samples PLA70-C1 (a), PLA70-C2 (b), PLA70-C3 (c), PLA70-S1 (d), PLA70-S5 (e) and PLA70-S6 (f). Apparently continuous domains of filled PA11 are highlighted in (e) and (f). (Scale bar = 10 μm)

The addition of 1 wt.% of nanoparticles does not have noticeable effects on the microstructure, which remains globular as in the unfilled blend. When the filler content is raised up to 2 wt.% of OMMT or 5 wt.% of MS, both spheroidal and elongated PA domains coexist, suggesting that these samples may be at the onset of co-continuity. The

morphological transition seems accomplishing by further increasing the filler content: irregularly-shaped PA11 domains interpenetrate the PLA major phase in the PLA70-C2 and PLA70-S6 samples, as expected for co-continuous morphologies. Actually, the analysis of SEM micrographs suffers from the intrinsic two-dimensional feature of the image and limitedness of the inspected region of sample [35]. To substantiate the previous conclusions, dynamic-mechanical analysis was carried out. Although providing indirect evidences of the morphological changes, DMA has the advantage of probing much greater, bulk regions of sample.

The temperature dependence of the elastic moduli E' at 1 Hz is shown in Figure 3.4.a,b for the neat polymers, the unfilled blend and their OMMT- and SM-filled counterparts.

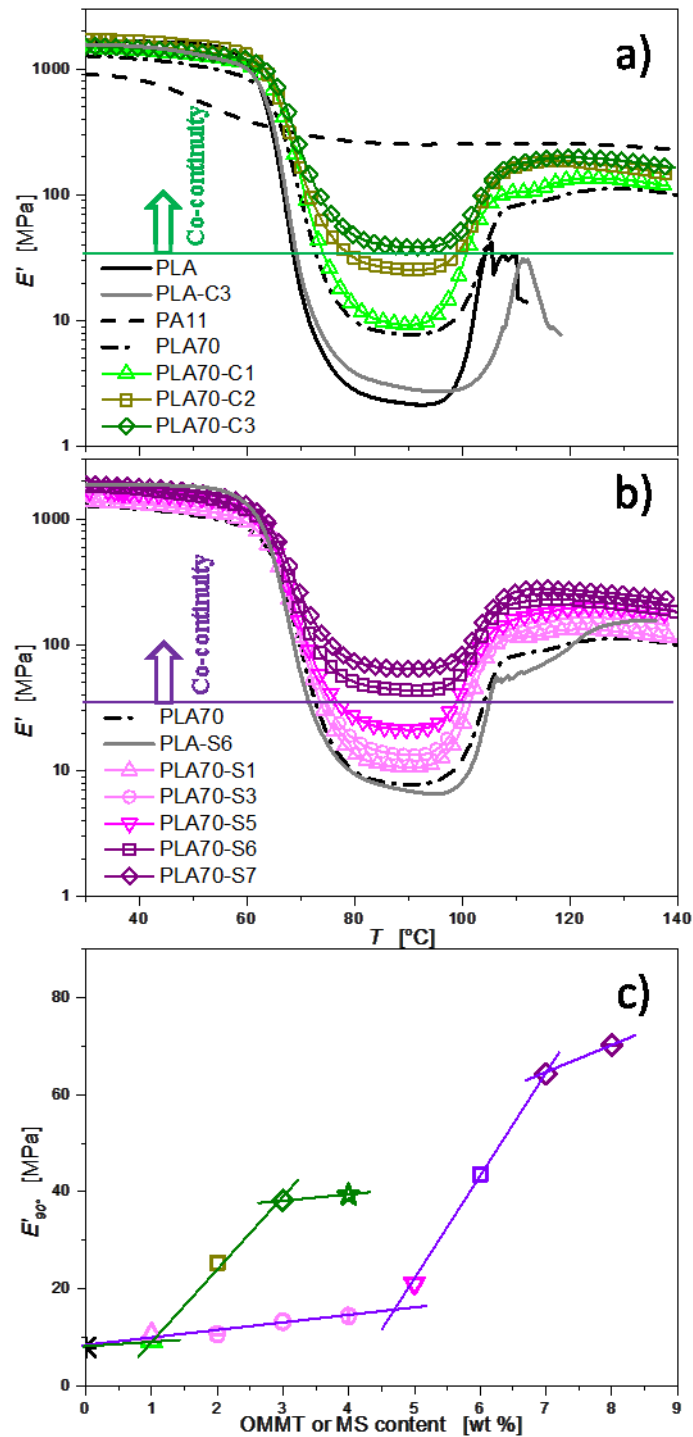


Fig. 3.4: Storage modulus as a function of Temperature of the (a) neat polymers, the unfilled blend PLA70, the OMMT-filled samples PLA-C3 and PLA70-Cx and (b) the MS-filled samples PLA-S6 and PLA70-Sy; the reference curve of the unfilled blend PLA70 is reported as well. (c) Storage modulus at 90 $^{\circ}\text{C}$ as a function of filler content for OMMT- (green symbols and line) and MS-based samples (violet symbols and line)

Consider first the pure polymers. The E' of the amorphous PLA decreases by about 3 decades at the T_g ($\sim 60^{\circ}\text{C}$), then it increases upon heating around 100°C due to cold crystallization [36]. Differently, the modulus of the semicrystalline PA11 does not fall down at the T_g

(~50°C) because of the bearing contribution of the crystalline phase. Concerning the blends, the behaviour is intermediate between those of the two polymer phases, whose incidence depends on the specific microstructure. Due to the drop-matrix morphology, the thermo-mechanical behaviour of the neat PLA70 blend is essentially governed by the PLA major phase. The overall response of the filled blends qualitatively resembles that of the unfilled sample, but the values of E' scale with particle loading. Note that, in case of multiphase systems, the increase of E' does not reflect the reinforcing action of the nanoparticles alone, but it contains information also about filler-induced morphological changes [37]. From now on we refer the rubbery moduli in the range $T=80-100^\circ\text{C}$, i.e. where the difference between the pure polymer phases is the biggest and, hence, morphological effects, if any, are amplified. The moduli at $T=90^\circ\text{C}$ (E'_{90}) are shown in Figure 6.c as a function of filler content. The growth of E'_{90} is not gradual, and a sudden jump is noticed around 2 wt.% of OMMT and 6 wt.% of MS. Note that the same amounts of filler do not generate a comparable increase of E'_{90} when added to pure PLA. It can be hence concluded that the observed critical behavior in the blend is indicative of morphological transition from drop-matrix to co-continuous morphology. A relevant consequence is shown in Figure 3.5, where the pictures of two samples, one below and the other above the identified co-continuity threshold, are compared. The bars were heated up from room temperature up to ~180°C at a heating rate of 2°C/min under a constant load of 0.455 MPa. The sample PLA70-S6 keeps its shape due to the continuous PA11 framework, while the sample PLA70-S1, having drop-matrix morphology, visibly deflects during the test.

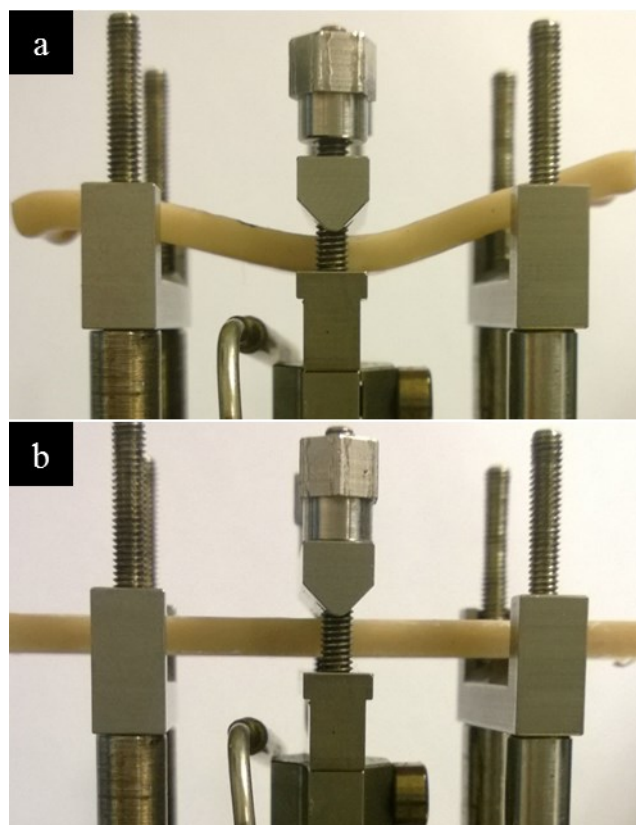


Fig. 3.5: Pictures of (a) PLA70-S1 and (b) PLA70-S6 soon after a creep test performed applying a constant load of 0.455 MPa while heating at 2°C/min from room temperature up to 180°C.

Summarizing, the previous analyses indicate that both OMMT and MS preferentially locate inside the PA11 minor phase of our blends, promoting co-continuity when the filler content exceeds a critical threshold. The latter is much lower in case of plate-like nanoparticles. Specifically, only 2 wt.% of OMMT (~0.9 vol.%) are as effective as 6 wt.% of needle-like MS (~3.3 vol.%). In the next paragraphs we discuss the reasons underlying the greater effectiveness of the former type of filler.

Role of the bulk rheology

While many different system-specific mechanisms are proposed in the literature to explain why nanoparticles are able to induce co-continuity in immiscible polymer blends, a general agreement exists in considering crucial the role of rheology. In our previous paper we noticed a relationship between the critical OMMT content for inducing co-continuity in a PLA/PA11 blend at 30 wt.% of PA11 and the particle threshold at which the host polyamide experiences a rheological transition from liquid-like (viscous shear modulus, G'' , much greater than the elastic one, G') to gel-like ($G' \sim G'' \sim \omega^n$, n being a constant) behaviour [4]. It was argued that the melt elasticity of the PA11 increases due to the addition of particles, eventually inhibiting the break-up and retraction phenomena of the elongated domains which form in the course of

melt-mixing. The interpenetration of the polymer phases is hence preserved, and the blends finally exhibit co-continuous morphology. To test this hypothesis, linear viscoelastic analyses were carried out on PA11-based composites filled with various amount of either OMMT or MS. The results are shown in Figure 3.6, where G' and $\tan\delta = G''/G'$ are reported as a function of frequency.

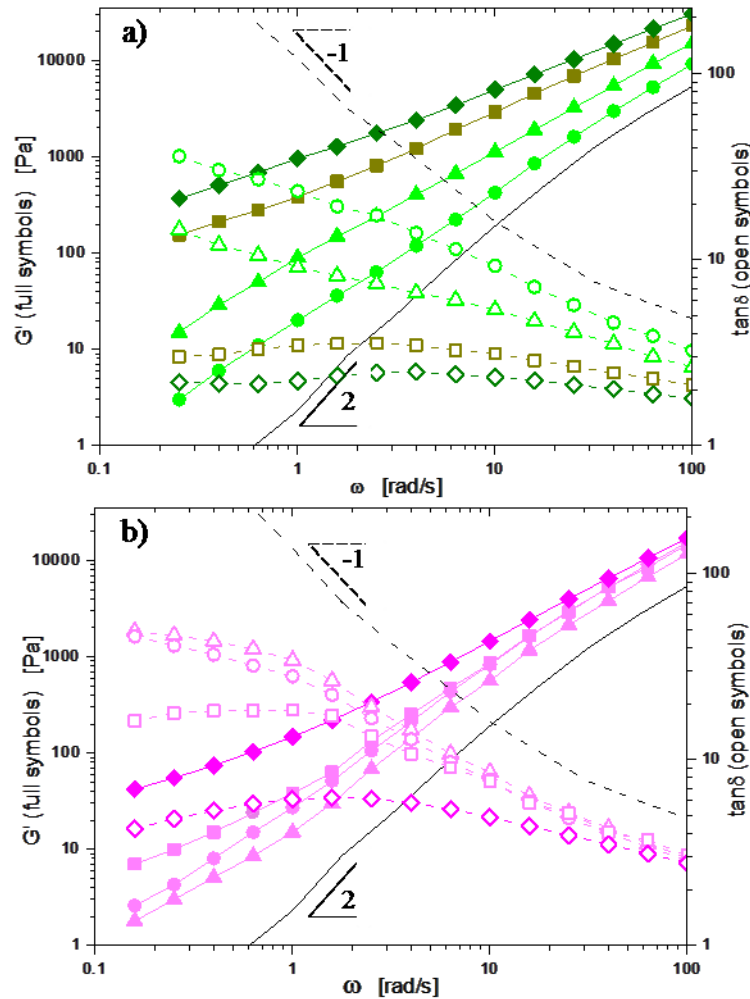


Fig 3.6: ω -dependent elastic modulus (full symbols, left axis) and loss factor $\tan\delta$ (open symbols, right axis) of PA11-based (a) OMMT- and (b) MS-nanocomposites at different filler content: (a) PA11-C1 (circles), PA11-C3 (triangles), PA11-C6 (squares), PA11-C8 (diamonds); (b) PA11-S1 (triangles), PA11-S3 (circles), PA11-S6 (squares), PA11-S15 (diamonds). The modulus and the loss factor of the neat PA11 are reported as the continuous (G') and dashed line ($\tan\delta$).

The unfilled polymer exhibits a predominant viscous feature ($\tan\delta > 1$) in the whole range of frequency investigated, approaching terminal Maxwellian behavior ($G' \sim \omega^2$ and $\tan\delta \sim \omega^{-1}$) at $\omega < 1 \text{ rad s}^{-1}$. The frequency dependence of G' of both the OMMT- and MS-filled samples progressively weakens with particle loading, reflecting the presence of slow populations of dynamical species unable to relax in the investigated frequency range. Flocs of particles

possibly involving fractions of adsorbed polymer are usually considered responsible for the observed phenomenology [38]. For filler contents high enough a space-spanning network of flocs eventually builds up, causing the arrest of the relaxation dynamics. Actually, in the accessed frequency range none of the samples exhibits a clear low-frequency plateau of G' . The latter is usually considered the fingerprint of three-dimensional particle networks embedded in host polymers. Nonetheless, a drastic slowing down of the relaxation dynamics is clearly recognizable at the highest particle concentration. In particular, the flattening of $\tan\delta$ denotes gel-like behavior [39]. The divergence of the longest relaxation times typical of gels essentially implies inability to flow. Such a condition is attained around 6 wt.% of OMMT and 15 wt.% of MS. Assuming that the particles exclusively reside inside the PA11 phase of our blends, the previous thresholds approximately correspond to the amounts of particles located inside the PA11 phase of the samples PLA70-C2 and PLA70-S5, i.e. where the first signs of co-continuity were detected. It is hence confirmed that the bulk rheology of the filled polymer phase could be a relevant parameter in the phenomenon of filler-induced co-continuity. However, in the next section we prove that slowing down the melt state dynamics of the minor polymer phase may not be sufficient, or rather that other mechanisms take part, alternatively or concurrently, to promote co-continuity.

CNTs-based blends

The OMMT has proved to be more effective than MS nanoparticles, being able to induce co-continuity at filler volume fractions much lower than required for the latter type of filler. Viscoelastic analyses have suggested that such a difference could reflect the much higher volume fractions of MS required to induce a comparable slowdown of the relaxation dynamics of the filled PA11. If the principle is general, therefore using a filler highly effective in altering the bulk rheology of the PA11 should ensure co-continuity at very low particle loadings. CNTs were selected to test this hypothesis. Besides being able to cause radical changes in the rheology of the PA11, this kind of nanoparticles fulfills also the requisite of preferential positioning inside the minor phase of our blends. This is shown in Figure 3.7, where representative TEM micrographs of the sample PLA90-N0.2 are shown.

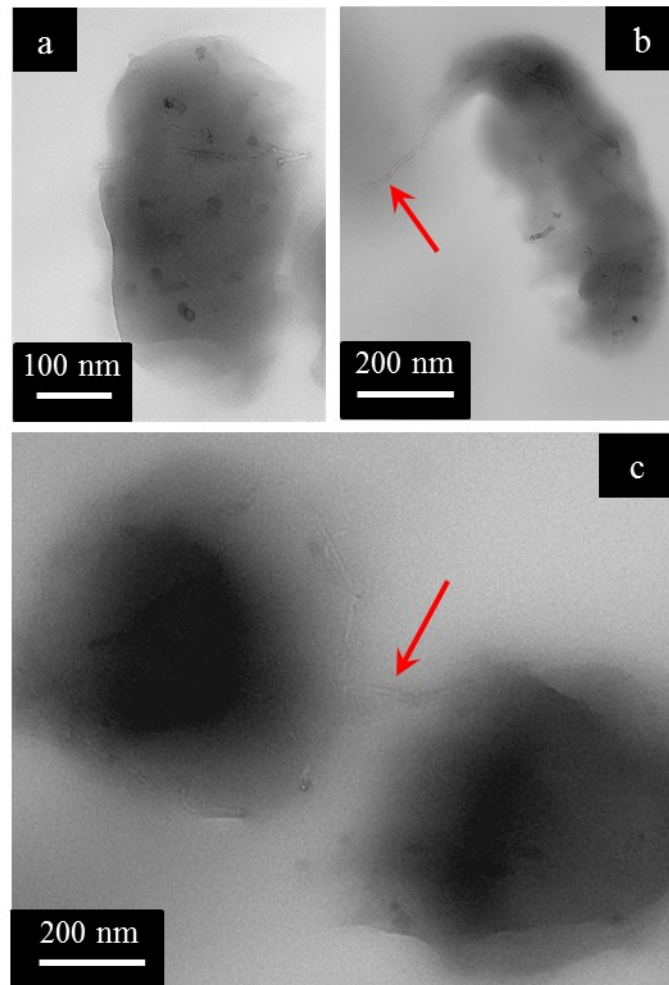


Fig. 3.7: TEM micrographs of CNT-rich PA11 droplets. The arrows indicate nanotubes protruding from the domain (b) or connecting contiguous drops (c).

The filler is predominantly located inside the PA11. Nanotubes extending beyond their domains or connecting contiguous drops are occasionally noticed. This is not surprising, since the CNTs may be longer than the characteristic sizes of the PA11 droplets. SEM micrographs of the sample PLA90-N0.75 are shown in Figure 3.8.

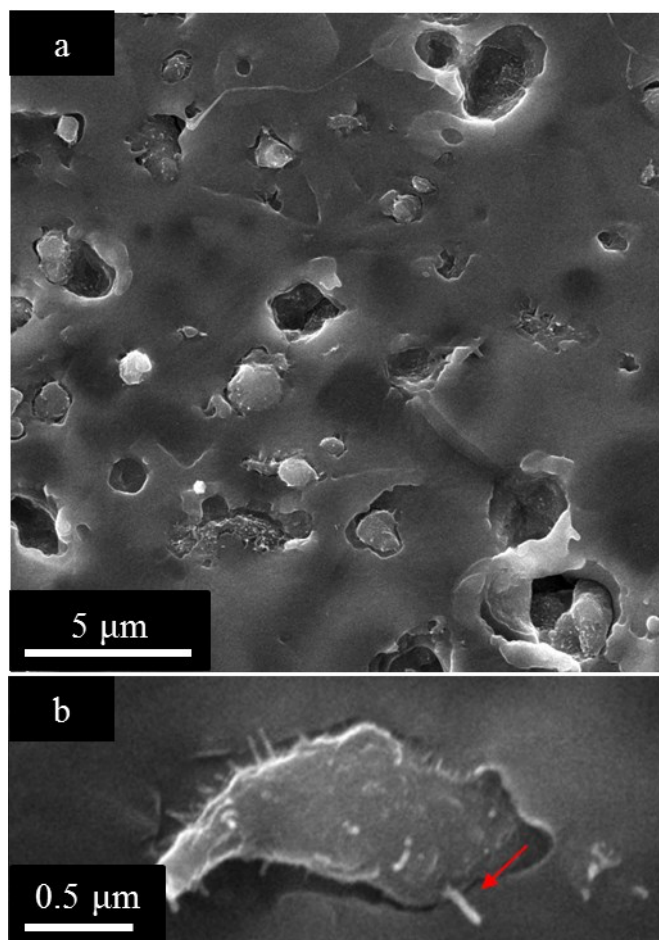


Fig. 3.8: (a) SEM micrograph of the sample PLA90-N0.75. A magnification of a CNTs-rich PA11 droplet is shown in (b). The arrows indicate part of CNTs.

The CNTs appear as bright spots and small fibrils gathered in the proximity of the PA11 drops. In agreement with the TEM analysis, some nanotubes protrude from the host domains. Particles can be also noticed in the PLA cavities remaining after the removal of PA11 domains during sample preparation. Pötschke *et al.* suggested that MWCNTs may bridge the polymer phases [40]. The propensity of the CNTs to enrich the PA11 phase of our blends, however, is evident, being supported also through electrical volume resistivity measurements. Adding 0.75 wt.% of CNTs in pure PLA results in an electrically conductive sample with volume resistivity $\rho_v \approx 10^3$ Ohm cm. On the contrary, the same amount of CNTs added to the blend at 10 wt.% of PA11 is not sufficient to ensure the percolating path of CNTs required to conduct current, the ρ_v of the PLA90-N0.75 being above 10^8 Ohm cm, that is outside the instrument limits.

The remarkable impact of the CNTs on the elasticity of the PA11 is shown in Figure 3.9.

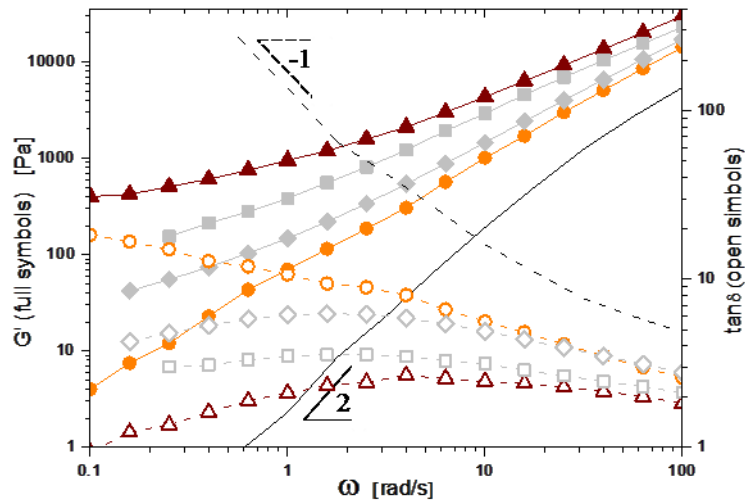


Fig. 3.9: ω -dependent elastic modulus (full symbols, left axis) and loss factor $\tan\delta$ (open symbols, right axis) of the samples PA11-N0.5 (circles), PA11-S15 (diamonds), PA11-C6 (squares) and PA11-N1 (triangles). The modulus and the loss factor of the neat PA11 are reported as the continuous (G') and dashed line ($\tan\delta$).

The addition of 1 wt. % (~ 0.6 vol.%) of CNTs has effects on rheology of the PA11 more significant than 6 wt.% of OMMT or 15 wt.% of MS. Notably, the first signs of gel-like behavior already emerge at 0.5 wt.% of CNTs. Nevertheless, the noticeable self-networking capability of CNTs on the basis of their remarkable impact on the rheology of PA11 is not sufficient to induce co-continuity in the blends. As reported in Figure 3.10.a, the sample PLA70-N0.3, that is where 1 wt. % of CNTs locates inside the PA11, only exhibits a slight increase of the rubbery elastic modulus with respect to the unfilled blend. Much higher filler contents are needed to generate the jump in the dynamic-mechanical response related to the morphological transition from drop-matrix to co-continuous morphology. Looking at the dependence of E'_{90} on the CNT content (Figure 3.10.b), the latter should take place around 2 wt.% of CNTs. This is also in line with the visual inspection of the SEM micrographs of Figure 3.11.

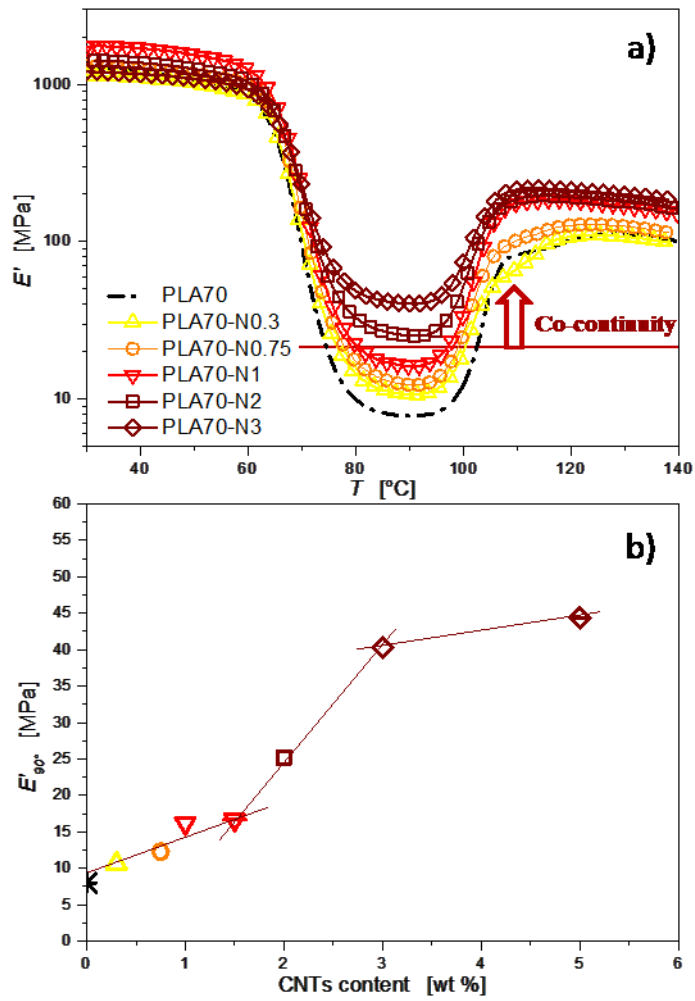


Fig. 3.10: (a) Storage modulus as a function of Temperature of the CNTs-filled blends PLA/PA11 70/30. The reference curve of the unfilled sample PLA70 is reported as well. (b) Storage modulus at 90°C of the CNTs-filled blends at 70% of PLA as a function of CNTs content.

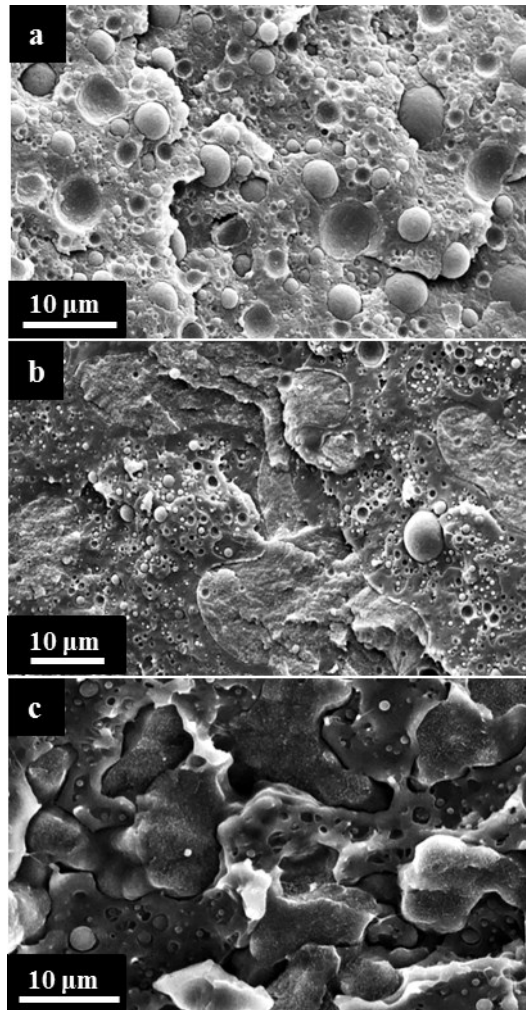


Fig. 3.11: SEM micrographs of the CNTs-filled samples (a) PLA70-N0.3 (b) PLA70-N1 (c) PLA70-N2.

The sample PLA70-N0.3 exhibits drop-matrix morphology. Signs of phase interpenetrations can be noticed at 1 wt.% of CNTs, and a clear co-continuous microstructure characterizes the sample PLA70-N2. It is important to observe that the presence of big CNT bundles exceeding the characteristic size of the polymer phases was noticed more and more frequently with increasing the filler content. In effect, volume resistivity tests reveal that conductive paths of CNTs start to establish around 0.75 wt.%, that is a bit lower than the content for inducing the continuity of the PA11 phase (see Figure 3.12). In other words, space-spanning CNT networks can build up even if the preferred PA11 phase is not continuous, being able to involve also CNT agglomerates and portions of single CNTs not confined in the PA11 domains.

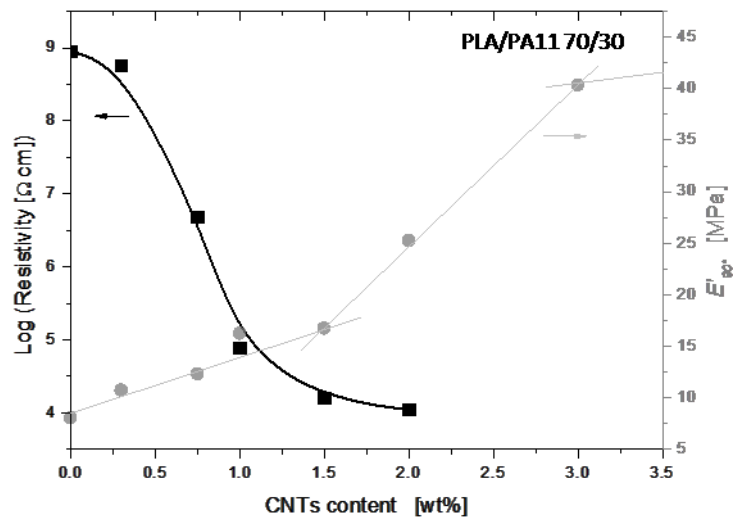


Figure 3.12: Resistivity versus CNTs content for the PLA/PA11 70/30 blends (left axis). E'_{90° as a function of CNTs content is reported, as well (right axis).

Summarizing, like OMMT and MS, also CNTs are able to induce co-continuity in the studied system. The difference with the other types of nanoparticles is that the noticeable impact of CNTs on the bulk rheology of the PA11 phase does not appear to be related with the morphological transition, which takes place at a CNTs content much higher than needed to slow down the melt state dynamics of the PA11 phase in the blend. Among the possible concurrent mechanisms playing a role in the phenomenon, in the next section we focus on the ability of the selected fillers to affect the polymer-polymer interfacial features, and in particular the interfacial tension.

Role of the interfacial features

Kinetically arresting the melt state dynamics of either of the phases of immiscible blends is a possible way to lower the volume fraction of the minority component at co-continuity. Such a condition can be achieved if nanoparticles selectively located inside one of the polymers arrange themselves in a space-spanning elastic network. Actually, in order that such a structure may preserve the three-dimensionality of the host polymer, the particles must be able to drag and pin the latter. On the other hand, the resulting extra polymer-polymer interfaces are thermodynamically unfavourable, unless the nanoparticles do not ensure a reduction of the polymer-polymer interfacial tension σ . In other words, the stability of co-continuity depends on a complex energetic balance involving the strength of the particle network and the mutual interactions among the polymer melts and solid phase. Contact angle

measurements were performed to estimate the effect of the fillers on the compatibility between the polymer phases. Although referring to high-temperature data would be more correct, here we consider the experimental values of the interfacial tensions as measured at room temperature. In fact, the strong assumption of linear dependence of σ on T to invoke in order to compute high temperature data, as well as the lack of reliable data of the $\partial\sigma/\partial T$ coefficient for our specific materials, would bring about unnecessary uncertainty about the conclusions.

The measured values of contact angles and the computed surface tensions are resumed in Table 3.2; the interfacial tensions between PLA and PA11 filled with the various types of nanoparticles are shown in Table 3.3.

Table 3.2: Experimental values of contact angle and surface energies.

Material	Contact Angle		Surface Energy		
	°		mJ/m ²		
	Water	Glycerol	σ	σ^d	σ^p
PLA	63.5	64.1	38.5	7.9	30.5
PA11	69.5	53.5	41.8	31.4	10.4
PA11-C1	73	65.2	32.1	16.9	15.2
PA11-S1	76.3	68.9	29.5	15.6	13.8
PA11-N1	94.9	84.1	20.5	16.4	4.1

Table 3.3: Interfacial tensions between PLA and various PA11-based nanocomposites.

Sample Pairs	σ_{ij} [mJ m ⁻²]
PLA/PA11	13.05
PLA/PA11-C1	4.35
PLA/PA11-S1	4.54
PLA/PA11-N1	13.86

Due to its aliphatic segments, PA11 is less polar than PLA. All three kinds of nanoparticles reduce the surface tension of PA11. However, in the case of CNTs such a result essentially reflects a drop of the polar component of PA11. Differently, σ^p increases when using the inorganic (although organo-modified) OMMT and MS. Ultimately, the data of interfacial tension indicate that CNTs do not appreciably alter the interfacial tension between the PLA and the filled PA11, while both OMMT and MS generate a significant decrease of σ_{ij} .

Provided the difference persists at the processing temperature, the lack of thermodynamic gain in terms of interfacial tension could destabilize the elongated domains of CNTs-filled PA11 which form during melt mixing despite their rheological gel-like behaviour. In contrast, both OMMT and MS seem able to partially relax the constraint of the interfacial tension. As a result, elongated domains of filled PA11 are stable enough to preserve interpenetrated structures with considerable interfacial area. A schematic of the morphology of the three nanocomposite blends is shown in Figure 3.13.

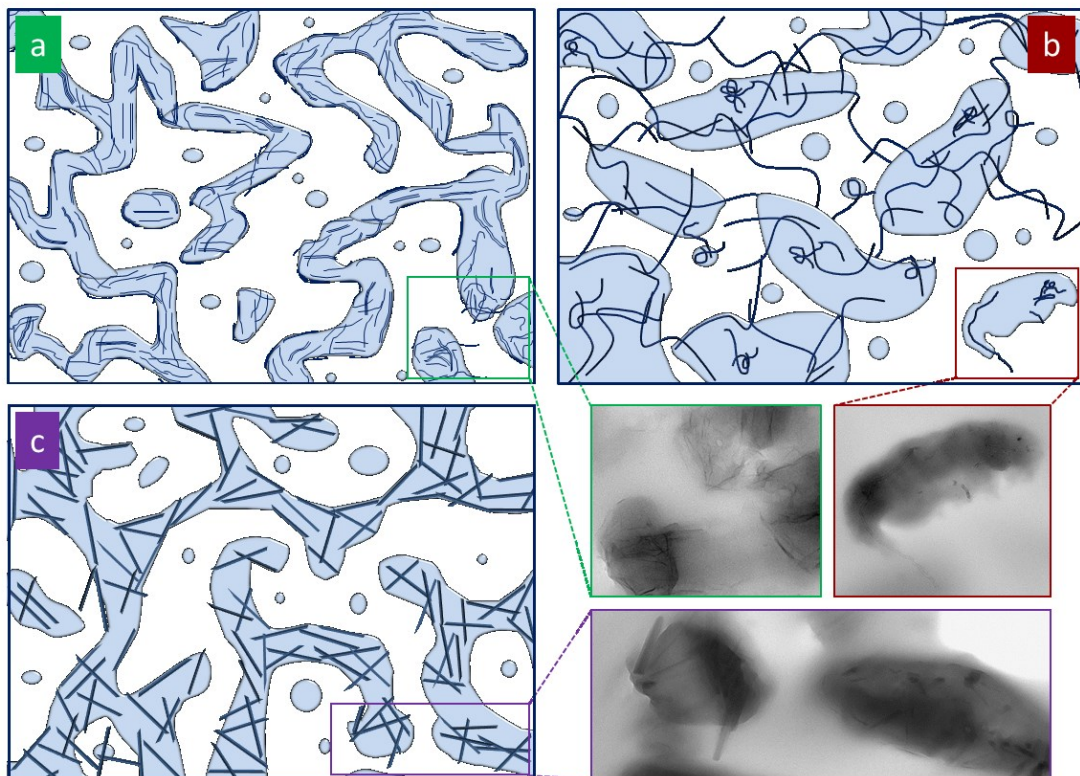


Fig. 3.13: Schematic illustration of the morphology of the filled blends at 70 % wt of PLA when the filled PA11 phase is at the gel-point: (a) PLA70-C3; (b) PLA70-N0.75; (c) PLA70-S6.

According to the previous considerations, it is stressed that CNTs percolation might occur irrespective of polymer phase co-continuity.

Finally, consider the greater effectiveness of OMMT compared to MS in inducing co-continuity. Both kinds of nanoparticles comparably reduce the interfacial tension between PLA and filled PA11. The differences between the two fillers can be hence essentially ascribed to their geometrical features. It is reasonable to expect that the flexible, plate-like OMMT adapt much better than the stiff, needle-like MS to the wavy, two-dimensional feature of the polymer-polymer interface. This picture is consistent with the detection of rigid rods

protruding from the PA11 drops noticed in the sample PLA90-S1.5 (see Figure 3.2). Moreover, besides bulk rheology and surface tension arguments, interfacial rheology should be also taken into account. Interfacially-located OMMT platelets mechanically hinder the shape relaxation of drops in polymer blends [28, 29], and this certainly contributes to some extent in preserving co-continuity. Unfortunately, isolating the interfacial contribution is a challenging task, and targeted analyses are needed to assess which one between surface rheology and bulk rheology plays the dominant role.

3.4. CONCLUSIONS

The possible underlying mechanisms of nanoparticles-induced co-continuity in immiscible polymer blends have been investigated through a comparative study on a blend of PLA and PA11 (PLA/PA11 70/30 wt/wt) filled with cloisite (OMMT), sepiolite (MS) and carbon nanotubes (CNTs). Specifically, we discussed the roles played by (*i*) bulk rheology of filled phase, (*ii*) self-networking propensity of nanoparticles and (*iii*) interfacial properties of the blend, which may be differently affected by changing chemistry and geometrical features of the nanoparticles.

Morphological and dynamic-mechanical analyses showed that the three fillers selectively distributed inside PA11, minor phase, and were all able to convert the drop-matrix morphology of the blend into a stable and highly co-continuous one, provided that a critical nanoparticles loading is exceeded.

Rheological analyses revealed that in the case of OMMT and MS the filler loading at which the morphological transition occurs corresponds to that at which a rheological transition from a liquid- to gel-like behaviour takes place in the filled polyamide, indicating the structuring of the filler inside the hosting phase. Conversely, the CNTs content necessary to promote co-continuity has been found much higher than needed to induce a comparable slowdown of the relaxation dynamics of the filled PA11 phase. Moreover, volume resistivity tests revealed that a space-spanning conductive CNTs network builds up across the sample even if the preferred PA11 phase is not continuous. These findings reveal that simply kinetically arresting the melt state relaxation dynamics of the filled polymer phase through the aggregation of nanoparticles into a percolating network may be not sufficient to promote co-continuity and other mechanisms may take part, concurrently and/or alternatively, in nanoparticle-induced co-continuity in immiscible polymer blends.

We believe that, among others, a critical role is played by the ability of nanoparticles to differently affect the properties of the blend interface. The data of interfacial tension indicated that CNTs do not appreciably alter the interfacial tension between the PLA and the filled PA11, while both OMMT and MS, which share a similar surface chemistry, generate a significant decrease of σ_{ij} . The lack of thermodynamic gain in terms of interfacial tension could destabilize the elongated domains of CNTs-filled PA11 which form during melt mixing despite their rheological gel-like behaviour.

With respect to MS, much lower contents of OMMT are needed to induce co-continuity. Both kinds of nanoparticles comparably reduce the interfacial tension between PLA and filled PA11. The differences between these two fillers may be essentially ascribed to their geometrical features, which affect differently the bulk rheology and, probably, also the surface rheology of the filled drops. It is reasonable to expect that, when the filler starts to accumulate at the drops contours, the flexible, plate-like OMMT adapts much better than the stiff, needle-like MS to the wavy, two-dimensional feature of the polymer-polymer interface, thus contributing in stabilizing elongated and irregular domains of the minor phase against break up or shape relaxation phenomena both thermodynamically and mechanically. The merging of these elongated structures during melt mixing eventually results into co-continuity. However, isolating the interfacial contribution remains a challenging task and more targeted analyses are needed to assess which one between surface rheology and bulk rheology plays the dominant role.

3.5. REFERENCES

- [1] Paul D. R., Bucknall C. B.; *Polymer Blends: Formulation & Performance*, John Wiley & Sons, New York **2000**.
- [2] Utracki LA.; *Commercial polymer blends*. London: Chapman and Hall; **1998** [Chapter 6].
- [3] *Formation of Co-continuous Structures in Melt-Mixed Immiscible Polymer Blends*; Pötschke P., Paul D. R.; *J Macromol Sci, Part C: Polymer Reviews*, 43:1, (**2003**) 87-141.
- [4] *Heat-Resistant Fully Bio-Based Nanocomposite Blends Based on Poly(lactic acid)*; Nuzzo A., Coiai S., Carroccio S. C., Dintcheva N. Tz., Gambarotti C., Filippone G.; *Macromol. Mater. Eng.* 299 (1) (**2014**) 31-40.
- [5] *Novel morphologies of poly(phenylene oxide) (PPO)/polyamide 6 (PA6) blend nanocomposites*; Li Y., Shimizu H., *Polymer* 45 (**2004**) 7381-7388.
- [6] *Morphology evolution of nanocomposites based on poly(phenylene sulfide)/poly(butylene terephthalate) blend*; Wu D., Wu L., Zhang M., Zhou W., Zhang Y.; *J Appl Polym Sci* 46 (**2008**) 1265-1279.
- [7] *Effect of Organoclay on the Morphology and Properties of Poly(propylene)/Poly[(butylene succinate)-co-adipate] Blends*; Ray S. S., Bandyopadhyay J., Bousmina M., *Macromol. Mater. Eng.* 292 (**2007**) 729-747.
- [8] *Co-continuous morphologies in polymer blends: a new model*; Willemse R.C., Posthuma de Boer A., Van Dam J., Gotsis A. D., *Polymer* 39 (24) (**1998**) 5879-5887
- [9] *Tailoring the morphology of polypropylene/polyamide 66 blend at an asymmetric composition by using organoclay and maleic anhydride grafted polypropylene*; Wang L., Shi C., Guo Z. X., Yu J., *Journal of Industrial and Engineering Chemistry* 20 (1) (**2014**) 259
- [10] *Retarded relaxation and breakup of deformed PA6 droplets filled with nanosilica in PS matrix during annealing*; Kong M., Huang Y., Chen G., Yang Q., Li G.; *Polymer* 52 (**2011**) 5231-5236.
- [11] *The dynamics of montmorillonite clay dispersion and morphology development in immiscible ethylene-propylene rubber/polypropylene blends*; Kontopoulou M., Liu Y., Austin J. R., Parent J. S.; *Polymer* 48 (**2007**) 4520-4528

- [12] *Influence of selective filling on rheological properties and phase inversion of two-phase polymer blends*; Steinmann S., Gronski W., Friedrich C.; *Polymer* 43 (2002) 4467-4477.
- [13] *Using organoclay to promote morphology refinement and co-continuity in high-density polyethylene/polyamide 6 blends-Effect of filler content and polymer matrix composition*; Filippone G., Dintcheva N.Tz., La Mantia F.P., Acierno D.; *Polymer* 51 (2010) 3956-3965.
- [14] *Kinetically Trapped Co-continuous Polymer Morphologies through Intraphase Gelation of Nanoparticles*; Li L., Miesch C., Sudeep P. K., Balazs A. C., Emrick T., Russell T. P., and Hayward R. C.; *Nano Lett.* 11 (2011) 1997-2003.
- [15] *Carbon black self-networking induced co-continuity of immiscible polymer blends*; Wu G., Li B., Jiang J.; *Polymer* 51 (2010) 2077-2083
- [16] *Morphology evolution of immiscible polymer blends as directed by nanoparticle self-agglomeration*; Cai X., Li B., Pan Y., Wu G.; *Polymer* 53 (2012) 259-266
- [17] *Cocontinuous morphology of immiscible high density polyethylene/polyamide 6 blend induced by multiwalled carbon nanotubes network*; Xiang F., Shi Y., Li X., Huang T., Chen C., Peng Y., Wang Y.; *European Polymer Journal* 48 (2) (2012) 350-361.
- [18] *Compatibilizing effect of a filler in binary polymer mixtures*; Nesterov A. E. and Lipatov Y. S.; *Polymer* 40 (5) (1999) 1347-1349
- [19] *Compatibilization of Immiscible Poly(propylene)/Polystyrene Blends Using Clay*; Wang Y., Zhang Q., Fu Q.; *Macromol Rapid Commun* 24 (2003) 231-235
- [20] *Role of organically modified layered silicate as an active interfacial modifier in immiscible polystyrene/polypropylene blends*; Ray S. S., Pouliot S., Bousmina M., Utracki L.A.; *Polymer* 45 (25) (2004) 8403-8413.
- [21] *Compatibilization efficiency of organoclay in an immiscible polycarbonate/poly(methyl methacrylate) blend*; Ray S. S. and Bousmina M.; *Macromolecular Rapid Communications* 26 (6) (2005) 450-455.
- [22] *A comparative thermal, optical, morphological and mechanical properties studies of pristine and C15A nanoclay-modified PC/PMMA blends: a critical evaluation of the role of nanoclay particles as compatibilizers*; Singh A. K., Prakash R., Pandey D.; *RSC Advances* 3 (35) (2013) 15411

- [23] *Efficiently suppressing coalescence in polymer blends using nanoparticles: role of interfacial rheology*; Vandebril S., Vermant J., Moldenaers P.; *Soft Matter* 6 (14) (2010) 3353-3362.
- [24] *The role of organically modified layered silicate in the breakup and coalescence of droplets in PBT/PE blends*; Hong J. S., Namkung H., Ahn K. H., Lee S. J., Kim C.; *Polymer* 47 (11) (2006) 3967-3975.
- [25] *Interfacial tension reduction in PBT/PE/clay nanocomposite*; Hong J. S., Kim Y. K., Ahn K. H., Lee S. J., Kim C.; *Rheologica acta* 46 (4) (2007) 469-478.
- [26] *Compatibilizing bulk polymer blends by using organoclays*; Si M., Araki T., Ade H., Kilcoyne A. L. D., Fisher R., Sokolov J. C., Rafailovich M. H.; *Macromolecules* 39 (14) (2006) 4793-4801.
- [27] *Pickering emulsions: interfacial tension, colloidal layer morphology, and trapped-particle motion*; Vignati E., Piazza R., Lockhart T. P.; *Langmuir* 19(17) (2003) 6650-6656.
- [28] *Role of Interface Rheology in Altering the Onset of Co-Continuity in Nanoparticle-Filled Polymer Blends*; Filippone G., Romeo G., Acierno D.; *Macromolecular Materials and Engineering* 296 (7) (2011) 658-665.
- [29] *Assembly of plate-like nanoparticles in immiscible polymer blends – effect of the presence of a preferred liquid–liquid interface*; Filippone G., Causa A., Salzano de Luna M., Sanguigno L., D. Acierno; *Soft Matter* (2014) DOI: 10.1039/C3SM52995A.
- [30] *Clustering of Coated Droplets in Clay-Filled Polymer Blends*, Filippone G., Acierno D.; *Macromolecular Materials and Engineering* 297 (9) (2012) 923-928.
- [31] S. Wu, *Polymer Interface and Adhesion*, Marcel Dekker, New York 1982.
- [32] D. K. Owens, R. C. Wendt, *J. Appl. Polym. Sci.* 13 (1969) 1741.
- [33] *Polar interactions at liquid/polymer interfaces*; Carrè A.; *J. Adhesion Sci. Technol.* 21 (10) (2007) 961-981.
- [34] *Uneven distribution of nanoparticles in immiscible fluids: Morphology development in polymer blends*; Fenouillot F., Cassagnau P., Majestè J.-C.; *Polymer* 50 (2009) 1333-1350
- [35] *Comparison of methods for the detection of cocontinuity in poly (ethylene oxide)/polystyrene blends*; Galloway J. A., Macosko C. W., *Polymer Engineering & Science* 44 (4) (2004) 714-727.

- [36] *Poly(lactic acid): plasticization and properties of biodegradable multiphase systems*; Martin O., Avérous L., Polymer 42 (14) (2001) 6209-6219.
- [37] *Phase continuity detection and phase inversion phenomena in immiscible polypropylene/polystyrene blends with different viscosity ratios*; Omonov T.S., Harrats C., Moldenaers P., Groeninckx G.; Polymer 48 (2007) 5917-5927.
- [38] *A unifying approach for the linear viscoelasticity of polymer nanocomposites*; Filippone G. and Salzano de Luna M., Macromolecules 45 (21) (2012) 8853–8860.
- [39] *Rheology of polymers near liquid-solid transitions. Neutron spin echo spectroscopy viscoelasticity rheology*; Winter H. H., and Mours M.; Springer Berlin Heidelberg (1997) 165-234.
- [40] *Morphology and electrical resistivity of melt mixed blends of polyethylene and carbon nanotube filled polycarbonate*; Pötschke P., Bhattacharyya A.R., Janke A., Polymer 44 (26) (2003) 8061-8069.

CONCLUSIONS

Nowadays, public concerns about the environment, climate change, and limited fossil fuel resources are driving governments, companies, and scientists to find an alternative to crude oil.

Bio-polymers, meant as polymers which are biodegradable and/or derived from biological resources, can form the basis for an environmentally preferable, sustainable alternative to current materials based exclusively on petroleum feedstock. Together with the high costs of production, the most limiting factor that makes a major shift to bio-polymers impractical is the fact that they exhibit physical and mechanical properties typically lower than the competing conventional plastics. This is the key point that most of the industrial and academic world underlines and is facing and this has been the main challenge in this dissertation.

In particular, the overall aim of the research activity has been the individuation of bio-based and eco-sustainable polymeric formulations with improved properties and suitable for applications of technological interest.

Among bio-polymers, we have focused on poly lactic acid (PLA), which until now represents the most promising candidate for the substitution, totally or partially, of many petroleum-based polymers. In fact, as widely discussed in the introduction of the thesis, PLA exhibits the best compromise among eco-sustainability, physical and mechanical features and industrial development prospect. However, the low mechanical resistance at high temperature (Heat Deflection Temperature = $50\div 60^{\circ}\text{C}$) has prevented its complete access to relevant industrial sectors.

The first part of the thesis (Part 1) has been dedicated to finding viable and simple routes to improve the poor mechanical properties of the amorphous PLA above its glass transition. The goal was achieved by blending PLA with Polyamide 11 (PA11), a semicrystalline, heat resistant and bio-based polymer, with lower eco-sustainability features with respect to PLA. In order to reduce the content of the less eco-sustainable PA11, while preserving the heat resistance of the blend, the continuity of the PA11 phase was promoted by the addition of small amounts of an organo-modified montmorillonite (OMMT). The selective positioning of the OMMT inside the PA11 and at the PLA/PA11 interface turned the blend morphology of a blend at 70 wt% of PLA from drop/matrix into a stable co-continuous one. In such a way,

remarkable improvements of the high temperature mechanical performances were achieved owing to the OMMT-rich PA11 framework, which interpenetrates the PLA, major phase, and contributes to bear stresses up to ~ 160 °C, i.e. ~ 100 °C above the PLA glass transition. Neither the mere reinforcing action of the filler nor changes in the crystallinity of the polymeric blend constituents was responsible for the observed improvement. Looking for optimized formulations, the room temperature tensile properties were investigated to critically test the degree of embrittlement of the material upon addition of OMMT. We found that reducing the PA11 content results in the loss of the high temperature creep resistance. On the other hand, increasing the OMMT content in the blend at 70 wt% of PLA may bring about an excessive material embrittlement at room temperature.

Nanoparticles-induced co-continuity in immiscible polymer blends has been previously observed in many systems, the underlying mechanisms being still unclear. Additional goal of this thesis has been to better clarify the mechanisms behind the co-continuity development observed in our bio-based nanocomposite polymer blend through a comparative study among three different kinds of fillers added to the blend at 70 wt% of PLA. Specifically, we used: cloisite (OMMT), sepiolite (MS) or carbon nanotubes (CNTs). We have discussed the roles played by (i) bulk rheology of filled phase, (ii) self-networking propensity of nanoparticles and (iii) interfacial properties of the blend, which may be differently affected by changing chemistry and geometrical features of nanoparticles.

Morphological and dynamic-mechanical analyses showed that, as in the case of OMMT, also MS and CNTs selectively distributed inside PA11, minor phase, and they were able to convert the drop-matrix morphology of the blend into a stable and highly co-continuous one, provided a critical nanoparticles loading is exceeded.

Rheological analyses revealed that in the case of OMMT and MS the filler loading at which the morphological transition occurs corresponds to that at which a rheological transition from a liquid- to gel-like behaviour takes place in the filled polyamide, indicating the structuring of the filler inside the hosting phase. Conversely, the CNTs content necessary to promote co-continuity has been found much higher than needed to induce a comparable slowdown of the relaxation dynamics of the filled PA11 phase. Moreover, volume resistivity tests revealed that a space-spanning conductive CNTs network builds up across the sample even if the preferred PA11 phase is not continuous. These findings reveal that simply kinetically arresting the melt state relaxation dynamics of the filled polymer phase by the aggregation of nanoparticles into a percolating network may be not sufficient to promote co-continuity and other mechanisms

may take part, concurrently and/or alternatively, in nanoparticle-induced co-continuity in immiscible polymer blends.

We believe that, among others, a critical role is played by the ability of nanoparticles to differently affect the properties of the blend interface. The data of interfacial tension indicated that CNTs do not appreciably alter the interfacial tension between the PLA and the filled PA11, while both OMMT and MS, which share a similar surface chemistry, generate a significant decrease of σ_{ij} . The lack of thermodynamic gain in terms of interfacial tension could destabilize the elongated domains of CNTs-filled PA11 which form during melt mixing despite their rheological gel-like behaviour. In contrast, both OMMT and MS seem able to partially relax the constraint of the interfacial tension. As a result, elongated domains of filled PA11 are stable enough to preserve interpenetrated structures with considerable interfacial area.

With regards to MS, much lower contents of OMMT are needed to induce co-continuity. Both kinds of nanoparticles comparably reduce the interfacial tension between PLA and filled PA11. The differences between these two fillers may be essentially ascribed to their geometrical features, which affect differently the bulk rheology and, probably, also the surface rheology of the filled drops. It is reasonable to expect that, when the filler starts to accumulate at the drops contours, the flexible, plate-like OMMT adapts much better than the stiff, needle-like MS to the wavy, two-dimensional feature of the polymer-polymer interface, thus contributing to stabilizing elongated and irregular domains of the minor phase against break up or shape relaxation phenomena both thermodynamically and mechanically. The merging of these structures eventually results into co-continuity. However, isolating the interfacial contribution remains a challenging task and more targeted analyses are needed to assess which one between surface rheology and bulk rheology plays the dominant role.

Concluding, our results provide the experimental evidence that a judicious selection of the blend constituents, combined with a clever manipulation of the blend microstructure through the addition of nanoparticles, may represent a simple and general strategy to obtain “engineered” materials with enhanced properties. Therefore, applying such an approach to bio-polymers is certainly a viable route to expanding and diversifying the field of possible applications of such promising materials.

Appendix

A.1. Melt state stability: linear viscoelasticity and degradation phenomena

In this section we present a rheological analysis of pure PLA, pure PA11 and PA11/OMMT, which are the constituents of the studied blends. In particular, we focus on the degradation phenomena (chain scission, chain extension, branching/crosslinking phenomena) which may occur during processing and rheological characterization. It is important to observe that the extrusions and rheological tests were performed in a dry nitrogen atmosphere, while the compression molding step to produce the specimens was carried out in air. In the former case the degradation is essentially thermally-activated, while thermo-oxidative degradation can take place on the outer surfaces of the disks prepared by compression-molding.

Performing oscillatory frequency scans in the linear regime is the simplest way to inspect the relaxation spectrum of a viscoelastic fluid. Such kind of test, however, strictly requires the stability of the properties in the melt state in the course of the test. Regarding this aspect, the thermally-induced changes in molecular structure of PLA and PA11 reflect in the time evolution of the linear viscoelastic properties, probed during dynamic time sweep tests (i.e. tests during which the linear viscoelastic moduli at fixed frequency and strain amplitude are monitored as a function of time).

The typically low stability of the polymers in the melt state precludes long time measurements. As a consequence, to measure the rheological characteristics of time-changing samples such as our PLA and PA11-based samples, a well-controlled experimental protocol has been established. Such experimental protocol, which is described in detail in the next section, has been used in this work to test the rheological behavior of pure PLA, pure PA11 and PA11/OMMT, PA11/MS, PA11/CNTs nanocomposites.

On the other hand, the outcomes of rheological investigations allow to study the alterations of the macromolecular structures induced by the exposure of the studied polymers to high temperatures. Chain scission, branching/crosslinking, chain extension have been documented for various thermally-degraded thermoplastic polymers, such as PET [1], polyamides [2-4],

PLA [5], and polyolefins [6]. These phenomena alter the molecular weight, its distribution (polydispersity) and the polymeric chain structure (branching/crosslinking), which, in turn, affect the melt rheology. Many models have been proposed in literature to correlate structural changes of the polymer chains to rheological properties like zero-shear viscosity, degree of shear thinning, storage modulus, loss modulus and phase angle [7-14]. However, the rheological analysis is often insufficient to differentiate among the various degradation mechanisms, which may occur singly or simultaneously. As an example, discriminating, even qualitatively, between the effects of branching and polydispersity on rheological behavior is still a challenging task. As a consequence, in many cases it may be difficult to discern between phenomena with similar rheological effects, such as for example branching and chain extension, or to evaluate the relative predominance of chain scission and branching potentially occurring simultaneously. The task becomes even more difficult when nanoparticles, specifically OMMT, are added to the polymers. Interactions between individual particles/aggregates and the matrix, as well as between particles, interfere with the polymer chains motion and relaxation, thus affecting the overall rheological behavior. On the other hand, nanoparticles may chemically or physically interfere with the degradation mechanisms, thus contributing in altering the molecular chain structure of the host polymer. Therefore, the rheological analysis of nanofilled polymers undergoing thermal degradation requires the employ of complementary methods to determine the alterations in polymer molecular weight and its distribution. Here we study the thermal degradation phenomena which occur in PLA, PA11 and PA11/OMMT through a critical analysis of data coming from rheological analysis and size exclusion chromatography (SEC-MALLS).

A.1.1. Experimental procedure

PA11/OMMT nanocomposites (PA11-C_x, where x denotes the weight percent of OMMT in the sample) were prepared by compounding the constituents in a co-rotating twin-screw extruder (Minilab Micro-compounder by Thermohaake) equipped with a cylindrical capillary die (diameter 1.5 mm, length 30 mm). The polymer and the filler, dried overnight under vacuum at T=80°C, were melt compounded under gaseous nitrogen at T=215°C and screw speed 80 rpm, corresponding to average shear rates of ~50 s⁻¹. The residence times, carefully controlled owing to an integrated back-flow channel, were set to ~1 min for each blend. Composites with three different concentrations of OMMT, namely 3, 6, 9 wt%, were prepared. The extruded materials were granulated, dried again and compression-molded in air

using a laboratory press (LP-20B by Lab. Tech. Eng. Company Ltd.) at $T=215^{\circ}\text{C}$ under a pressure $P\approx 40\text{ MPa}$ for 5 min, then the samples were cooled down to room temperature at about $30^{\circ}\text{C min}^{-1}$. Pure PLA and pure PA11 were processed under similar conditions and used as reference materials.

Rheological analyses were carried out under nitrogen atmosphere at 215°C using a strain-controlled rotational rheometer (mod. ARES by Rheometrics Scientific) in parallel plate geometry (plate diameter 25 mm). Low-frequency ($\omega=1\text{ rad s}^{-1}$) time sweep measurements were performed on pure PA11 and PLA in linear regime, which was preliminarily estimated through strain scan experiments. The time evolution of the linear viscoelastic properties demonstrates the low stability of the polymers in the melt state. Therefore, long time measurements are precluded. Additionally, since changes in the rheological properties occur during testing, a well-controlled experimental protocol has been established to ensure the data reproducibility. In particular, a sequence of four consecutive frequency scans was performed on each sample from $\omega=10^2$ down to $10^{-1}\text{ rad s}^{-1}$ in the linear regime. The elastic (G') and viscous (G'') shear moduli were recorded as a function of angular frequency. Then, the moduli at time-zero were extrapolated for each value of the frequency.

Size-exclusion chromatography (SEC-MALLS) were performed on PA11 and PA11/OMMT composites at the end of each rheological step to follow the changes of molecular weight and its distribution.

A.1.2. Thermal degradation of pure PLA

The thermally-promoted changes in molecular structure of PLA are proved by the time evolution of the linear viscoelastic properties obtained during the dynamic time sweep test.

In Figure A.1 the PLA complex viscosity, η^* , is plotted as a function of time.

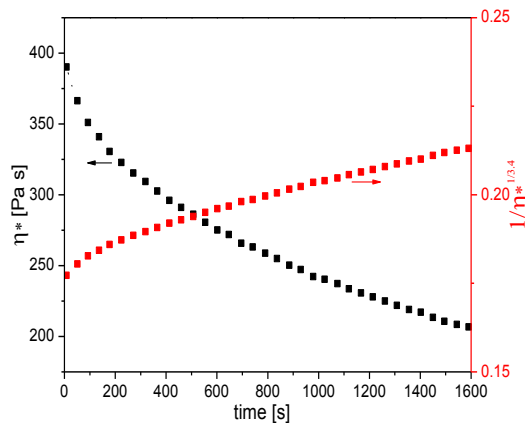


Fig. A.1. Time evolution of the PLA complex viscosity η^* and linearization of the rheological data.

The (complex) viscosity decreases during time, reflecting the thermal degradation of the polymer. The reduction of the viscosity is ascribed to the decrease in the weight-average molecular weight (M_w) due to several different complex degradation processes which causes a random chain scission [15]. Some mechanical degradation may occur during rheological tests in addition to thermal degradation. However, the very low strain amplitudes involved (less than 5%) suggest that thermal degradation is largely predominant. The plot of $1/\eta^{3.4}$ versus time exhibits a linear trend, suggesting that the thermal degradation behavior of PLA is consistent with a first-order chain scission, quite common in biodegradable polyesters [16, 17]. According to this first-order model, because of random chain scission, M_w changes during time t scaling as $M_w \sim 1/t$. For linear polymers the viscosity η scales with M_w as $\eta \sim M_w^{3.4}$ [18]. Thus, the linear trend $1/\eta^{3.4} \sim t$.

In Figure A.2.a the elastic (G') and viscous (G'') shear moduli are plotted as a function of frequency. In particular, to get linear viscoelastic properties before the degradation process, four consecutive frequency scans have been performed. Then, for each frequency the experimental points have been plotted as a function of the time at which they were acquired, and the moduli at “time zero” have been finally extrapolated. The previous procedure is summarized for some representative frequencies in Figure A.2.b.

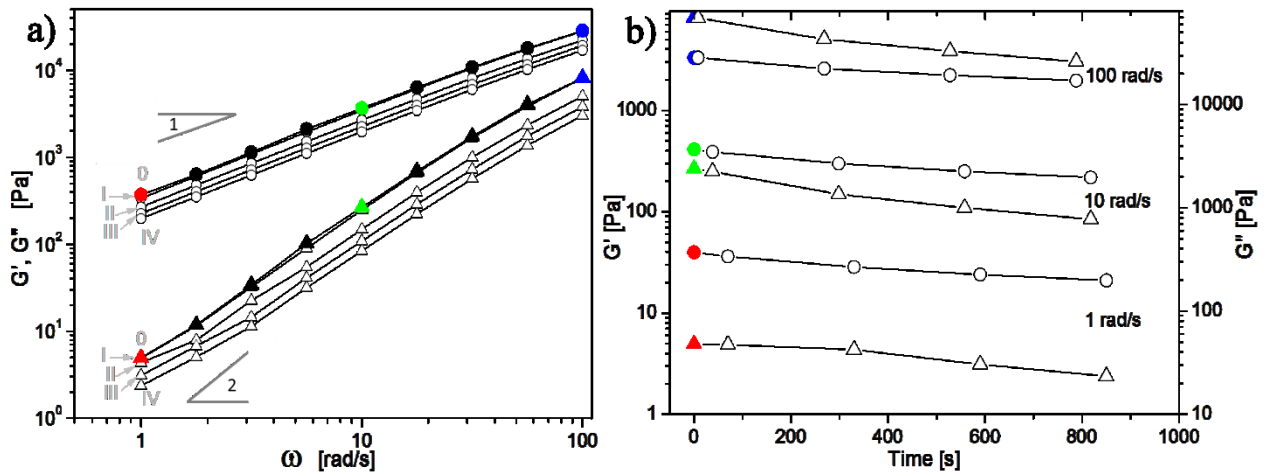


Fig. A.2: (a) Frequency dependence of elastic G' (triangles) and viscous G'' (circles) moduli obtained during the four consecutive frequency scans (from I to IV, empty symbols) performed on PLA sample. Full symbols are the moduli extrapolated at time-zero according to the procedure described in (b). The moduli are plotted as a function of the time at which they were acquired. Colored symbols are the extrapolated moduli at time-zero for some representative frequencies.

A decrease of both moduli is observed, with G' which degrades a bit faster than G'' . This is expected since the melt elasticity is very sensitive to the molecular weight. Focusing on the moduli at “time zero”, a predominantly viscous feature ($G'' \gg G'$) emerges in the whole range

of frequency investigated, and the typical terminal Maxwellian behavior (G' and G'' scaling as ω^2 and ω , respectively) is approached at low frequencies.

5.1.3. Thermal degradation of PA11

As in the case of PLA, also the rheological behavior of the PA11 reflects its low thermal stability. The PA11 complex viscosity is plotted in Figure A.3 as a function of time.

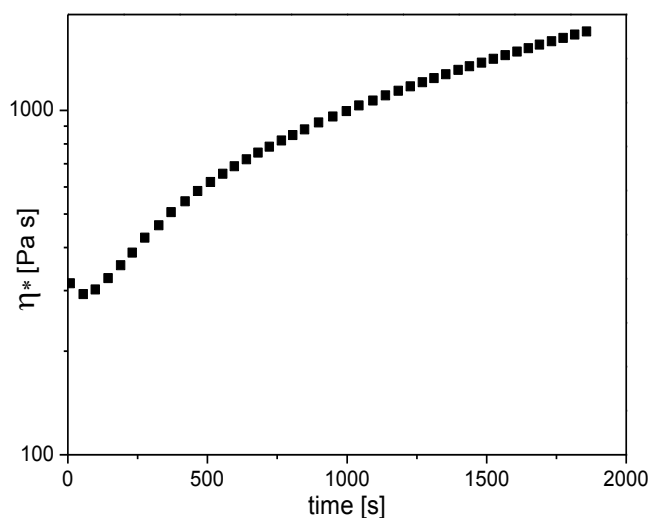


Fig. A.3: Time evolution of the PA11 complex viscosity η^* .

Unlike the PLA, the complex viscosity of PA11 noticeably increases during time, which reflects a post-condensation reaction of the polymer that leads to an increase in molecular weight. A similar mechanism is well known for nylons. The poly-condensation of polyamides is a reversible reaction between amine groups and carboxylic groups that produces amide linkages and water [2-4]. As a result, chain branching and/or extension take place. Polyamide degradation may occur at high temperature (around 200°C) in oxygen-poor atmosphere, which are the conditions adopted in this work. Looking at Figure A.3, it can be noticed that the increase of the complex viscosity is faster in the earlier stages. Over long timescales, when the molecular weight is high, the degradation kinetic slows down, being controlled by the diffusion of the reactive end groups.

The overlay of the linear viscoelastic moduli of PA11 is reported in Figure A.4 as a function of frequency as obtained during the four consecutive frequency scans. The moduli extrapolated at “time zero” are reported as full symbols.

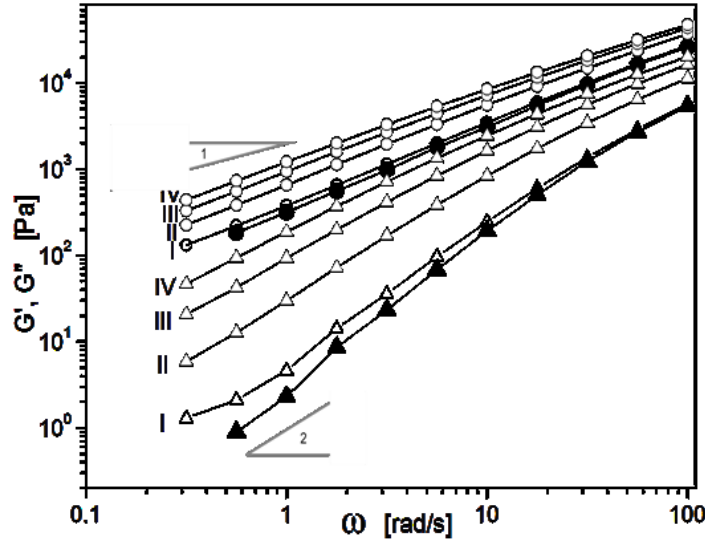


Fig. A.4: Frequency dependence of elastic G' (triangles) and viscous G'' (circles) moduli obtained during the four consecutive frequency scans performed on PA11 (from I to IV, empty symbols). Full symbols are the moduli extrapolated at “time-zero”.

The elasticity remarkably increases during time, reflecting the increase of M_w . The growth rate of G' is more pronounced at low frequencies. In fact, the segmental relaxation governing the response of a polymer at high frequencies is typically insensitive to M_w , as well as to difference in polymer architecture [18]. A similar trend is also detected for G'' , but the ageing effect appears less prominent. The thermally-promoted changes in molecular weight and, probably, in chain architecture slow down the relaxation process and changes the shape of G' curve. More precisely, the relaxation spectrum progressively widens and the terminal behavior disappears, at least in the investigated frequency range. Such a behavior may be correlated to the increased polydispersity and/or chain branching, as indicated more clearly by Van Gorp plot shown in Figure A.5 [19]. The loss phase angle, $\delta = \arctan(G''/G')$, is reported as a function of the complex modulus, $G^* = \sqrt{G'^2 + G''^2}$. Hatzikiriakos used this kind of plot aiming at correlating the rheological response to the presence of long chain branching and/or polydispersity [20]. More specifically, as the degree of polydispersity and/or branching increases the mode and the characteristic times of polymer relaxation process increase. As a consequence, the Van-Gorp plot becomes less steep, the terminal flow plateau at 90° is reached at lower values of G^* and the area under the Van-Gorp curve decreases [21, 22]. The effects of polydispersity and branching on rheological properties, such as viscoelastic moduli, shear thinning behavior, Van-Gorp plot, are similar. On the other hand, polydispersity can be affected by the occurrence of chain extension and/or chain branching. Chain extension and branching can alter the molecular weight and its distribution, thus the polydispersity, but, unlike chain branching, chain extension results in the formation of longer chains, which

remain linear. Therefore, to discern between polydispersity and branching, rheology need to be coupled to SEC-MALLS analyses.

Figure A.5 reveals that the Van Gulp area decreases during time. We are inclined to ascribe such a decrease to the occurrence of chain branching. In fact, SEC-MALLS results, summarized in Table A.1, reveal the increase of molecular weight without significant alterations in polydispersity index. Linear chains, despite with a higher molecular weight, could not justify the trend of Van-Gulp curves.

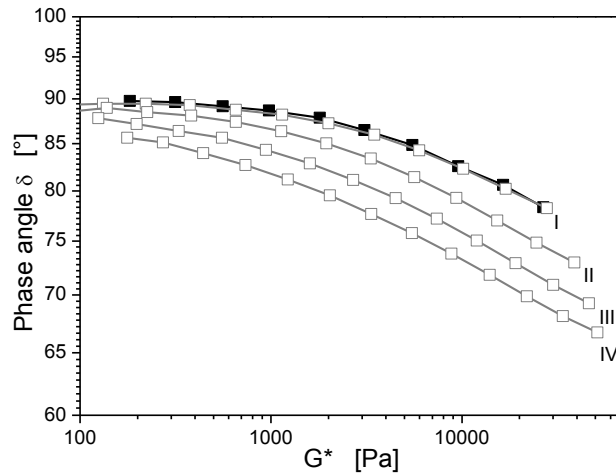


Fig. A.5: Van Gulp plots computed from the four consecutive frequency scans performed on PA11 (from I to IV, empty symbols). The Van Gulp plot extrapolated at “time-zero” is reported as well (full symbols).

Table A.1: SEC-MALS of PA11 before and after the rheological characterization

Sample	M_p [g/mol]	M_n [g/mol]	M_w [g/mol]	M_z [g/mol]	M_w/M_n	M_z/M_w	R_{gp} [nm]
PA11 before rheological characterization	28,071	16,814	28,853	43,249	1.72	1.50	9.5
PA11 after IV frequency sweep	34,133	22,251	44,840	77,137	2.02	1.72	13.6

A.1.4. Thermal degradation of PA11/OMMT nanocomposites

Since the organoclay resides inside the PA11 phase in our PLA/PA11/OMMT blends, we focused on the rheological behavior of PA11-organoclay nanocomposites. The addition of nanoparticles is well-known to radically alter the linear viscoelastic properties of a polymer matrix. However, besides the effects on the relaxation dynamics of polymer chains, the impact of the organoclay needs to be interpreted by considering also their possible effect on the

degradation pathways of the PA11. Regarding the latter aspect, a molecular weight reduction of the host polymer has been documented for various polyamide-organoclay nanocomposites prepared by melt processing due to a catalytic effect of the nanoparticles, which promote the cleavage of the polymer chains under thermo-oxidative conditions [23-25]. In particular, the double bonds in the alkyl ammonium surfactant of the organo-modified clay are susceptible to free radical formation [26-28]. In turn, these free radicals can attack the polyamide resulting in chain scission, i.e. a reduction in polymer molecular weight. The higher the number of double bonds in the organic surfactant, the greater the degradation. However, alternative not thermo-oxidative degradation pathways are also proposed. As an example, Xie et al. showed that alkyl ammonium organoclays decompose between 200 and 300°C producing, among other organic species, α -olefins and amines which is suggestive of the Hofmann elimination mechanism [29, 30]. This mechanism generally occurs when a quaternary ammonium hydroxide is converted at high temperatures into an alkene and an amine (see Figure A.6.a). However, in the case of organoclays, elimination of the ammonium modifier may result in a substitution of the ammonium linkage on the clay with a hydrogen proton on the β -carbon (Figure A.6.b). Possible evidence of protons bound to clay surface has been reported by Davis et al. [31]. Ultimately, the α -olefins, by-products, or intermediates produced in this reaction could attack the polymer.

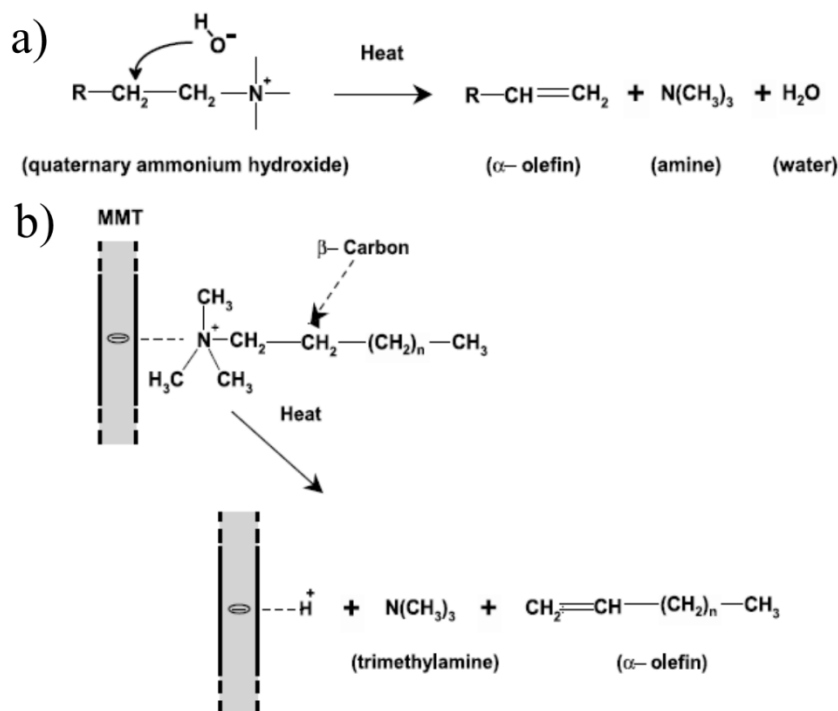


Fig. A.6: The Hofmann elimination reaction for quaternary ammonium compounds: (a) general reaction scheme and (b) a proposed scheme for organically modified MMT.

Summarizing, when Cloisite 30B is added to PA11, two competitive chemical phenomena could take place: (i) the PA11 matrix at high temperatures experiences poly-condensation phenomena, which result in an increase of M_w ; (ii) on the other hand, the nanoparticles may catalyze the cleavage of the polymer chains, causing a lowering of M_w .

The results of SEC-MALS for some PA11/OMMT composites before and after the rheological characterization are reported in Table A.2.

Table A.2: SEC of some representative samples

Designation	Sample	M_n	M_w	M_w/M_n
		[g/mol]	[g/mol]	
A	PA11 before rheological characterization	16.814	28.853	1.72
B	PA11 after IV frequency sweep	22.251	44.840	2.02
C	PA11-C3 before rheological characterization	14.026	25.411	1.81
D	PA11-C3 after IV frequency sweep	19.544	38.959	1.99
E	PA11-C9 after IV frequency sweep	19,491	41,134	2.11
Comparison	Effect of....	Percentage Variation		
b vs a	Temperature on PA11 degradation during rheological characterization (not oxidative conditions)	32.3	55.4	17.4
c vs a	OMMT addition on PA11 degradation during processing (extrusion under nitrogen atmosphere and compression moulding in air)	16.6	-11.9	5.6
d vs c	OMMT addition on PA11 degradation during rheological characterization (not oxidative conditions)	39.3	53.3	10.0
e vs d	OMMT content on PA11 degradation during rheological characterization (not oxidative conditions)	-0.3	5.6	5.9

The PA11-C3 sample exhibits a lower M_w than pure PA11 after the extrusion under nitrogen atmosphere and compression moulding in air. This can be ascribed to two phenomena. As extensively discussed by other authors and summarized above, Cloisite 30B can catalyze the cleavage of polyamide chains during processing. Therefore, the lower M_w of PA11-C3 sample can be the consequence of filler-induced chain scission, which could occur concurrently and/or alternatively to thermally-induced poly-condensation of PA11. However, we cannot completely exclude that the organoclay may hinder chain branching through a shielding mechanism of polymer chains. We can suppose that the latter is favored by the good exfoliation degree of OMMT in PA11 matrix, demonstrated by both WAXD (see Figure 2.4) and dynamic-mechanical analyses (see Figure 2.8).

After rheological characterization an increase of M_w is observed for the filled samples PA11-C3 and PA11-C9. An almost comparable percentage increment of M_w is observed for filled and pure PA11, suggesting that OMMT does not significantly alter the degradation pathways of PA11, experimented during rheological characterization.

Consider now the rheological response of PA11/OMMT composites.

Figure A.7 shows the elastic modulus (normalized over its value at “time zero”) as a function of time at which it was acquired during the four consecutive frequency scans performed on the neat and OMMT-filled PA11.

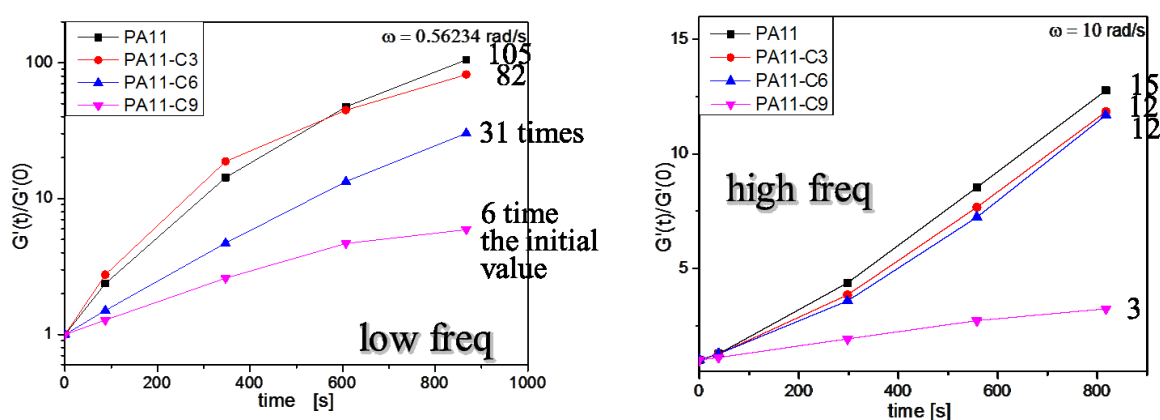


Fig. A.7: Elastic modulus (normalized over its value at time zero) as a function of time for the neat and OMMT-filled PA11.

The elastic modulus grows during time for all samples, the growth rate being more prominent at low frequencies when the relaxation dynamics of large portions of macromolecules are probed. The addition of filler remarkably reduces the growth of G' . Such a reduction becomes more pronounced increasing the filler content. SEC-MALLS data revealed that, irrespective of OMMT presence and content, the polymer matrix undergoes comparable modifications of molecular weight and its distribution. Therefore, in the present case, the slower G' increase during time for the filled samples, compared to the pristine PA11, should not be ascribed to different chemical alterations of the hosting matrix possibly induced by OMMT. We believe that such a rheological behavior originates from the orientation of nanoparticles induced by the squeezing flow experimented during sample loading, as reported by Macosko et al. for PC/Graphene composites. Above a critical concentration, excluded volume interactions between anisotropic nanoparticles may prevent the relaxation of the anisotropic state induced by squeezing or shear flows. Orientation of nanoparticles often results in a decrease of viscosity, storage and loss moduli [32]. However, more targeted rheological analyses are necessary to verify the latter hypothesis. Additionally, other characterization techniques need

to be performed, such as FTIR and MALDI to assess the effective degradation pathways experimented by pure and OMMT-filled PA11.

A.2. References

- [1] *Chain branching detection by Cole-Cole modeling of rheological properties changes during PET mechanical recycling*; Nait-Ali K.L., Bergeret A., Ferry L., Colin X.; Polymer Testing 31 (2012) 500-504.
- [2] *Degradation of polyamide 11 in rotational moulding*; Maria Jovita Oliveira, Gabriela Botelho; Polym. Degrad. Stab. 93 (2008) 139-146.
- [3] *Rheological behavior of polyamide 11 with varying initial moisture content*; Acierno S. and Van Puyvelde P.; J. Appl Polym Sci 97 (2005) 666-670.
- [4] *Postcondensation and oxidation processes in molten polyamide 6*; Marechal P., Legras R., Dekoninck J. M.; J. Polym. Sci. Part A Polym. Chem. 31 (1993) 2057-67.
- [5] *Mechanistic aspects of the thermal degradation of poly(lactic acid) and poly(b-hydroxybutyric acid)*; Kopinke F.D., Mackenzie K.; J Anal Appl Pyrolysis 40 (1997) 43-53.
- [6] *Competition Between Chain Scission and Branching Formation in the Processing of High-Density Polyethylene: Effect of Processing Parameters and of Stabilizers*; Scaffaro R., La Mantia F.P., Botta L., Morreale M., Dintcheva N. Tz., Mariani P.; Polym Eng Sci (2009).
- [7] *Influence of long-chain branching on linear viscoelastic flow properties and dielectric relaxation of polycarbonates*; Liu C., Chen P., He J., Fan Q., Polymer 45 (2004) 2803-2812.
- [8] *Work of fracture of PBT/PC blend: effect of specimen size, geometry, and rate of testing*; S. Hashemi, Polym. Eng. Sci. 37 (1997) 912-921.
- [9] *Effect of molecular structure on the linear viscoelastic behavior of poly-ethylene*; Wood-Adams P.M., Dealy J.M., De Groot A.W., Redwine O.D.; Macromolecules 33 (2000) 7489-7499.
- [10] *Reactive dual-component compatibilizers for polycarbonate/high-density polyethylene blends*; Mascia L., Valenza A.; Adv. Polym. Technol. 14 (1995) 327-335.

- [11] *Polycarbonate/ABS blends: a literature review*; R. Greco, A. Sorrentino; Adv. Polym. Technol. 13 (1994) 249-258.
- [12] *Phase morphology of polystyrene-polyarylate block copolymer/polycarbonate blends and their application to disk substrates*; Ohishi H., Ikehara T., Nishi T., J. Appl. Polym. Sci. 82 (2001) 2566-2582.
- [13] *Time-temperature superposition for polymeric blends*; Van Gurp M., Palmen J.; Rheol Bull. 67 (1998) 5–8.
- [14] *On the use of time-temperature superposition in multicomponent/multiphase polymer systems*; Han C.D., Kim J.K., Polymer 34 (1993) 2533-2539.
- [15] *Thermal decomposition of biodegradable polyesters-II. Poly(lactic acid)*; Kopinke F.-D., Remmler M., Mackenzie K., Möder M., Wachsen O., Polym. Degrad. and Stab. 43 (1996) 329-342.
- [16] *Thermal degradation kinetics of poly (3-hydroxybutyrate-co-3-hydroxyhexanoate)*; Daly P. A., Bruce D. A., Melik D. H., Harrison G. M.; J. Appl. Polym. Sci. 98 (2005) 66-74.
- [17] *Steady shear and dynamic properties of biodegradable polyesters*; Ramkumar D. H. S., Bhattacharya M.; Polym. Eng. Sci. 38 (1998) 1426-1435.
- [18] Larson R.G. The structure and rheology of complex fluids. New York: Oxford University Press; 1999.
- [19] M. van Gurp, J. Palmen; Rheology Bulletin, 67 (1) (1998) 5-8.
- [20] *Long chain branching and polydispersity effects on the rheological properties of polyethylenes*; Hatzikiriakos S. G.; Polym Eng Sci 40 (11) (2000) 2279-2287.
- [21] *Van Gurp-Palmen-Plot: a way to characterize polydispersity of linear polymers*; Trinkle S., Friedrich C.; Rheologica acta 40 (2001) 322-328.
- [22] *Van Gurp-Palmen-Plot II – classification of long chain branched polymers by their topology*; Trinkle S., Walter P., Friedrich C.; Rheologica acta 41 (2002) 103-113.
- [23] *Nylon 6 nanocomposites: The effect of matrix molecular weight*; Fornes T. D., Yoon P. J., Keskkula H., Paul D. R.; Polymer 42 (2001) 9929-9940.
- [24] *Polymer matrix degradation and color formation in melt processed nylon 6/clay nanocomposites*; Fornes T. D., Yoon P. J., Paul D. R., Polymer 44 (2003) 7545-7556.
- [25] *Nylon 6 nanocomposites by melt compounding*; Cho J. W., Paul D. R., Polymer 42 (2001) 1083-1094.
- [26] McCreeedy K., Keskkula H.; Polymer 20 (1975) 1155-9.

- [27] Anderson C., Rodriguez F., Polym. Mater. Sci. Eng. 51 (1984) 608.
- [28] Schnabel W., Polymer degradation: principles and practical applications, New York: Hanser Publishers; 1981.
- [29] Grassie N., Scott G., Polymer degradation and stabilization, New York, Cambridge University Press; 1985.
- [30] [30] *Thermal degradation chemistry of alkyl quaternary ammonium montmorillonite*; Xie W., Gao Z., Pan W.-P., Hunter D., Singh A., Vaia R.; Chem Mater 13 (2001) 2979-90.
- [31] *Processing degradation of polyamide 6/montmorillonite clay nanocomposites and clay organic modifier*; Davis R., Gilman J., VanderHart D.; Polym. Degrad. Stab. 79 (2003) 111-21.
- [32] *Processing-property relationships of polycarbonate/graphene composites*; Kim H., Macosko C. W.; Polymer 50 (2009) 3797-3809.